Contents of issue 4 vol. L

Polish Academy of Sciences

Institute of Fundamental Technological Research

Archives of Mechanics

Archiwum Mechaniki Stosowanej

volume 50 issue 4

FIFTY YEARS OF THE ARCHIVES OF MECHANICS

Agencja Reklamowo-Wydawnicza A. Grzegorczyk
Warszawa 1998

ARCHIVES OF MECHANICS IS DEVOTED TO

Theory of elasticity and plasticity • Theory of nonclassical continua • Physics of continuous media • Mechanics of discrete media • Nonlinear mechanics • Rheology • Fluid gas-mechanics • Rarefied gas • Thermodynamics

---

Printed in Poland, Editorial Office: Świętokrzyska 21,
00-049 Warszawa (Poland)
e-mail: publikac@ippt.gov.pl

Arkuszy wydawniczych 12. Arkuszy drukarskich 9.
Papier offset. kl III 70 g. B1.
Oddano do składania 13 lipca 1998 r.
Druk ukończono w październiku 1998 r.
Skład i łamanie: G. Wasilewska
Druk i oprawa: Drukarnia OMIKRON, Stare Babice ul. Kutrzeby 15,
tel. (022) 752 94 16

Arch. Mech., 50, 4, pp. 675–689, Warszawa 1998
FIFTY YEARS OF THE ARCHIVES OF MECHANICS

Variational bounds on the effective moduli of anisotropic piezoelectric composites

A. GAŁKA, B. GAMBIN and J. J. TELEGA (WARSZAWA)

INEQUALITIES of Thompson and Dirichlet type have been used to derive the elementary bounds on elastic, piezoelectric and dielectric macroscopic moduli. The Ritz method has been applied to determine approximately the effective moduli.

1. Introduction

PIEZOELECTRIC MATERIALS are often used in modern technical devices. The necessity of modelling the behaviour of intelligent materials significantly influences the interest of many researchers in finding effective properties of piezoelectric composites, cf. [1 – 5] and the references cited therein. We observe that biological materials such like dry bones also exhibit piezoelectric properties, cf. [6]. It seems that the paper by the third author [6] was the first on non-uniform homogenization of piezoelectric composites, which includes periodic homogenization as a particular case. In an accompanying paper [5], a detailed study of Γ-convergence for a class of physically nonlinear piezocomposites has been performed. This class includes the linear case, which is the starting point for the present paper. To determine the effective moduli one has to solve appriopriate periodic boundary value problems posed on the so-called basic cell. For two- and three-dimensional problems such cell problems cannot be exactly solved, hence the need for approximate methods and bounding techniques. In the present contribution we shall consider the problem of variational bounds for the effective moduli. Inequalities of Thompson and Dirichlet type are used to derive elementary bounds on elastic, piezoelectric and dielectric macroscopic moduli. Moreover, for two-phase composites the Ritz method is applied to determine approximately the effective moduli. The results obtained by using Ritz's method compare favourably with upper and lower bounds on the corresponding coefficients.

2. Piezoelectric solid with a microperiodic structure

The elastic, piezoelectric and dielectric moduli are denoted by c_{ijkl}, g_{ijk}, ε_{ij}, respectively, $(i, j, k, l = 1, 2, 3)$. The constitutive relations are given by

$$D_i = \varepsilon_{ij} E_j + g_{ikl} e_{kl}, \tag{2.1}$$

$$\sigma_{ij} = c_{ijkl} e_{kl} - g_{kij} E_k, \tag{2.2}$$

or equivalently

$$E_k = \kappa_{kj} D_j - h_{kij} e_{ij}, \tag{2.3}$$

$$\sigma_{ij} = a_{ijkl} e_{kl} - h_{kij} D_k, \tag{2.4}$$

or

$$D_i = \hat{\kappa}_{ij} E_j - \hat{h}_{ikl} \sigma_{kl}, \tag{2.5}$$

$$e_{ij} = \hat{a}_{ijkl} e_{kl} - \hat{h}_{kij} E_k, \tag{2.6}$$

where

$$\kappa_{ij} = (\boldsymbol{\varepsilon}^{-1})_{ij}, \quad h_{kij} = (\boldsymbol{\varepsilon}^{-1})_{kn} g_{nij}, \quad a_{ijkl} = c_{ijkl} + (\boldsymbol{\varepsilon}^{-1})_{rn} g_{rij} g_{nkl} \tag{2.7}$$

and

$$\hat{a}_{ijkl} = (\mathbf{c}^{-1})_{ijkl}, \qquad \mathbf{c}_{ijkl} = a_{ijkl} - h_{mij} (\boldsymbol{\kappa}^{-1})_{mn} h_{nkl}, \tag{2.8}$$

$$(\hat{\boldsymbol{\kappa}}^{-1})_{ij} = \kappa_{ij} - h_{ikl} (\mathbf{a}^{-1})_{klmn} h_{jmn}, \quad \hat{h}_{ijk} = -h_{lmn} (\boldsymbol{\kappa}^{-1})_{il} \hat{a}_{mnjk}. \tag{2.9}$$

By $(\boldsymbol{\varepsilon}^{-1})_{ij}, (\mathbf{c}^{-1})_{ijkl}$ etc. we denote the components of matrices being inverse of matrices $(\varepsilon_{ij}), (c_{ijkl})$ etc., respectively. Here D_i, E_i, σ_{ij}, e_{ij} are components of the electric displacement vector, the electric field, the stress tensor and the strain tensor, respectively. In the linear case, being the subject of the present contribution, the internal energy $U(y, \mathbf{e}, \mathbf{D})$, $y \in Y$ and its dual $U^*(y, \boldsymbol{\sigma}, \mathbf{E})$, have the following form:

$$U(y, \mathbf{e}, \mathbf{D}) = \frac{1}{2} a_{ijkl}(y) e_{ij} e_{kl} - h_{ijk}(y) D_i e_{jk} + \frac{1}{2} \kappa_{ij}(y) D_i D_j, \tag{2.10}$$

$$U^*(y, \boldsymbol{\sigma}, \mathbf{E}) = \frac{1}{2} \hat{a}_{ijkl}(y) \sigma_{ij} \sigma_{kl} - \hat{h}_{ijk}(y) E_i \sigma_{jk} + \frac{1}{2} \hat{\kappa}_{ij}(y) E_i E_j. \tag{2.11}$$

The set $Y \subset \mathbb{R}^3$ is called the basic cell, cf. [2, 3] and the references cited therein. The dual function U^* is calculated as the Fenchel conjugate of U, see [7]

$$U^*(y, \boldsymbol{\sigma}, \mathbb{E}) = \sup \left\{ \sigma_{ij} e_{ij} + E_i D_i - U(y, \mathbf{e}, \mathbf{D}) | \mathbf{e} \in \mathbb{E}^3_s, \mathbf{D} \in \mathbb{R}^3 \right\}, \tag{2.12}$$

where $\mathbb{E}^3_s$ stands for the space of symmetric 3×3 matrices. The functions a_{ijkl}, h_{ijk} and κ_{ij} are Y-periodic. The elastic, piezoelectric and dielectric coefficients satisfy obvious symmetry conditions. The function $U(y, \cdot, \cdot)$ is assumed to be strictly convex, cf. [1, 6].

3. Homogenization

The density of the macroscopic or homogenized potential U^h is expressed as follows [6]:

$$(3.1)\qquad U^h(\mathbf{e}^h,\mathbf{D}^h)=\inf_{\mathbf{v}\in\mathbf{H}_{\rm per}}\inf_{\mathbf{D}\in\Delta_{\rm per}}\frac{1}{|Y|}\int_Y\Big[\frac{1}{2}a_{ijkl}(y)\left(e^y_{ij}(\mathbf{v})+e^h_{ij}\right)\cdot\left(e^y_{kl}(\mathbf{v})+e^h_{kl}\right)-h_{kij}(y)\left(D_k(y)+D^h_k\right)\left(e^y_{ij}(\mathbf{v})+e^h_{ij}\right)+\frac{1}{2}\kappa_{ij}(y)\left(D_i(y)+D^h_i\right)\left(D_j(y)+D^h_j\right)\Big]dy,$$

where $\mathbf{e}^h\in\mathbb{E}^3_s$, $\mathbf{D}^h\in\mathbb{R}^3$ and $e^y_{ij}(\mathbf{v})=\dfrac{1}{2}\left(\dfrac{\partial v_j}{\partial y_i}+\dfrac{\partial v_i}{\partial y_j}\right)$.

The superscript h stands for a homogenized quantity and

$$(3.2)\qquad \mathbf{H}_{\rm per}=\{\mathbf{u}=(u_i)\in H^1(Y)^3|\mathbf{u}\ \text{takes equal values on the opposite faces of } Y\},$$

$$(3.3)\qquad \Delta_{\rm per}=\{\mathbf{D}=(D_i)\,|D_i\in L^2(Y),\ \mathrm{div}_y\mathbf{D}=0\ \text{ in } Y,\ \int_Y\mathbf{D}(y)dy=0,$$

D_iN_i takes opposite values on the opposite sides of Y $\}$.

The density of the macroscopic dual potential U^{*h} is expressed as follows:

$$(3.4)\qquad U^{*h}(\boldsymbol{\sigma}^h,\mathbf{E}^h)=\inf_{\phi\in H^1_{\rm per}}\inf_{\sigma\in S_{\rm per}}\frac{1}{|Y|}\int_Y\Big[\frac{1}{2}\hat{a}_{ijkl}(y)\left(\sigma_{ij}(y)+\sigma^h_{ij}\right)\cdot\left(\sigma_{kl}(y)+\sigma^h_{kl}\right)-\hat{h}_{kij}(y)\left(E^y_k(\phi)+E^h_k\right)\left(\sigma_{ij}(y)+\sigma^h_{ij}\right)+\frac{1}{2}\hat{\kappa}_{ij}(y)\left(E^y_i(\phi)+E^h_i\right)\left(E^y_j(\phi)+E^h_j\right)\Big]dy,$$

where $\boldsymbol{\sigma}^h\in\mathbb{E}^3_s$, $\mathbf{E}^h\in\mathbb{R}^3$, $E^y_i(\phi)=-\dfrac{\partial\phi}{\partial y_i}$, and

$$(3.5)\qquad H^1_{\rm per}=\left\{\varphi\in H^1(Y)\mid\varphi\ \text{ is } Y\text{-periodic}\right\},$$

$$(3.6)\qquad S_{\rm per}=\left\{\boldsymbol{\sigma}\in L^2(Y,\mathbb{E}^2_s)\,|\mathrm{div}_y\boldsymbol{\sigma}=0\ \text{ in } Y,\ \int_Y\boldsymbol{\sigma}(y)dy=0,\right.$$

$\left.\sigma_{ij}N_j\ \text{takes opposite values on the opposite faces of } Y\right\}$.

Here $\mathbf{N}$ is the outward unit vector normal to ∂Y.

REMARK. The formula (3.1) results from the theory of Γ-convergence applied to convex periodic homogenization problems [6, 8]. The general case of convex

homogenization of piezoelectric composites with periodic or non-uniformly periodic microstructure has been investigated in our accompanying paper [5].

The form (3.4) of the dual potential U^{*h} is obtained by applying Azé's theory of duality, cf. [5, 6, 9].

4. Elementary bounds

The homogenized internal energy (3.1) can be written in the following form [6]:

$$U^h(\mathbf{e}^h, \mathbf{D}^h) = \frac{1}{2} a^h_{ijkl} e^h_{ij} e^h_{kl}, -h^h_{kij} D^h_k e^h_{ij} + \frac{1}{2} \kappa^h_{ij} D^h_i D^h_j, \tag{4.1}$$

where

$$a^h_{ijkl} = \frac{\partial^2 U^h}{\partial e^h_{ij} \partial e^h_{kl}}, \qquad h^h_{kij} = \frac{\partial^2 U^h}{\partial e^h_{ij} \partial D^h_k}, \qquad \kappa^h_{ij} = \frac{\partial^2 U^h}{\partial D^h_i \partial D^h_j}.$$

Explicit expressions in terms of a solution $(\tilde{\mathbf{v}}, \tilde{\mathbf{D}}) \in \mathbf{H}_{\text{per}} \times \Delta_{\text{per}}$ of the minimization problem appearing on the r.h.s of (3.1) were derived in [6]. Supose that the trial fields are: $e^y_{ij}(\mathbf{v}) = 0$, $D_i(y) = 0$, $\sigma_{ij}(y) = 0$, and $\phi(y) = 0$. Then we get

$$U^h(\mathbf{e}^h, \mathbf{D}^h) \leq \frac{1}{2} < a_{ijkl}(y) > e^h_{ij} e^h_{kl} - < h_{kij}(y) > D^h_k e^h_{ij} + \frac{1}{2} < \kappa_{ij}(y) > D^h_i D^h_j, \tag{4.2}$$

and

$$U^{*h}(\boldsymbol{\sigma}^h, \mathbf{E}^h) \leq \frac{1}{2} < \hat{a}_{ijkl}(y) > \sigma^h_{ij} \sigma^h_{kl} - < \hat{h}_{kij}(y) > E^h_k \sigma^h_{ij} + \frac{1}{2} < \hat{\kappa}_{ij}(y) > E^h_i E^h_j, \tag{4.3}$$

where

$$< \cdot > = \frac{1}{|Y|} \int_Y (\cdot) dy. \tag{4.4}$$

For convex functions f and g the inequality $f(x) \leq g(x)$ implies $f^*(x^*) \geq g^*(x^*)$, cf. [7]. Hence

$$U^h(\mathbf{e}^h, \mathbf{D}^h) \geq \frac{1}{2} a^v_{ijkl} e^h_{ij} e^h_{kl} - h^v_{kij} D^h_k e^h_{ij} + \frac{1}{2} \kappa^v_{ij} D^h_i D^h_j, \tag{4.5}$$

where a^v_{ijkl} and κ^v_{ij} are the components of the matrices inverse to the matrices $\mathbf{A}$ and $\mathbf{K}$ respectively, where

$$A_{ijkl} = < \hat{a}_{ijkl} > - < \hat{h}_{mij} > (< \hat{\kappa} >^{-1})_{mn} < \hat{h}_{nkl} >, \tag{4.6}$$

$$K_{ij} = < \hat{\kappa}_{ij} > - < \hat{h}_{ikl} > (< \hat{a} >^{-1})_{klmn} < \hat{h}_{jmn} >, \tag{4.7}$$

and

$$h^v_{ijk} = -(< \hat{h}_{lmn} > (< \hat{\kappa} >^{-1})_{il} a^v_{mnjk}. \tag{4.8}$$

The inequalities (4.2), (4.5) are the elementary bounds on the homogenized internal energy cf. [3]. Taking into account (4.1), (4.2) and (4.5) and taking $\mathbf{D}^h = 0$ or $\mathbf{e}^h = 0$, we obtain two particular bounds

$$a^v_{ijkl} e^h_{ij} e^h_{kl} \leq a^h_{ijkl} e^h_{ij} e^h_{kl} \leq < a_{ijkl}(y) > e^h_{ij} e^h_{kl}, \quad \text{for each } \mathbf{e}^h \in \mathbb{E}^3_s, \tag{4.9}$$

$$\kappa^v_{ij} D^h_i D^h_j \leq \kappa^h_{ij} D^h_i D^h_j \leq < \kappa_{ij}(y) > D^h_i D^h_j, \quad \text{for each } \mathbf{D}^h \in \mathbb{R}^3. \tag{4.10}$$

The inequalities (4.9) and (4.10) are equivalent to positive definiteness of the following quadratic forms:

$$(a^h_{ijkl} - a^v_{ijkl}), \ (< a_{ijkl}(y) > - a^h_{ijkl}), \ (\kappa^h_{ij} - \kappa^v_{ij}), \ (< \kappa_{ij}(y) > - \kappa^h_{ij}). \tag{4.11}$$

By using these inequalities one can derive the elementary bounds on the diagonal elements of Voigt matrices, that is the bounds on these particular homogenized material coefficients. Now they are of the form

$$a^v_{ijkl} \leq a^h_{ijkl} \leq < a_{ijkl}(y) >, \tag{4.12}$$

$$\kappa^v_{ij} \leq \kappa^h_{ij} \leq < \kappa_{ij}(y) >, \tag{4.13}$$

provided that

$$\begin{aligned} (ijkl) \ &\in \ \{(1111), (2222), (3333), (1212), (1313), (2323)\}, \\ (ij) \ &\in \ \{(11), (22), (33)\}. \end{aligned} \tag{4.14}$$

Every inequality for the homogenized coefficients a^h_{ijkl} and κ^h_{ij} with indices not belonging to (4.14) includes at least two elements from the set of the homogenized moduli a^h_{ijkl} and κ^h_{ij} with indices from (4.14). For instance, for a^h_{1133} the inequalities which include a^h_{1111} and a^h_{3333} have the form:

$$|a^h_{1133} - < a_{1133} > | \ \leq \ \sqrt{(a^h_{1111} - < a_{1111} >)(a^h_{3333} - < a_{3333} >)}, \tag{4.15}$$

$$|a^h_{1133} - a^v_{1133}| \ \leq \ \sqrt{(a^h_{1111} - a^v_{1111})(a^h_{3333} - a^v_{3333})}. \tag{4.16}$$

Any inequality satisfied by h^h_{kij} results directly from (4.2) and (4.5). It always contains at least two elements from the set of the homogenized coefficients a^h_{ijkl} and κ^h_{ij} with indices from the sets defined by (4.14). For instance, the inequalites satisfied by h^h_{113} and involving a^h_{1313} and κ^h_{11} have the following form:

$$|h^h_{113} - h^v_{113}| \ \leq \ \sqrt{(a^h_{1313} - a^v_{1313})(\kappa^h_{11} - \kappa^v_{11})}\,, \tag{4.17}$$

$$|h^h_{113} - < h_{113} > | \ \leq \ \sqrt{(a^h_{1313} - < a_{1313} >)(\kappa^h_{11} - < \kappa_{11} >)}\,. \tag{4.18}$$

The bounds obtained in this way are rather wide. Substituting

$$e_{ij}^h = P_{kij} D_k^h , \qquad D_i^h = Q_{ikl} e_{kl}^h, \tag{4.19}$$

into (4.2) and (4.5) and performing optimization of the expressions thus obtained with respect to P_{kij} and Q_{ikl}, we get

$$\kappa_{ij}^v + (h_{ikl}^h - h_{ikl}^v)((\mathbf{a}^h - \mathbf{a}^v)^{-1})_{klmn}(h_{jmn}^h - h_{imn}^v) \leq \kappa_{ij}^h, \tag{4.20}$$

$$\kappa_{ij}^h \leq < \kappa_{ij} > \\ +(h_{ikl}^h - < h_{ikl} >)((\mathbf{a}^h - < \mathbf{a} >)^{-1})_{klmn}(h_{jmn}^h - < h_{imn} >, \tag{4.21}$$

and

$$a_{ijkl}^v + (h_{mij}^h - h_{mij}^v)\left((\boldsymbol{\kappa}^h - \boldsymbol{\kappa}^v)^{-1}\right)_{mn}(h_{nkl}^h - h_{nkl}^v) \leq a_{ijkl}^h, \tag{4.22}$$

$$a_{ijkl}^h \leq < a_{ijkl} > \\ +(h_{mij}^h - < h_{mij} >)((\boldsymbol{\kappa}^h - < \boldsymbol{\kappa} >)^{-1})_{mn}(h_{nkl}^h - < h_{nkl} >). \tag{4.23}$$

For indices from the set (4.14) these bounds are narrower than the Voigt-Reuss bounds (4.12), (4.13).

5. Example: two-phase composite

Let us consider a fibre-reinforced composite, in which the matrix and fibre materials are both homogeneous and transversely isotropic, with the axis of transverse isotropy oriented in the direction of the fibres. The fibres are distributed in such a manner that the symmetry of the homogenized material is the same as that of the plane basic cell.

For convenience, six independent Cartesian components of the strain tensor $\mathbf{e}$ and three Cartesian components of the electric displacement vector $\mathbf{D}$ are arranged in the following manner:

$$\mathbf{F}^T = (e_{11}, e_{22}, e_{33}, 2\,e_{23}, 2\,e_{31}, 2\,e_{12}, D_1, D_2, D_3) , \tag{5.1}$$

where the superscript T denotes the transpose. The free-energy densities of the fibres and of the matrix are quadratic functionals of $\mathbf{F}$, and hence are characterized by two 9×9 symmetric positive-definite matrices, say $\overset{(1)}{\mathbf{A}}$ and $\overset{(2)}{\mathbf{A}}$

$$\overset{(1)}{U}(\mathbf{F}) = \frac{1}{2}\mathbf{F}^T \cdot \overset{(1)}{\mathbf{A}} \cdot \mathbf{F}, \tag{5.2}$$

$$\overset{(2)}{U}(\mathbf{F}) = \frac{1}{2}\mathbf{F}^T \cdot \overset{(2)}{\mathbf{A}} \cdot \mathbf{F}. \tag{5.3}$$

The material constants for the fibre material PZT-7A and for the matrix material are given by

$$\overset{(1)}{\mathbf{A}} = \left[\begin{array}{c|c} \overset{(1)}{\mathbf{a}} & \overset{(1)}{\mathbf{h}}{}^{T} \\ \hline \overset{(1)}{\mathbf{h}} & \overset{(1)}{\boldsymbol{\kappa}} \end{array}\right] \quad \text{and} \quad \overset{(2)}{\mathbf{A}} = \left[\begin{array}{c|c} \overset{(2)}{\mathbf{a}} & \overset{(2)}{\mathbf{h}}{}^{T} \\ \hline \overset{(2)}{\mathbf{h}} & \overset{(2)}{\boldsymbol{\kappa}} \end{array}\right], \tag{5.4}$$

where $\overset{(1)}{\mathbf{a}}$ are the elastic moduli in [GPa]

$$\overset{(1)}{\mathbf{a}} = \begin{bmatrix} 157 & 85.4 & 73 & 0 & 0 & 0 \\ 85.4 & 157 & 73 & 0 & 0 & 0 \\ 73 & 73 & 175 & 0 & 0 & 0 \\ 0 & 0 & 0 & 47.2 & 0 & 0 \\ 0 & 0 & 0 & 0 & 47.2 & 0 \\ 0 & 0 & 0 & 0 & 0 & 35.8 \end{bmatrix}. \tag{5.5}$$

By using (2.7) we find

$$\overset{(1)}{\mathbf{c}} = \begin{bmatrix} 154.84 & 83.237 & 82.712 & 0 & 0 & 0 \\ 83.237 & 154.84 & 82.712 & 0 & 0 & 0 \\ 82.712 & 82.712 & 131.39 & 0 & 0 & 0 \\ 0 & 0 & 0 & 25.696 & 0 & 0 \\ 0 & 0 & 0 & 0 & 25.696 & 0 \\ 0 & 0 & 0 & 0 & 0 & 35.8 \end{bmatrix}, \tag{5.6}$$

since the piezoelectric coefficients $\overset{(1)}{\mathbf{h}}$ in [V/nm] and $\overset{(1)}{\mathbf{g}}$ in [V/F] are specified by

$$\overset{(1)}{\mathbf{h}} = \begin{bmatrix} 0 & 0 & 0 & 0 & -2.3 & 0 \\ 0 & 0 & 0 & -2.3 & 0 & 0 \\ 1.02 & 1.02 & -4.58 & 0 & 0 & 0 \end{bmatrix}, \tag{5.7}$$

$$\overset{(1)}{\mathbf{g}} = \begin{bmatrix} 0 & 0 & 0 & 0 & -9.35 & 0 \\ 0 & 0 & 0 & -9.35 & 0. & 0 \\ 2.121 & 2.121 & -9.52 & 0 & 0 & 0 \end{bmatrix}. \tag{5.8}$$

Here the dielectric coefficients $\overset{(1)}{\boldsymbol{\kappa}}$ in [m/nF] and $\overset{(1)}{\boldsymbol{\varepsilon}}$ in [nF/m] are given by

$$\overset{(1)}{\boldsymbol{\kappa}} = \begin{bmatrix} 0.246 & 0 & 0 \\ 0 & 0.246 & 0 \\ 0 & 0 & 0.481 \end{bmatrix}, \tag{5.9}$$

$$\overset{(1)}{\boldsymbol{\varepsilon}} = \begin{bmatrix} 4.065 & 0 & 0 \\ 0 & 4.065 & 0 \\ 0 & 0 & 2.079 \end{bmatrix}. \tag{5.10}$$

Let us pass to the specification of the material coefficients of the epoxy matrix. Now the elastic moduli are given by

$$\overset{(2)}{\mathbf{a}} = \overset{(2)}{\mathbf{c}} = \begin{bmatrix} 8 & 4.4 & 4.4 & 0 & 0 & 0 \\ 4.4 & 8 & 4.4 & 0 & 0 & 0 \\ 4.4 & 4.4 & 8 & 0 & 0 & 0 \\ 0 & 0 & 0 & 1.8 & 0 & 0 \\ 0 & 0 & 0 & 0 & 1.8 & 0 \\ 0 & 0 & 0 & 0 & 0 & 1.8 \end{bmatrix}. \tag{5.11}$$

The piezoelectric coefficients are specified by

$$\overset{(2)}{\mathbf{g}} = \overset{(2)}{\mathbf{h}} = \begin{bmatrix} 0 & 0 & 0 & 0 & 0 & 0 \\ 0 & 0 & 0 & 0 & 0 & 0 \\ 0 & 0 & 0 & 0 & 0 & 0 \end{bmatrix}, \tag{5.12}$$

while the dielectric coefficients are given by

$$\overset{(2)}{\boldsymbol{\kappa}} = \begin{bmatrix} 26.9 & 0 & 0 \\ 0 & 26.9 & 0 \\ 0 & 0 & 26.9 \end{bmatrix}, \tag{5.13}$$

$$\overset{(2)}{\boldsymbol{\varepsilon}} = \begin{bmatrix} 0.0372 & 0 & 0 \\ 0 & 0.0372 & 0 \\ 0 & 0 & 0.0372 \end{bmatrix}. \tag{5.14}$$

Let us introduce the following matrices:

$$\mathbf{A}^s = f_1 \overset{(1)}{\mathbf{A}} + f_2 \overset{(2)}{\mathbf{A}}, \tag{5.15}$$

$$\mathbf{A}^r = \left(f_1 \left(\overset{(1)}{\mathbf{A}} \right)^{-1} + f_2 \left(\overset{(2)}{\mathbf{A}} \right)^{-1} \right)^{-1}, \tag{5.16}$$

where f_1 stands for the fibre volume fraction, and $f_2 = 1 - f_1$.

If $f_1 = 0.4$, $f_2 = 0.6$ then we have

(5.17)

$$\mathbf{A}^r = \begin{bmatrix} 12.9 & 7.09 & 7.06 & 0 & 0 & 0 & 0 & 0 & 0.042 \\ 7.09 & 12.9 & 7.06 & 0 & 0 & 0 & 0 & 0 & 0.042 \\ 7.06 & 7.06 & 12.9 & 0 & 0 & 0 & 0 & 0 & -0.28 \\ 0 & 0 & 0 & 2.93 & 0 & 0 & 0 & -0.141 & 0 \\ 0 & 0 & 0 & 0 & 2.93 & 0 & -0.141 & 0 & 0 \\ 0 & 0 & 0 & 0 & 0 & 2.90 & 0 & 0 & 0 \\ 0 & 0 & 0 & 0 & -0.141 & 0 & 0.349 & 0 & 0 \\ 0 & 0 & 0 & -0.141 & 0 & 0 & 0 & 0.339 & 0 \\ 0.042 & 0.042 & -0.28 & 0 & 0 & 0 & 0 & 0 & 0.669 \end{bmatrix},$$

(5.17)

[cont.]

$$\mathbf{A}^s = \begin{bmatrix} 67.6 & 36.8 & 31.84 & 0 & 0 & 0 & 0 & 0 & 0.408 \\ 36.8 & 67.6 & 31.84 & 0 & 0 & 0 & 0 & 0 & 0.408 \\ 31.84 & 31.84 & 74.8 & 0 & 0 & 0 & 0 & 0 & -1.83 \\ 0 & 0 & 0 & 19.96 & 0 & 0 & 0 & -0.92 & 0 \\ 0 & 0 & 0 & 0 & 19.96 & 0 & -0.92 & 0 & 0 \\ 0 & 0 & 0 & 0 & 0 & 15.4 & 0 & 0 & 0 \\ 0 & 0 & 0 & 0 & -0.92 & 0 & 16.2 & 0 & 0 \\ 0 & 0 & 0 & -0.92 & 0 & 0 & 0 & 16.2 & 0 \\ 0.408 & 0.408 & -1.83 & 0 & 0 & 0 & 0 & 0 & 16.33 \end{bmatrix}.$$

The inequalities (4.2) and (4.5) are equivalent to

$$\mathbf{A}^r \leq \mathbf{A}^h \leq \mathbf{A}^s \tag{5.18}$$

where $\mathbf{A}^h$ denotes the effective matrix. The matrix inequalities (5.18) imply immediately upper and lower bounds on the diagonal coefficients. Better estimates can be obtained from (4.20) – (4.23). In this case, however, on account of a weak influence of coupling, the differences are small. At present no explicit bounds are avaiable on the off-diagonal components. BISEGNA and LUCIANO [1, 2] claim that they have provided bounds on the off-diagonal elements by taking appropriate elements of the matrices $\mathbf{A}^r$ and $\mathbf{A}^s$. Such a statement is in general not true since bounds on matrices do not coincide with bounds on their elements. Similar remark concerns Hashin-Shtrikman type bounds given in [1]. We observe that the bounds derived in [11] on off-diagonal coefficients are accurate only for the elastic matrix. Therefore below, by using the formulae (4.20) – (4.23) we provide examples of determination of the bounds on off-diagonal elements for piezoelectric coupling matrix of material coefficients. This seems to be an important novelty of our paper.

Let us summarize these results:

(i) The bounds on the coefficient a^h_{1122} are depicted in Fig. 1. The part of the plane inside the parallelogram contains points with coordinates (a^h_{1111}, a^h_{1122}). In particular, we have $-5.41 \leq a^h_{1122} \leq 49.3$. The bounds lie in the plane because in the example studied it was assumed that a^h_{1111} and a^h_{2222} coincide. The sign + denotes the point determined by the Ritz method [3].

(ii) Figure 2 depicts the surface determined by maximal values of the coefficients a^h_{1133} (the upper bound) as a function of a^h_{1111} and a^h_{3333}. The last two coefficients vary within the Voigt-Reuss bounds. In Fig. 3 the surface of lower bounds is represented. Similar surfaces can be constructed for other off-diagonal homogenized coefficients, cf. Figs. 6 and 7.

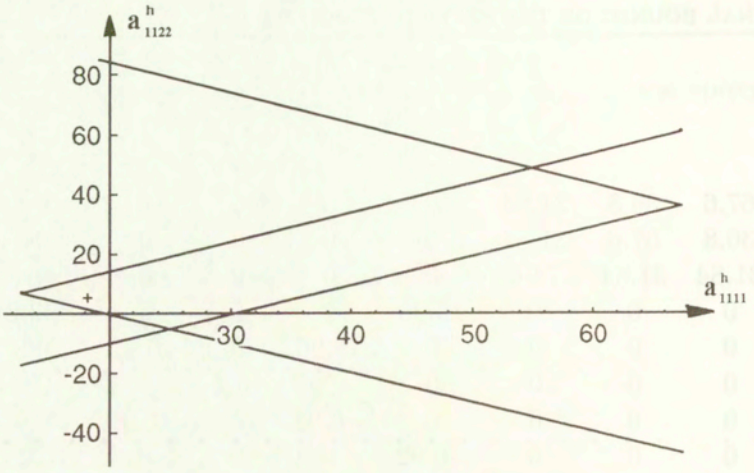

FIG. 1.

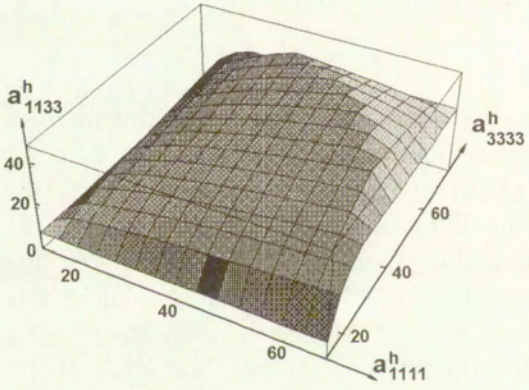

FIG. 2.

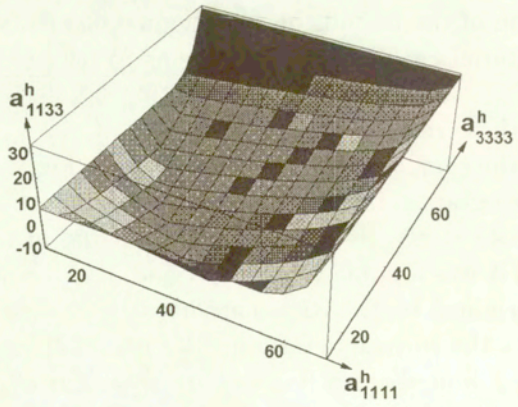

FIG. 3.

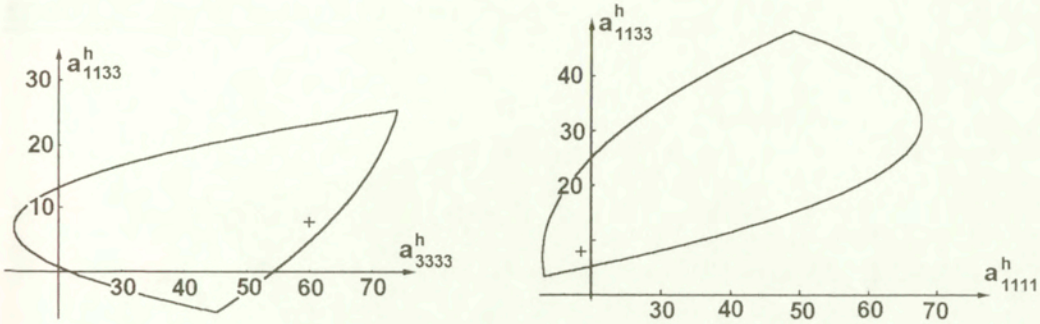

FIG. 4.

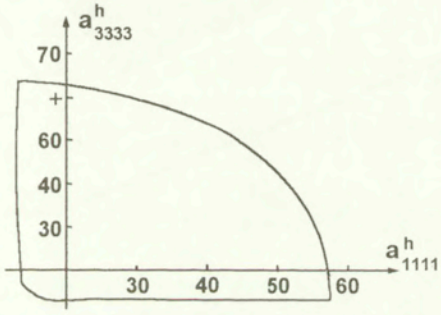

FIG. 5.

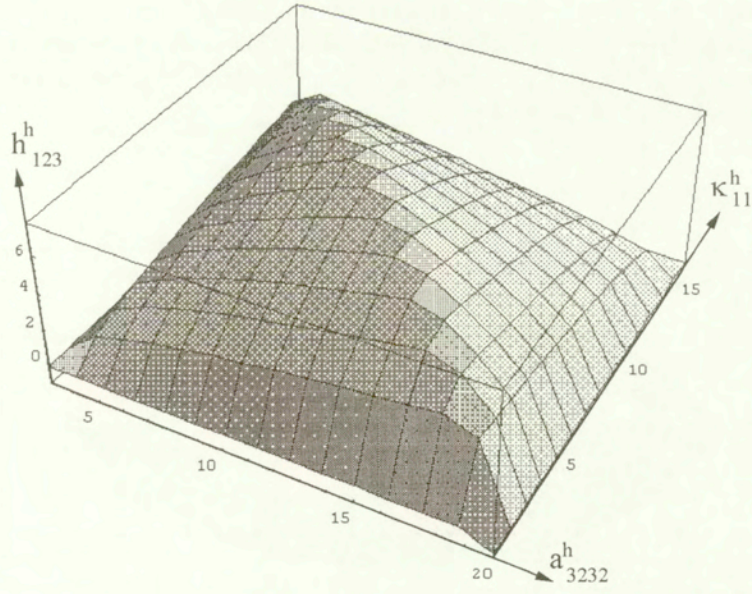

FIG. 6.

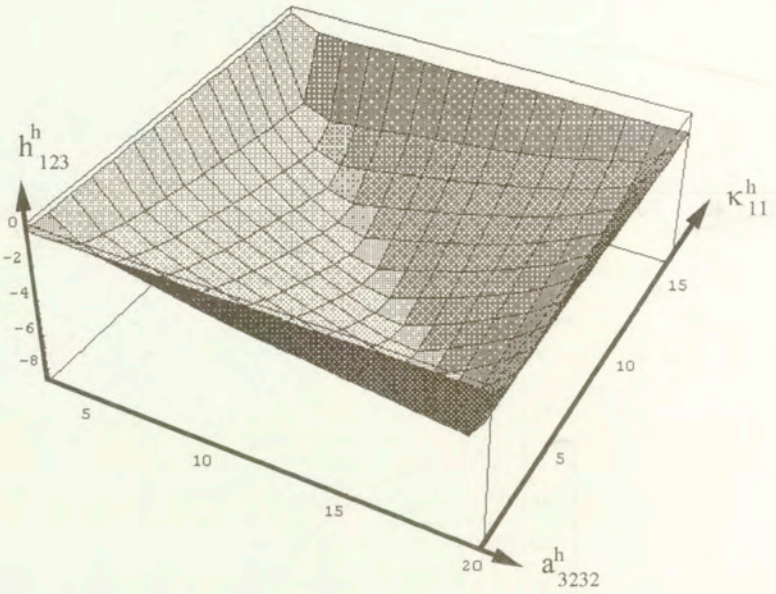

FIG. 7.

The domain contained between these two surfaces is called "the bounds region", cf. Fig. 8. Figures 4a, 4b, 5, 9 and 10 represent cross-sections of the bounds region within planes orthogonal to the coordinate axis and containing the Ritz point, denoted here by +. The coordinates of this point were determined in [3] by using the Ritz method. It is worth noting that the Ritz point lies within the bounds region.

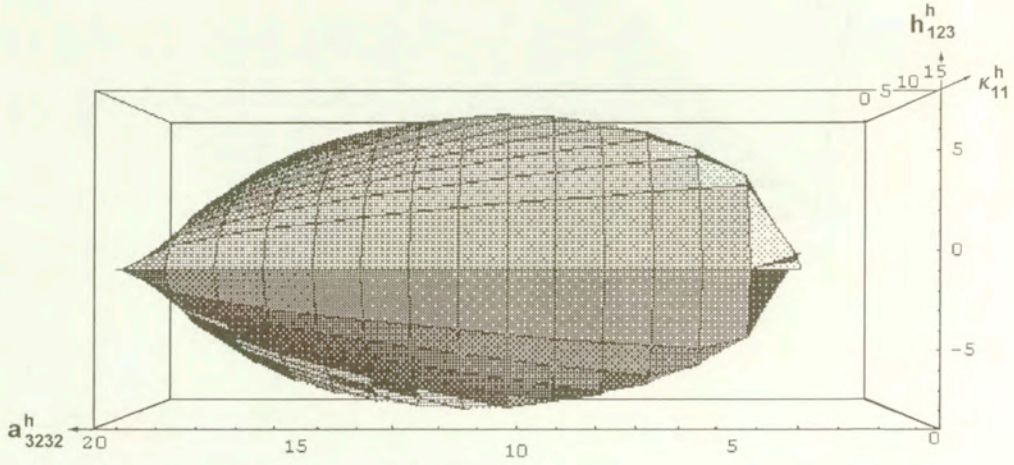

FIG. 8.

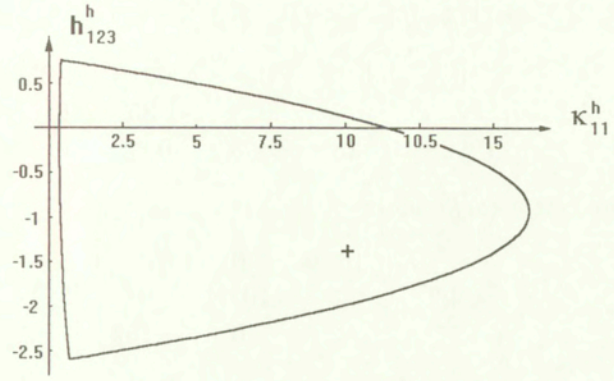

FIG. 9.

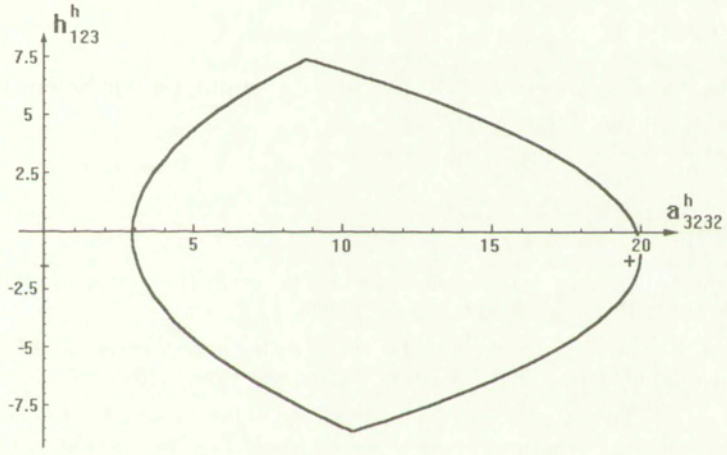

FIG. 10.

Let us now pass to providing the values of the homogenized coefficients for the same composite as they were obtained by employing the Ritz method [3]. Now they are given by:

a. *The elastic moduli*

$$\mathbf{a}^h = \begin{bmatrix} 18.46 & 5.81 & 7.96 & 0 & 0 & 0 \\ 5.81 & 18.46 & 7.96 & 0 & 0 & 0 \\ 7.96 & 7.96 & 59.98 & 0 & 0 & 0 \\ 0 & 0 & 0 & 19.82 & 0 & 0 \\ 0 & 0 & 0 & 0 & 19.82 & 0 \\ 0 & 0 & 0 & 0 & 0 & 3.19 \end{bmatrix}; \tag{5.19}$$

b. *The piezoelectric coefficients*

$$\mathbf{h}^h = \begin{bmatrix} 0 & 0 & 0 & 0 & -1.35 & 0 \\ 0 & 0 & 0 & -1.35 & 0 & 0 \\ 0.128 & 0.128 & -4.98 & 0 & 0 & 0 \end{bmatrix}; \tag{5.20}$$

c. *The dielectric coefficients*

$$\mathbf{k}^h = \begin{bmatrix} 10.04 & 0 & 0 \\ 0 & 10.04 & 0 \\ 0 & 0 & 1.152 \end{bmatrix}. \tag{5.21}$$

By comparing the method of bounds with the Ritz method we conclude that in this particular case of two-phase composite, Ritz's method yields results which fall within the upper and lower bounds.

Acknowledgement

The authors were supported by the State Committee for Scientific Research through the grant No 7 T07A 016 12.

References

1. P. BISEGNA, R. LUCIANO, *Variational bounds for the overall properties of piezoelectric composites*, J. Mech. Phys. Solids, **44**, 583–602, 1996.
2. P. BISEGNA, R. LUCIANO, *On methods for bounding the overall properties of periodic piezoelectric fibrous composites*, J. Mech. Phys. Solids, **45**, 1329–1356, 1997.
3. A. GAŁKA, J. J. TELEGA, R. WOJNAR, *Some computational aspects of homogenization of thermopiezoelectric composites*, Comp. Assisted Mech. Eng. Sci., **3**, 133–154, 1996.
4. K. KYCIA, A. NOWICKI, O. GAIL, T. D. HIEN, *Calculation of effective material tensors and the electromechanical coupling coefficient of a type 1-3 composite transducer*, Arch. Acoustics, **21**, 371–386, 1996.
5. J. J. TELEGA, A. GAŁKA, B. GAMBIN, *Effective properties of physically nonlinear piezoelectric composites*, Arch. Mech., **50**, 321–340, 1998.
6. J. J. TELEGA, *Piezoelectricity and homogenization. Application to biomechanics.* [In:] Continuum Models and Discrete Systems, Vol. 2, G. A. MAUGIN [Ed.], Longman, pp. 221–229, Essex 1991.
7. R. T. ROCKAFELLAR, *Convex Analysis*, Princeton University Press, Princeton 1970.
8. G. DAL MASO, *Introduction to Γ-convergence*, Birkhäuser, Boston 1993.
9. D. AZÈ, *Epi-convergence et dualité. Applications a' la convergence des variables primales et duales pour des suites d'optimization convexe*, Publications AVAMAC, Université de Perpignan, Report No. 84 – 12.
10. G. W. MILTON and R. V. KOHN, *Variational bounds on the effective moduli of anisotropic composites*, J. Mech. Phys. Solids, **36**, 6, 597–629, 1988.

11. P. BISEGNA, R. LUCIANO, *Bounds on the off-diagonal coefficients of the constitutive tensor of a composite material*, Mech. Res. Comm., **23**, 239–245, 1996.

POLISH ACADEMY OF SCIENCES
INSTITUTE OF FUNDAMENTAL TECHNOLOGICAL RESEARCH
e-mail: agalka@ippt.gov.pl
e-mail: jtelega@ippt.gov.pl
e-mail: bgambin@ippt.gov.pl

Received January 30, 1998.

Arch. Mech., 50, 1, pp. 691–701, Warszawa 1998
FIFTY YEARS OF THE ARCHIVES OF MECHANICS

Effect of miss-distance on the airfoil-vortex interaction Experiment

W. SELEROWICZ, G. SOBIERAJ, A. SZUMOWSKI
and J. PIECHNA (WARSZAWA)

THE EFFECT of a strong vortex interacting with an airfoil flow is investigated experimentally by means of a shock tube. The experiments follow the previous theoretical work [11] on this subject. The instantaneous pressure distributions and histories of lift coefficient during the vortex passage are presented. The flow is visualised using the schlieren method. It is found that due to the viscosity of the air not taken into account in numerical study, the effect of miss-distance in the range of up to 0.5 chord length is weaker than it was initially predicted.

1. Introduction

A TIP VORTEX shed from the helicopter rotor blade can interact with the following blade. This happens during the helicopter descent with a deep turn and its low-powered approach to landing. The strongest interaction occurs when the vortex filament passes parallel at a small distance from the blade plane. A specific case of this type of interaction shows the head-on impact of the vortex core on the leading edge.

The parallel airfoil-vortex interaction (AVI) was investigated by many authors. Both the numerical and the experimental methods were used. Considering a wide range of the flow Mach number which can exist during the helicopter blade rotation, the incompressible and compressible (also transonic) flows were studied. In the experiments the vortex needed for interaction was produced by a preceding pitched airfoil singly [1] or continuously in wind [2] or water [3] tunnels. The wind tunnel experiments, however, do not provide strong vortices and hence do not allow one to obtain sufficiently strong effects of the vortex interaction. This especially concerns the acoustic effects. For a weak vortex, the sound pressure produced during the interaction appears to be of the order of magnitude of the background disturbances. This disadvantage can be partly avoided by using starting vortex of a lifting airfoil placed in a shock tube. This technique was used by LENT *et al.* [4], LEE and BESHADER [5] and KAMIŃSKI and SZUMOWSKI [6]. By applying the interferometric [4, 5] and schlieren method [6] for flow visualisation, they observed an acoustic wave generated during the head-on collision.

Majority of the papers on the AVI phenomenon consider the acoustic effects, but only a few of them deal with the loading. References [1, 2, 7, 8] present

variation of the loading for very low flow velocities. Even in this case considerable changes of the airfoil surface pressure and the lift coefficient have been observed. For the transonic flow range [9, 10] these changes are additionally strengthened due to the shock waves which move along the airfoil surfaces (suction and pressure surfaces) during the interaction.

The parallel airfoil-vortex interaction is controlled, first of all, by the following parameters:

(i) the miss-distance which is defined as a distance measured at infinity between the vortex trajectory and the stream line passing through the stagnation point;

(ii) radius of the vortex core (r_0),

(iii) circulation (Γ_0) at $r = r_0$, and

(iv) flow Mach number at infinity.

The present experimental work concerns the effect of the first of four parameters mentioned above. It follows the previous numerical study [11] in which the airfoil flow was computed by means of the Euler solver. This paper, like [11], is focussed on aerodynamic effects: surface pressure and loading variations during the interaction.

The experiments conducted in this work correspond to the calculation results presented in Ref. [11]. However, the period of time in which the pressure histories during the interaction were possible to be measured, was much longer than the period available in computation. This was due to the relatively large length of the shock tube which enabled the authors to have a steady background flow (not disturbed by the waves reflected at closed ends of the shock tube or by the entropy discontinuity surface) for a relatively long time.

2. Experimental facility

The experiments were conducted in a conventional two-chamber shock tube of dimensions shown in Fig. 1. The rectangular cross-section of the tube was modified by mounting the triangular slots along the top and bottom walls to conceal the oblique waves which appear during the shock wave-airfoil interaction. Each experiment was prepared by evacuating the air from the low pressure chamber to obtain a vacuum up to 8 kPa of absolute pressure. In the high pressure chamber the atmospheric pressure was maintained. The two NACA 0012 airfoils of chord length $c = 120$ mm were placed at a distance of 530 mm in the shock tube. The preceding airfoil was used to generate the vortex, and the following one to induce the AVI process. The former could be displaced across the shock tube to adjust the vortex trajectory. A constant angle of attack equal to 20° of this airfoil was maintained. The instantaneous pressure was measured by means of miniature Kulite pressure transducers distributed at the side wall

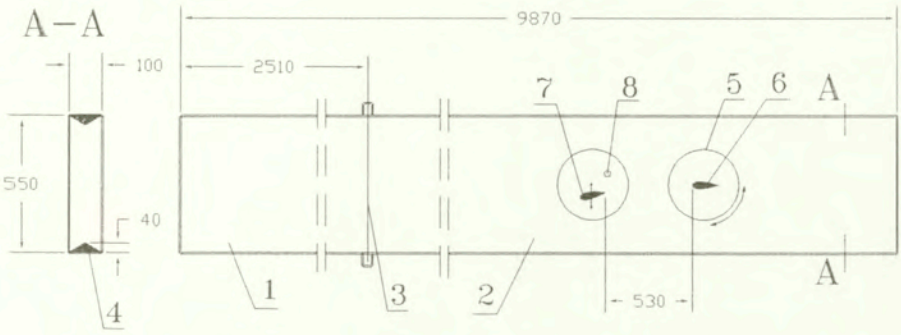

FIG. 1. Shock tube: *1* – high pressure chamber, *2* – low pressure chamber, *3* – diaphragm, *4* – slot, *5* – test section window, *6* – test airfoil, *7* – vortex generator, *8* – triggering transducer.

of the tube along the airfoil contour (Fig. 2). It was believed that due to their small diameters (2.3 mm), the measured pressure was equal to the actual airfoil surface pressure. This supposition was checked by comparing the measured wall pressure with the computed (Euler solver) airfoil surface pressure for the flow without the vortex (the vortex generator was removed during this experiment). The results are shown in Fig. 3. Good agreement between the corresponding pressure histories in each point except one (at the leading edge) can be noted. The discrepancy between the measured wall pressure and the calculated surface pressure at $x/c = 0$ appears to be caused by the nonuniform pressure distribution is the region close to the stagnation point (the transducer shows average pressure on its face).

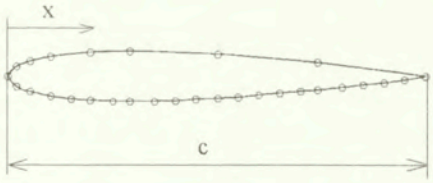

FIG. 2. Distribution of pressure transducers.

The vortex trajectory was identified by measuring the pressure histories at ten points densely distributed along the line normal to the airfoil plane, one chord upstream the airfoil.

The flow was visualised by means of the schlieren method. The Cranz-Schardin system which allows one to have 8 consecutive photographs during one experiment was used.

The experiments were performed with a constant flow Mach number $M_1 = 0.69$ which in this case corresponds to the following values of the flow velocity,

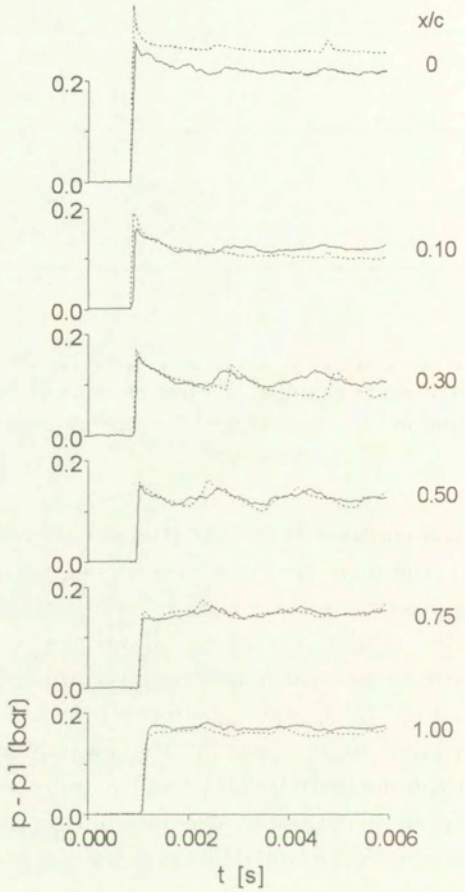

FIG. 3. Wall pressures (continous lines) measured at selected points (see Fig. 2) and the corresponding calculated airfoil surface pressures (dashed lines). Flow without a vortex.

the speed of sound and pressure, respectively: $u_1 = 276$ m/s, $a_1 = 400$ m/s and $p_1 = 22.6$ kPa. The vortex properties were as follows: relative radius of the vortex core $r_0/c = 0.045$, maximum circulation (at r_0) 50 m^2/s. Decay coefficient of velocity in the vortex $\alpha = 0.15$ (see [12]).

3. Results

The starting vortex shed from the airfoil (vortex generator) at 20 deg. angle of attack is followed by a wide vortex path. This causes that the flow at the test airfoil when it is reached by the vortex path, becomes strongly turbulent. The vortex path, however, forms with some delay after the starting vortex leaves the test airfoil and actually does not affect the AVI process. This can be seen in Fig. 4 which shows the wall pressure histories measured at two points

($x/\ c = 0.05$ and 0.5) in the upper and bottom contours of the airfoil, for identical experimental conditions. It can be observed that the random disturbances due to the vortex path are insignificant in the initial period (up to 3 ms after the shock wave passage) of the presented pressure histories. This period is nearly ten times longer than the time of the vortex passage along the airfoil. Nevertheless, the experiments were repeated a few times for each miss-distance considered to avoid random effects during the interaction. Then the average histories of the wall pressure measured at selected points in the airfoil contour were determined. They are presented below.

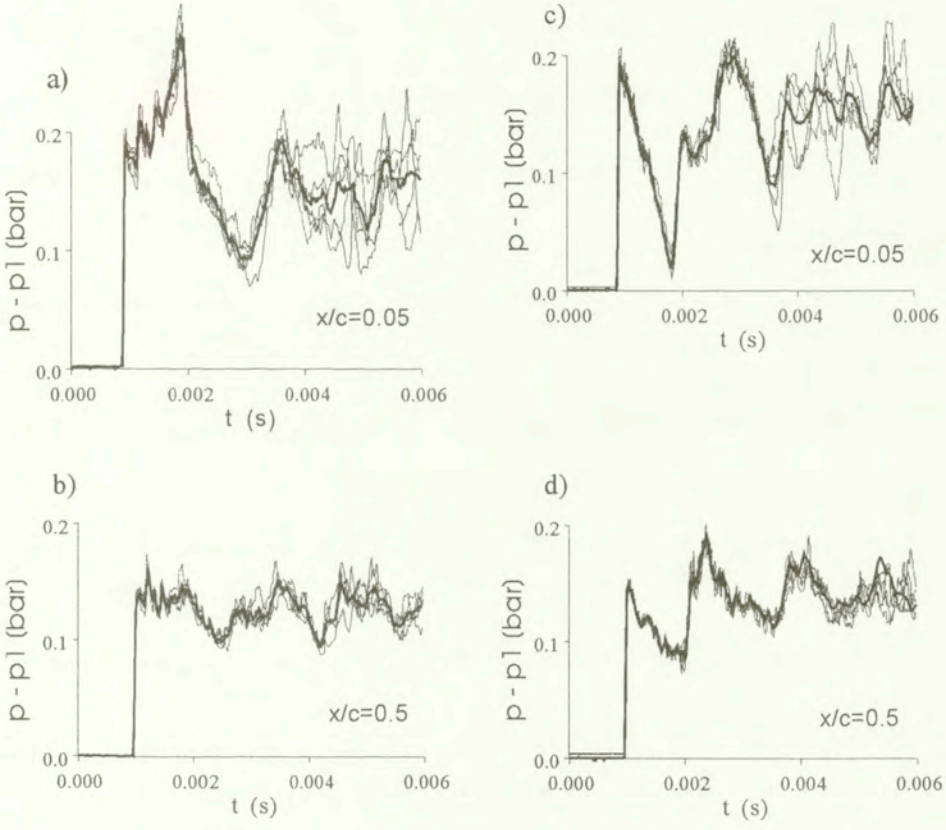

FIG. 4. Histories of wall pressure at two point in the bottom (a,c) and upper (b,d) airfoil contour (see Fig. 2) obtained for five identical experiments. Thick line – average of five histories.

In Fig. 5 the wall pressure signals for transducers symmetrically distributed along the upper and the bottom airfoil contour are presented. One can see that the pressure considerably varies during the interaction. This concerns, first of all, the leading section of the airfoil. Initially the pressure increases at the upper surface (p_u) and decreases at the bottom one (p_b). It is due to the stagnation

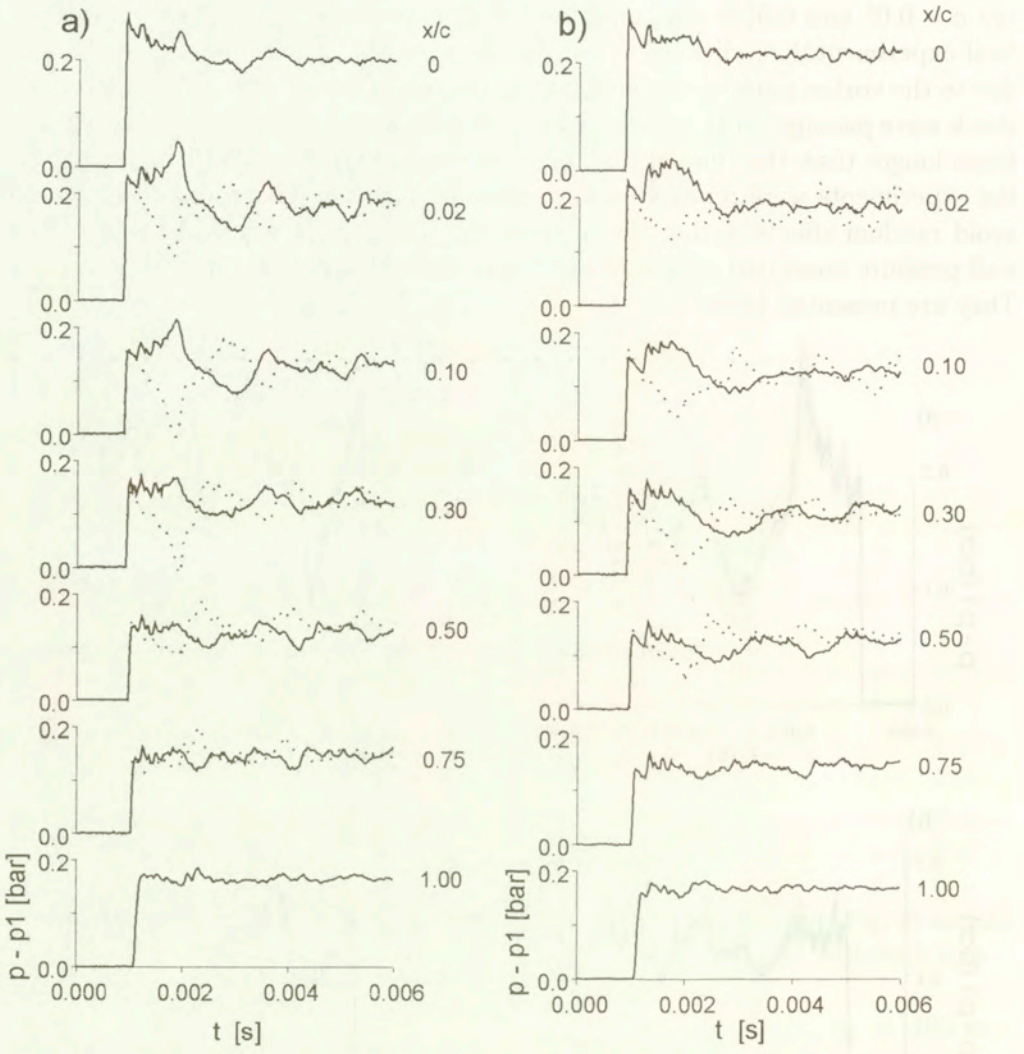

FIG. 5. Wall pressure histories for the upper (continuous lines) and bottom (dotted lines) airfoil contour.

point displacement on the upper surface when the clockwise rotating vortex approaches the airfoil. After some delay, when the stagnation point comes back to its previous position, p_u decreases and p_b increases. The pressure oscillations which are induced in this way exist for a relatively long time after the vortex leaves the airfoil. This effect was also observed by KAMIŃSKI and SZUMOWSKI [6]. The strongest pressure variations in the present experiments were noted at the point $x/c = 0.05$ at the bottom contour of the airfoil (Fig. 2). The pressure histories at that point are shown in Fig. 6 for several values of miss-distance. It is visible that the pressure decreases with nearly the same rate for all miss-distances considered

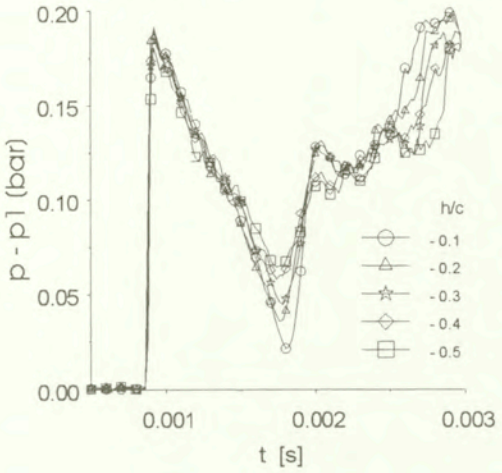

FIG. 6. Histories of wall pressure at $x/c = 0.0$ (bottom contour) for various miss--distances.

when the vortex approaches the airfoil. For small miss-distances, however, the pressure reaches a lower minimum.

Instantaneous pressure distributions along the chord for extreme values of miss-distance considered are shown in Fig. 7 (they are compared with the pressure distributions for steady flow without the vortex). One can observe an increasing pressure difference between the bottom and the upper surface during the initial phase of interaction (Fig. 7a, b and 7g, h). As a result, the lift coefficient decreases (Fig. 8) and reaches negative values. In the following phase of interaction the lift coefficient grows due to increasing bottom surface pressure and decreasing upper surface pressure (Fig. 7c and 7i). After some delay it reaches a maximum and decreases again. The measured lift coefficient histories shown in Fig. 8 are compared with the calculated ones for $x/c = -0.1$ obtained in [11]. Qualitative agreement between the corresponding curves can be noted. However, the rate of changes of c_l predicted by theory is about twice as large as the measured one.

The following explanation of this discrepancy can be proposed. The time required by the vortex to travel along the airfoil is about 0.4 ms (see data given in the second section). This time is represented in Fig. 8 by the section of abscissa which follows the minimum of the curve $c_l(t)$. During this interval (and also the preceding one) it was predicted [11] that the vortex maintains its coherent structure. Taking into account this feature one can suppose that the steep increase of c_l predicted in calculations appears to be a direct effect of the vortex travelling along the airfoil.

The calculations presented in Ref. [11] were performed for inviscid gas. However, due to the viscosity of the real air and the presence of shock waves with

complicated structure, the flow velocity induced by the vortex in the vicinity of the air surface is strongly disturbed.

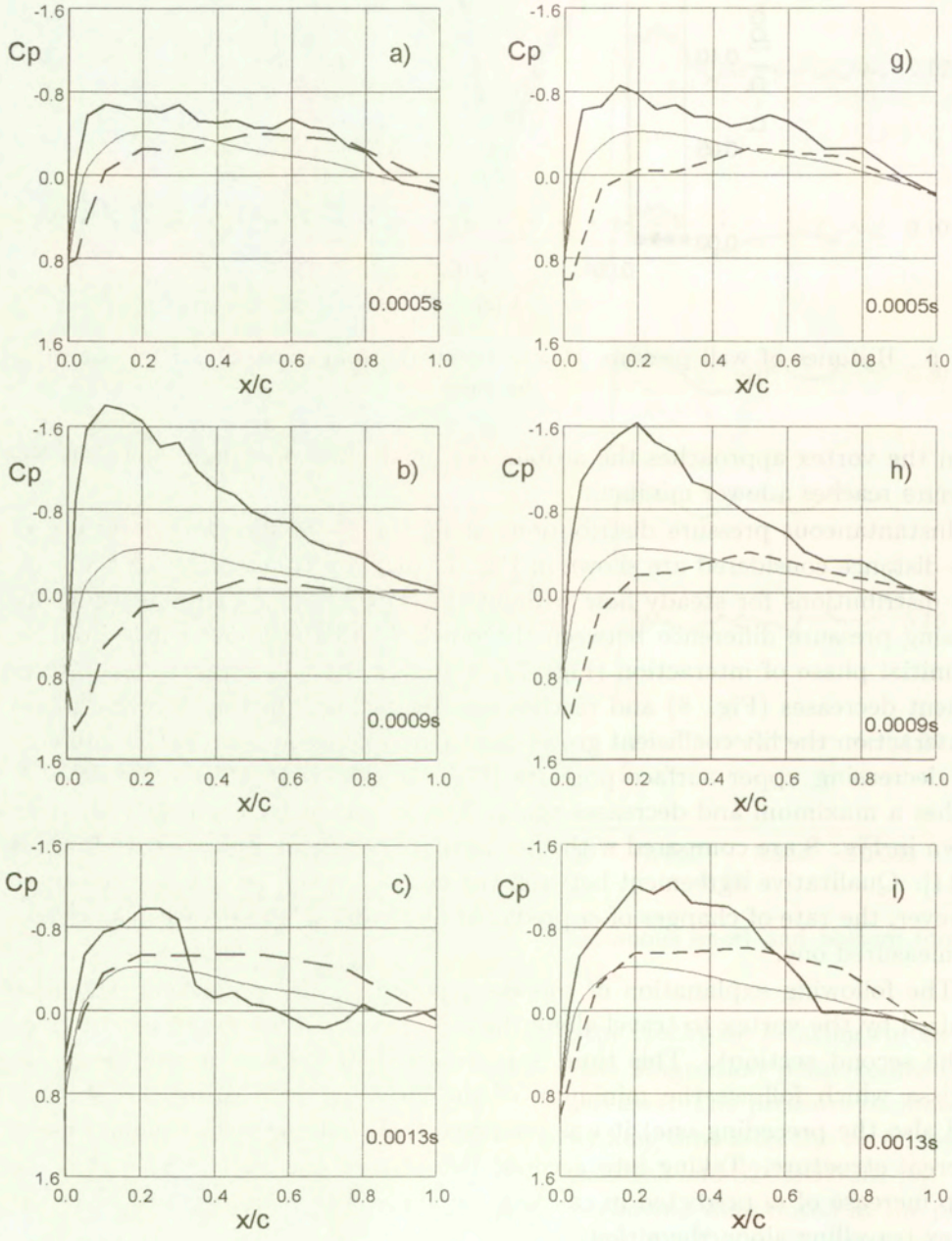

[FIG. 7.]

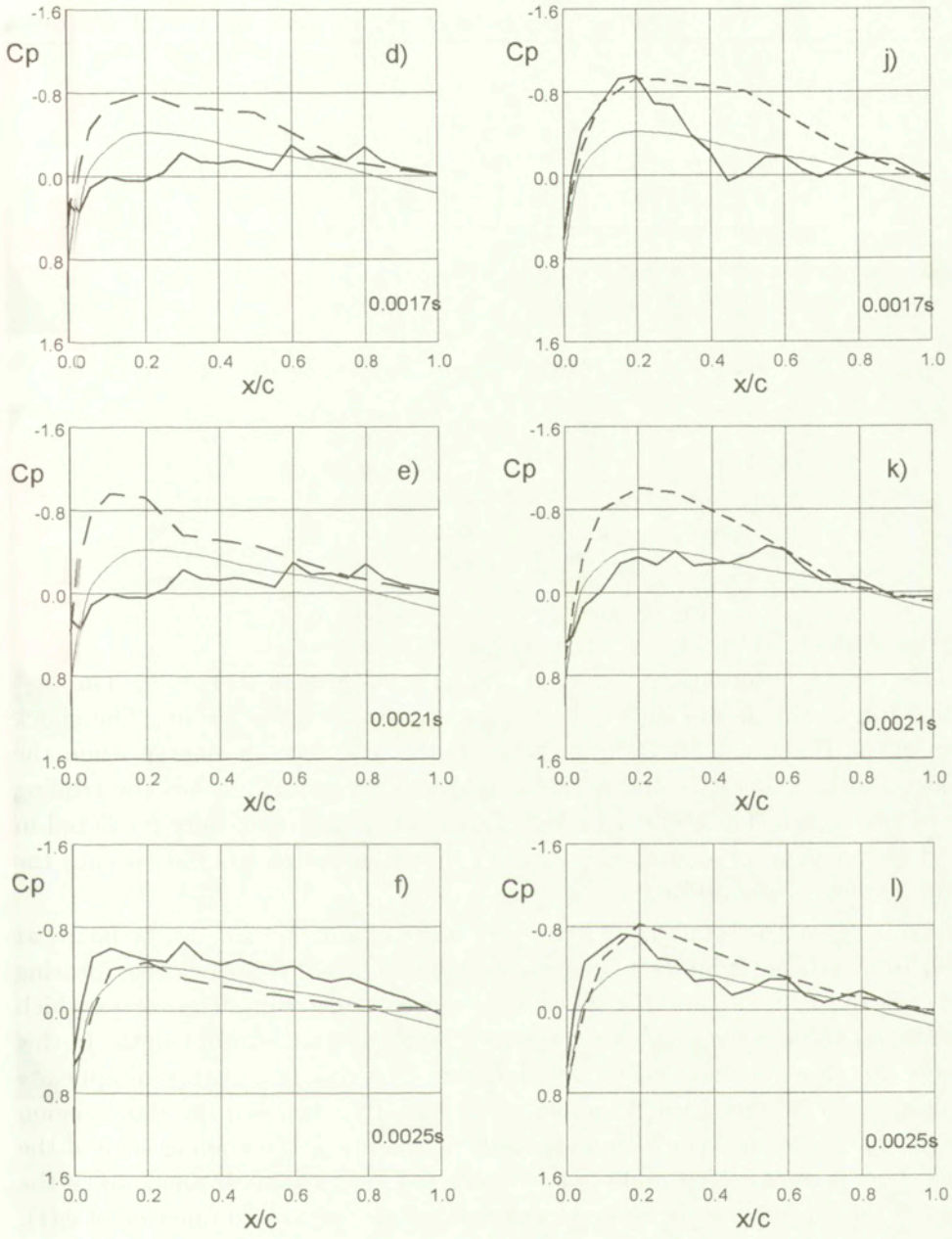

FIG. 7. Steady (thin continuous line) and instantaneous (thick continuous and dashed lines) presure distributions for $h/c = -0.1$ (first column) and $h/c = -0.5$ (second column) along upper (continuous) and bottom (dashed) airfoil contour.

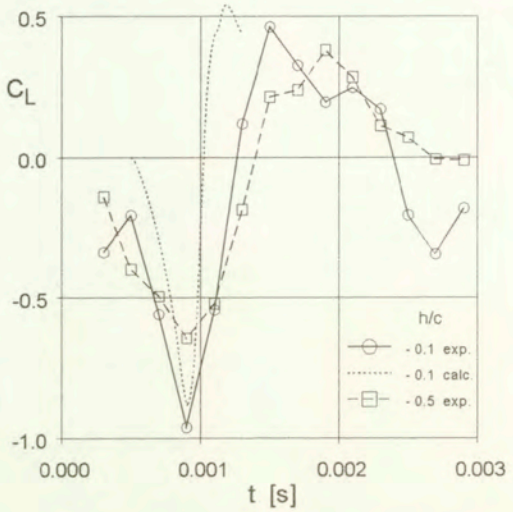

FIG. 8. Histories of a lift coefficient.

This can be noted in the schlieren photographs present in Fig. 9. The first photograph in this figure shows the vortex approaching the airfoil. The shock waves on both sides of the airfoil visible in this photograph emerge when the incident shock (generated due to the diaphragm break-up) reaches the trailing edge of the airfoil. These shocks which move slowly upstream were predicted in [11]. The following photographs (b and c) show the vortex when it reaches the leading section of the airfoil.

In this phase the "lambda" – like shock wave of a long stem can be noted at the bottom surface. It limits a supersonic region induced by a clockwise rotating vortex. Both the vortex and the shock wave move downstream. The vortex which moves faster reaches the shock wave approximately at a half-chord length. In this moment the flow pattern drastically changes. The coherent vortex disappears. Simultaneously, the separation bubble which initially existed in the shock region (along the stem of the shock wave) spreads out as far as the trailing edge of the airfoil. This process which could not be predicted for inviscid air seems to be the reason of the discrepancy between the calculated and measured function of $c_l(t)$.

4. Concluding remarks

The effect of miss-distance (in the range considered) on the airfoil flow is weaker than it was predicted in a previous numerical study [11]. This is due to the turbulent viscous stresses which are considerably influenced by the passing vortex, even for relatively large h/c. The vortex induces flow oscillations which exist for a long time after the vortex leaves the airfoil flow region.

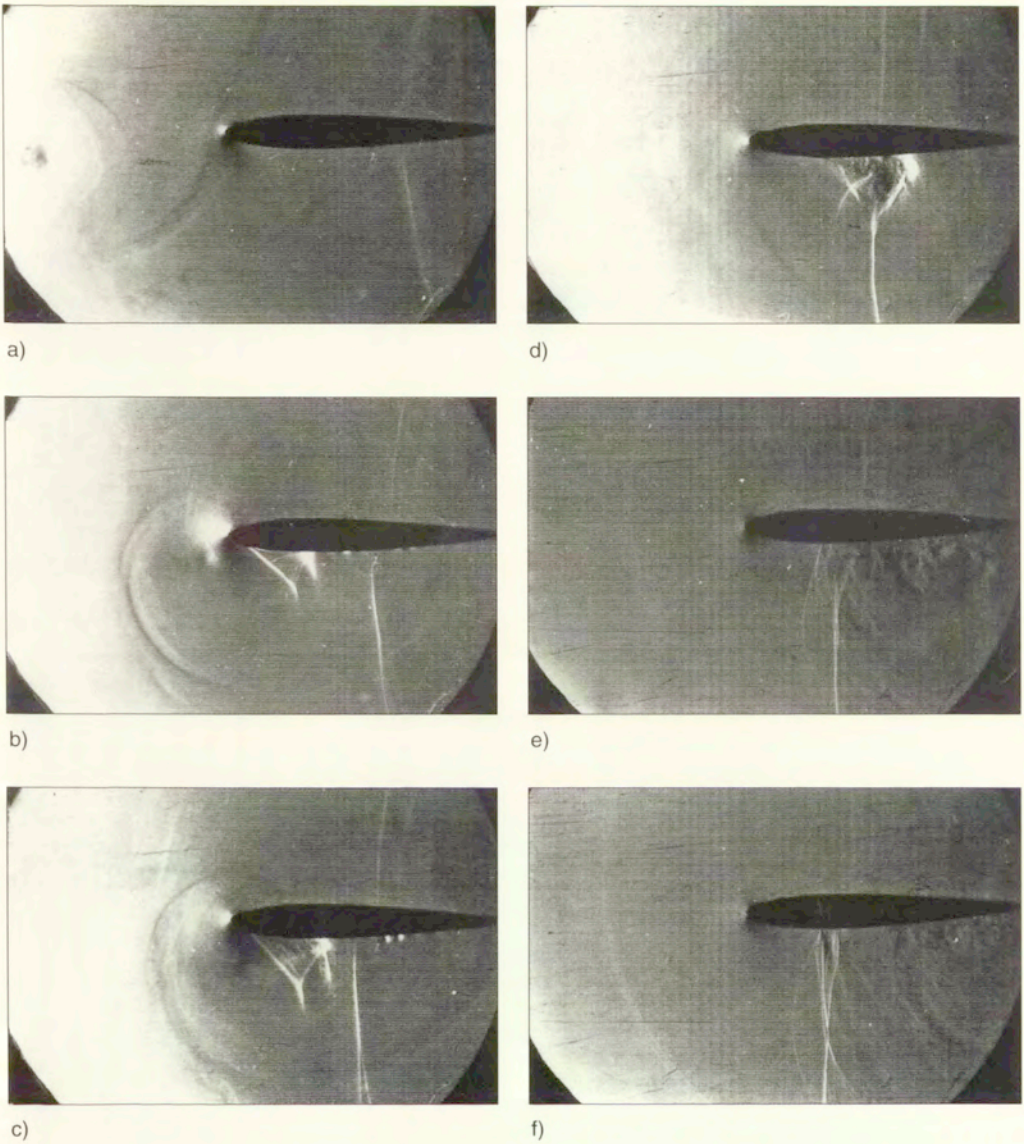

FIG. 9. Photographs of the flow during the AVI. Time interval between photographs (a) and (b) – 0.2 ms, for the following photos – 0.1 ms.

References

1. P. STRAUS, P. RENZONI and R.E. MAYLE, *Airfoil pressure measurements during a blade-vortex interaction and a comparison with theory*, AIAA J., **28**, 222–228, 1990.
2. E.R. BOOTH Jr., *Experimental observations of two-dimensional blade-vortex interaction*, AIAA J., **28**, 1353–1359, 1990.
3. D.R. POLING, M.C. WILDER and D. PEIONIS, *Fundamental research in helicopter rotor blade-vortex interaction modelling*, 17th Annual Forum of the AHS, Phoenix, Arizona, 421–433, 1991.
4. H.M. LENT, G. LOHR, G.E.-A. MEIER, K. MILLER, U. SCHIEVELBUSCH, O. SCHÜRMAN and A. SZUMOWSKI, *Noise mechanisms of transonic vortex airfoil interaction*, AIAA Paper, No. 90–3972.
5. D. BERSHADER, *Shock tube studies of vortex structure behaviour*, Proc. of the XVIth International Symposium on Shock Tubes and Waves, Aachen, Germany 1987.
6. W. KAMIŃSKI and A. SZUMOWSKI, *Acoustic effects of parallel vortex-airfoil interaction*, J. Sound and Vibration, 183, 209–220, 1995.
7. D. POLIN and L. DADONE, *Blade-vortex interaction*, AIAA J., **27**, 694–699, 1987.
8. D.J. LEE and C.A. SMITH, *Effect of vortex core distortion on blade-vortex interaction*, AIAA J., **29**, 1355–1362, 1991.
9. S. LEE and D. BESHANDER, *Head-on parallel blade-vortex interaction*, AIAA J., **32**, 16–22, 1994.
10. U. SCHIEVELBUSCH, *Stosswellenentstehung bei transonischer Wirbel-Profil- Wechselwirkung*, Max-Planck-Institut für Strömungsforschung. Göttingen Bericht 3/1990.
11. J. PIECHNA and A. SZUMOWSKI, *Effect of miss-distance on the air-vortex interaction. Numerical study*, Arch. Mech., **50**, 1, 127–138, 1998.
12. A. SZUMOWSKI, J. PIECHNA, W. SELEROWICZ and G. SOBIERAJ, *Modified formula for the velocity distribution in a vortex* [to be published in J. Fluids Engng.].

WARSAW UNIVERSITY OF TECHNOLOGY

ul. Nowowiejska 24, 00-665 Warszawa, Poland.

Received September 8, 1997; new version January 28, 1998.

Arch. Mech., 50, pp. 703–713, Warszawa 1998
FIFTY YEARS OF THE ARCHIVES OF MECHANICS

Coupling in thermo-mechanical wave propagation in NaF at low temperature

K. FRISCHMUTH (ROSTOCK) and V. A. CIMMELLI (POTENZA)

IN THE PRESENT PAPER we consider a linearly elastic heat conductor for which the semi-empirical heat transfer model [7] is assumed. Material functions are defined in accordance with measured parameters for NaF at 15 K. At that temperature, first and second sound waves have been observed in experiments. Both waves are reproduced by our coupled thermo-mechanical model.

1. Introduction

IN RECENT YEARS there has been considerable interest in hyperbolic models of heat conduction. The motivation for this comes from experimental observations of *heat pulses*, [1, 16, 22] at very low temperatures. The temperature is measured at one end of a specimen which is exposed to a (nearly) rectangular heat impulse at the other end. In those experiments an input pulse results in (at least) two impulses at the far end of the specimen, usually the first and the smaller one can be associated with a longitudinal mechanical wave, and the slower but greater one is a thermal wave called *second sound*.
We represent the state of the specimen by the following Fig. 1; all slices are assumed to have the same thickness in the initial state, gray level corresponds to the stress.

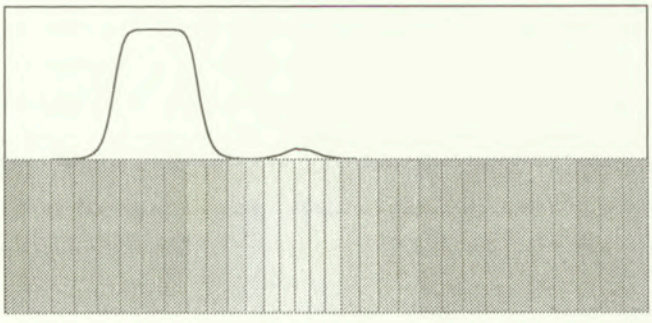

FIG. 1. Cut through deformed specimen.

Until now most models (which were developed to a level allowing numerical evaluation) concentrated on the second sound peak, disregarding the mechanical wave. There exist models for rigid heat conductors in the framework of materials

with memory [15], of rate-type materials [24], and of materials with internal state variables [18]. The quantitative differences between those models are minor, in fact for the constant coefficient case (small pulses at a constant and homogeneous background state) all they reduce to the classical Maxwell/Cattaneo/Vernotte equation

$$\tau\dot{q} + q = -\kappa\nabla\theta\,.$$

Since the second sound speed depends strongly on the background temperature, more realistic models include variable coefficients, what requires a careful thermodynamical analysis, cf. [17, 13].

Classical heat conduction theory is often criticised for the infinite wave speed it predicts [3] (Cattaneo's paradox), cf. [11] for a discussion. Here we reject the parabolic heat equation just for the simple reason that it totally failes to model the phenomenon described above. The flat curve in Fig. 2 of Sec. 4 shows the solution of the classical heat equation, which is obviously not acceptable as an approximation to the measured data, cf. [16].

The model accuracy of rigid conductor equations is obviously limited by the height of the first peak – which is absent from those models. For several experiments this lower error bound is quite large. For the internal state variable model, a pure thermal approach restricts also the possibility to obtain correct arrival times of the second sound peak, cf. [13]. Hence our present goal is to study coupled thermo-mechanical model equations.

General considerations about thermo-mechanical coupling have been published recently on the basis of the *semi-empirical heat conduction model* [5, 19]. In the present paper we present a hyperbolic system of four equations in one space variable which describes mechanical motion and heat conduction along the axis of the specimen. We will show that such a simple model can nicely reproduce the measured temperature behaviour if suitable constitutive constants are chosen. For the numerical calculations, we used values measured for NaF at 15 K, although the data come from different sources and samples of the material.

The presented model does not contain any information about the lateral motion of the specimen, hence also a peak indicated in the experimental curves as lateral mechanical wave can not be obtained. This problem has to be left to further investigation since these peaks are poorly distinguished, and the lateral mode is rather decoupled from the heat problem (at least for the isotropic case), cf. [4].

2. The coupled model

We consider here a simple 1D elastic model in the framework of classical thermo-elasticity [23] together with the basic variant of the previously studied

semi-empirical model of heat conduction. The coupling between both model components is brought about by thermal stress which acts as a source term in the mechanical subsystem, and by a heat source in the energy equation which depends on strain.

For the mechanical submodel we introduce the strain w and the velocity v as components of the state $U_{\text{mech}} = U_{\text{mech}}(x,t) = (w,v)^T$. The displacement vector is assumed to have only one non-vanishing component u – that directed along the x-axis, and this component depends only on x. We put $w = u_{,x}$ and $v = u_{,t}$. As the first balance equation we have $w_{,t} = v_{,x}$ – which is in fact, just the symmetry of the second derivatives of the displacement $u = u(x,t)$. The next balance law expresses the equation of motion, $\rho v_{,t} = \sigma_{,x}$, where σ is the stress (body forces are neglected). We adopt for the mechanical stress the linear relation $\sigma = (2\mu + \lambda)w + m\theta$, where μ and λ are Lamé constants, θ is the temperature deviation from some reference level θ_0, and m is a negative coefficient connected with thermal expansion. This gives us for the mechanical subsystem, the equations

$$w_{,t} = v_{,x}\,, \tag{2.1}$$

$$v_{,t} = c_m^2 w_{,x} + c_{mt}\theta_{,x} \tag{2.2}$$

with the mechanical wave speed $c_m = \pm\sqrt{2\mu + \lambda/\rho}$ and the coupling coefficient $c_{mt} = m/\rho$, which describes the influence of the thermal subsystem on the mechanical part.

Note that for constant temperature the above system is equivalent to the classical wave equation $u_{,tt} = c_m^2 u_{,xx}$. In the present case, however, θ has to fulfil the energy equation together with suitable constitutive equations for the heat flux.

For the thermal part of the system, the state U_{therm} is composed of just two variables, $U_{\text{therm}} = (\theta, g)^T$, where g denotes the gradient of the semi-empirical temperature β.

For the semi-empirical heat conduction theory in general, the heat flux q is given in terms of gradients of θ and β, while for β there is a kinetic equation. Taking gradients we obtain an evolution equation for $g = \nabla\beta$, cf. [17]. Throughout the present paper we restrict ourselves to the simplest case where β itself does not appear explicitly in that equation, i.e., we postulate a linear kinetic equation.

Let us further assume that θ is small enough so that we can regard heat capacity c and conductivity κ as constants (measured at θ_0). Thus we obtain for the thermal state

$$\theta_{,t} = \kappa c^{-1} g_{,x} + r, \tag{2.3}$$

$$g_{,t} = \tau^{-1}\theta_{,x} - \tau^{-1}g. \tag{2.4}$$

The first equation expresses the energy balance, the term r represents the influence of the mechanical subsystem. We found

$$r = c_{ttv}\theta_0 v_{,x}\,, \qquad c_{ttv} = m/c\,.$$

We disregard other heat sources, such as e. g. cooling through the lateral boundary – which would result in a negative source term for a 1D model.

The second equation is the extended kinetic equation in its meanwhile classical form, τ is the relaxation time; we denote $1/\tau = \gamma$ and $\kappa = K/c_0$. We observe that in the rigid conductor case ($v \equiv 0$), the above equations are equivalent to $\theta_{,tt} + \gamma\theta_{,t} = c_t^2\theta_{,xx}$, where $c_t = \pm\sqrt{\kappa/c\tau}$ is the characteristic wave speed of the thermal submodel.

The coupled system of equations becomes now

$$w_{,t} = v_{,x}\,, \tag{2.5}$$

$$v_{,t} = c_m^2 w_{,x} + c_{mt}\theta_{,x}\,, \tag{2.6}$$

$$\theta_{,t} = kg_{,x} + c_{ttv}\theta_0 v_{,x}\,, \tag{2.7}$$

$$g_{,t} = \gamma\theta_{,x} - \gamma g\,. \tag{2.8}$$

For a fully nonlinear variant – with all material parameters temperature-dependent – the energy equation should be rewritten in terms of internal energy rather than temperature. This case will be studied in a forthcoming paper.

3. Material constants and functions

Our goal is to describe a real-world situation, hence we need all relevant material constants of a material for which heat pulse experiments have been performed.

We found the best availability of measurements in the case of NaF, a cristalline solid which shows second sound effects in some interval around 16 K. In order to keep things simple we set $\theta_0 = 15$. For this temperature heat capacity, heat conductivity and second sound speed have been measured, and a temperature plot is also available [6]. So we don't use approximations but just the measured values from [16].

To complete the set of model parameters we need mass density, thermal expansion coefficient and the longitudinal wave speed. For this we use values

given in [14], concerning the speed identified from the position of the corresponding peak in the temperature plot. The following table contains all material constants we used in the numerical calculations described in the next section.

mechanical model:			
$\rho = 2.866$	$[\mathrm{g/cm^3}]$	$m = -1.1464$ E-5	$[\mathrm{g/\mu s^2/cm/K}]$
$c_m = 0.5477$	$[\mathrm{cm/\mu s}]$	$c_{mt} = -4.0$E-6	$[\mathrm{cm^2/\mu s^2/K}]$
thermal model:			
$c = 7950$	$[\mathrm{Ws/m^3/K}]$		
$\kappa = 205$	[W/cm/K]	$c_{ttv} = -144.8$	[1]
$c_t = 0.19531$	$[\mathrm{cm/\mu s}]$		
$\tau = \kappa/c_t^2/c = 0.675986$	$[\mu s]$		
$\gamma = 1/\tau = 1.47932$	$[1/\mu s]$		

4. Numerical method

In this section we study initial-boundary value problems for the above system (2.5) - (2.8). We assume that the body is initially at equilibrium: there is no motion, no temperature gradient, no heat flux. Then, at the left-hand boundary $x = 0$, we apply a trapezoidal heat impulse. The temperature is continuously but quickly increased, then it is kept constant, and then decreased,

$$\theta = at\chi_{[0,t_1]} + at_1\chi_{[t_1,2t_1+t_2]} + a(t_1 + t_2 - t)\chi_{[t_1+t_2,2t_1+t_2]}\,.$$

Here is $2t_1 + t_2$ the total duration of the pulse, t_1 is the time needed for heating or cooling, cf. [10]. By χ we denote the characteristic functions.

At the right-hand boundary $x = l$ we "measure" the temperature $\theta(l, \cdot)$, the velocity $v(l, \cdot)$ and the strain $w(l, \cdot)$ which are caused by that impulse.

For a fast numerical solution we want to apply an explicit method with constant stepsizes, cf. [21]. Such methods as Lax-Friedrich or Lax-Wendroff schemes are available and well understood for conservation laws of the form [2]

$$u_{,t} + f(u)_{,x} = 0\,.$$

In this section we denote by $u = u(x,t)$ the state $u = (U_{\mathrm{mech}}, U_{\mathrm{therm}})^T$. In our case we have a source term $b(u)$ on the right-hand side, the system is not in divergence form.

Observe that for the isothermal case $\theta \equiv \mathrm{const}$, the mechanical subsystem has the classical form, and we obtain nice numerical results with any of the mentioned methods.

Let us explain shortly the idea of the methods for this case. We replace the flux f by a consistent numerical flux $F^{(h)}$ which depends on the step-size h of the equidistant mesh in x-direction. A time-step is then carried out according to

$$U_{n+1} = U_n - \Lambda h \Delta F^{(h)},$$

where U_n is the numerical solution at time-step n, Δ denotes the forward difference, and Λ is the ratio of time to space step-size.

Classical requirements for such methods are the consistency of the numerical flux with the analytical one, i.e. $f(u) = F^{(h)}(u, \ldots, u)$ (the numerical flux depends on the state in several nodes, for Lax-Friedrich and Lax-Wendroff on two, cf. [21]), and the CFL condition (Courant, Friedrich, Levy) which imposes a bound on the ratio Λ. The latter has to be smaller than one over the largest sound speed (here c_m) [9].

The Lax-Friedrich scheme is monotone – it does not introduce artificial oscillations – but it also introduces considerable numerical diffusion; it is only of the first order accuracy. On the other hand, the second order Lax-Wendroff scheme often shows unphysical oscillations near shocks [20].

For our mechanical problem, however, both give quite good results for appropriate Λ. We obtain the best accordance with the known analytical solution just before violating the CFL condition, i.e. with $\Lambda \approx 1/c_m$ (see Figs. 2 and 3).

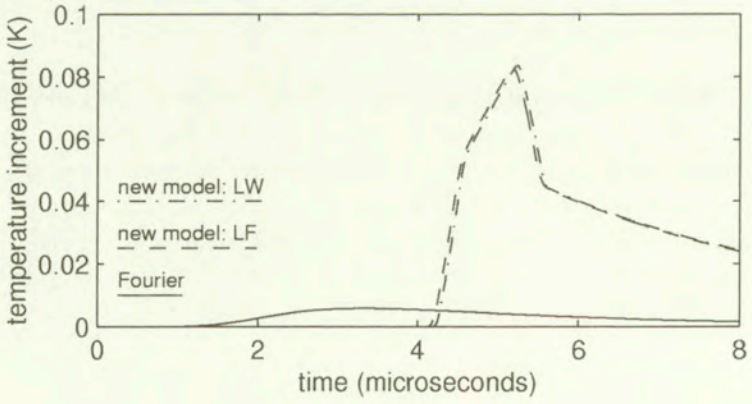

FIG. 2. Thermal submodel.

In the same manner we can consider the rigid thermal subsystem, cf. [12]. However, here we encounter already a source term which spoils the performance of the Lax-Friedrich scheme.

In order to understand that fact, we can decompose the state u in the eigenbasis of $\nabla_u f$. Then the differential part of the system is nicely diagonalized, but

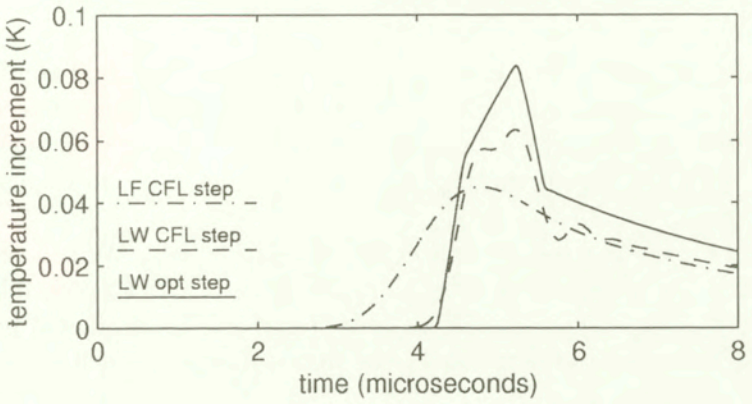

FIG. 3. Dependence on step-size and method.

there is a coupling via the right-hand side. This leads to an exponential decay of the amplitude of a pulse running into an equilibrium region. The Lax-Wendroff method (with Λ near $1/c_t$) reproduces this behaviour correctly.

For the thermo-mechanical system, the optimal step-size for the thermal subsystem is forbidden by the CFL condition (in all second-sound materials, the speed of the longitudinal elastic wave is larger than the speed of the thermal pulses).

However, the Lax-Wendroff results with a wrong Λ are still quite acceptable (Fig. 4). A method which removes the error caused by numerical diffusion is under preparation. The idea is to integrate both subsystems in their own meshes and just to exchange the coupling terms (waveform relaxation).

Let us discuss now some results for sodium fluoride (NaF) at 15 K.

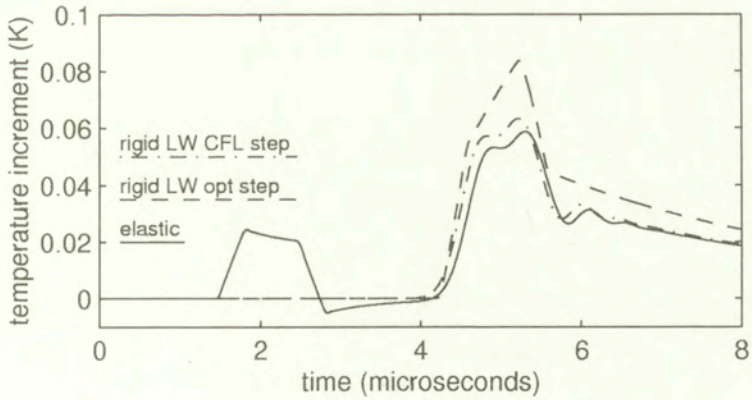

FIG. 4. Temperature at far end.

5. Results and conclusions

We omit the mechanical subsystem, and start with the rigid conductor. We compare a classical heat conductor (Fourier law) with our present second sound model. We give the temperatures at the right end of the specimen versus time as calculated by Lax-Friedrich and Lax-Wendroff schemes, with optimal step-size in Fig. 2.

Figure 2 shows so-called *arrival prints* of temperature. We can see that the classical heat conduction theory (flat curve) is obviously not applicable, and the Lax-Friedrich scheme is not distinguishable from Lax-Wendroff. On both curves we can still recognize the 4 jumps of the first derivative which come from the applied trapezoidal impulse.

A comparison between the optimal Lax-Wendroff solution and those obtained with the step-size imposed by the CFL condition for the full system shows the failure of the Lax-Friedrich method (Fig. 3).

We use 600 time steps and 110 space steps if the mechanical wave is relevant, 316 space steps otherwise. The Lax-Friedrich solution adds too much numerical viscosity, it looks like a solution to the classical parabolic equation.

Now we come to the full system. We do not apply any non-vanishing mechanical initial or boundary conditions, just a thermal pulse as in the rigid case. As a result we obtain a compression wave, combined with an increase of temperature, which travels approximately 3 times faster than the second sound pulse.

In the wake of the first pulse we see a tiny drop of the temperature level below the temperature of the environment – an observation confirmed by the experimental plots, cf. [16]. We present here the arrival situation for temperature (Fig. 4), velocity (Fig. 5) and strain (Fig. 6).

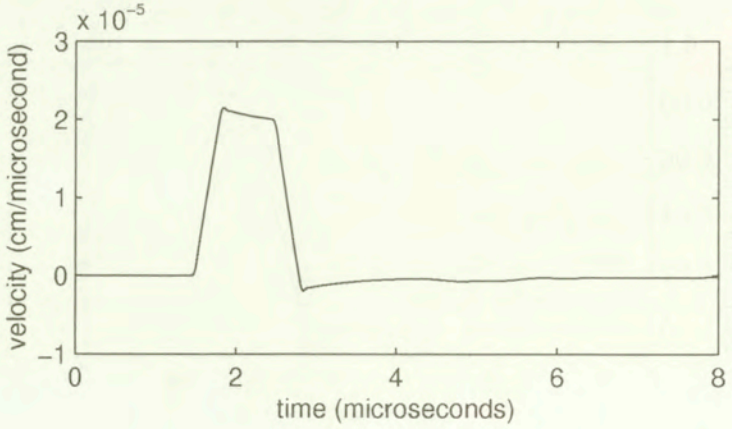

FIG. 5. Velocity at far end.

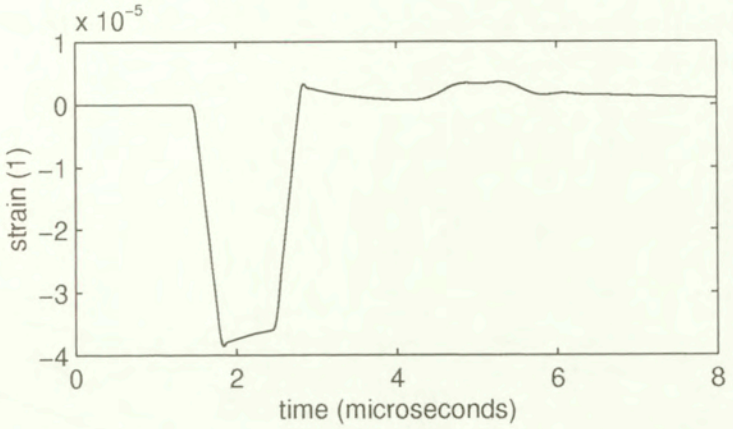

FIG. 6. Strain at far end.

We superimpose onto the plot of the temperature (Fig. 4) in the coupled model, the plots for θ as it results for the rigid conductor equations, once calculated with optimal step-sizes, and for comparison that calculated at the same mesh as in the coupled case. It is very clear that after 4 microseconds, the influence of the mechanical wave has nearly vanished. We suppose that the true solution after that time is similar to the rigid conductor solution – which is consistent with our expectation on the basis of the large difference between both wave speeds.

Finally, we visualize the result by a density plot and a 3D temperature distribution as a function of space and time, Figs. 7 and 8. The two pulses are

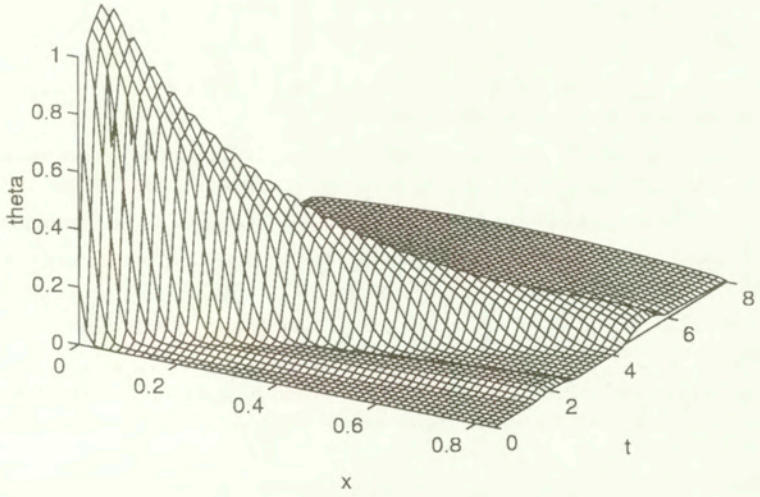

FIG. 7. 3D-plot of temperature.

clearly visible, the slopes of the isolines in the density plot are the reciprocals of the characteristic speeds c_m and c_t.

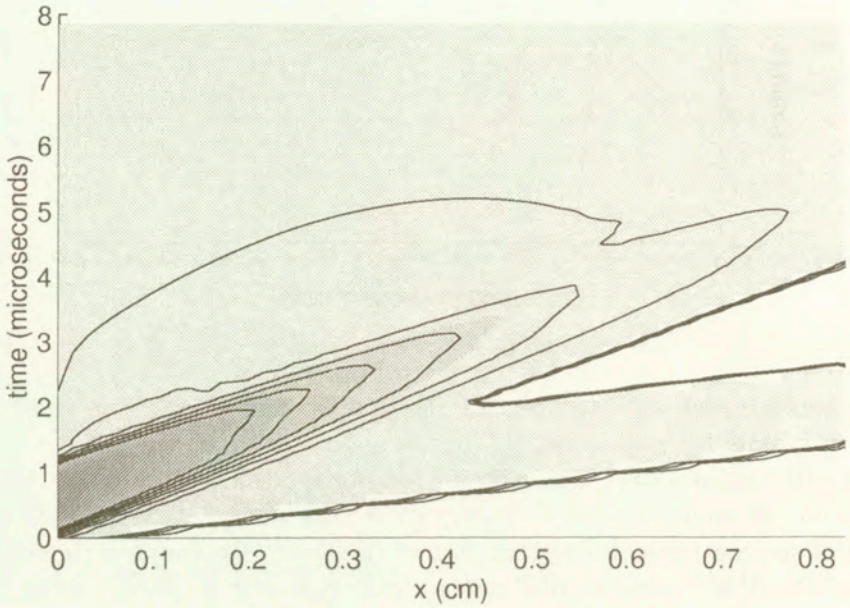

FIG. 8. Density plot: two characteristic speeds.

We hope to get an even better accordance between our numerical results and the real measurements by improving the model as well as the solver. Next steps will be the variable coefficients and more realistic boundary conditions, as well as a (negative) source term.

References

1. C. C. ACKERMAN, B. BERTAM, H. A. FAIRBANKS and R. A. GUYER, *Second sound in solid Helium*, Phys. Rev. Letters, **16**, 789, 1966.
2. R. ANSORGE, *A lecture on entropy conditions and their numerical analogues for conservation laws*, Hamburger Beiträge zur Angewandten Mathematik, B14, April 1991.
3. C. CATTANEO, *Sulla conduzione del calore*, Atti Sem. Mat. Fis. Univ. Modena, **3**, 83, 1948.
4. G. CAVIGLIA, A. MORRO, and B. STRAUGHAN, *Thermoelasticity at cryogenic temperatures*, Int. J. Non-Linear Mechanics, **27**, 2, 251–263, 1992.
5. V. A. CIMMELLI, *Thermodynamics of anisotropic solids near absolute zero*, Math. Comput. Modelling 1998 (in press).
6. V. A. CIMMELLI and K. FRISCHMUTH, *Determination of material functions through second sound measurements in a hyperbolic heat conduction theory*, Math. Comput. Modelling, **24**, 12, 19, 1996.
7. V. A. CIMMELLI and W. KOSIŃSKI, *Nonequilibrium semi-empirical temperature in materials with thermal relaxation*, Arch. Mech., **43**, 6, 753–767, 1991.

8. B. D. COLEMAN and M. E. GURTIN, *Thermodynamics with internal state variables*, J. Chem. Phys., **47**, 597–613, 1967.

9. R. COURANT, K. O. FRIEDRICHS, and H. LEWY, *Über die partiellen Differenzengleichungen der mathematischen Physik*, Math. Ann., **100**, 32–74, 1928.

10. W. DREYER and H. STRUCHTRUP, *Heat pulse experiments revisited*, Continuum Mech. Thermodyn., **5**, 3, 1993.

11. G. FICHERA, *Is the Fourier theory of heat propagation paradoxical?* Rendiconti del Circolo Matematico di Palermo, Serie II, Tomo XLI, 5–28, 1992.

12. K. FRISCHMUTH and V. A. CIMMELLI, *Numerical reconstruction of heat pulse experiments*, Int. J. Engng. Sc., **33**, 2, 209, 1995.

13. K. FRISCHMUTH and V. A. CIMMELLI, *Identification of constitutive functions and verification of model assumptions in semi-empirical heat conduction theory*, Quaderni del Dipartimento di Matematica, Potenza, Report No. 4, 1994.

14. *Gmelin handbook of inorganic and organometallic chemistry*, Springer, Berlin 1993.

15. M. E. GURTIN and A. C. PIPKIN, *A general theory of heat conduction with finite wave speeds*, Arch. Rat. Mech. Anal., **31**, 113–126, 1968.

16. R. J. HARDY and S. S. JASWAL, *Velocity of second sound in NaF*, Phys. Rev. B, **3**, 4385, 1971.

17. W. KOSIŃSKI, *Thermodynamics of continua with heat waves*, in Proc. ASME Joint Applied Mechanics and Materials Summer Meeting, UCLA 1995, AMD, **18**, 19, 1995.

18. W. KOSIŃSKI and P. PERZYNA, *Analysis of acceleration waves in materials with internal parameters*, Arch. Mech., **24**, 4, 629, 1972.

19. W. KOSIŃSKI and W. WOJNO, *Gradient generalization to internal state approach*, Arch. Mech., **47**, 3, 523, 1995.

20. P. D. LAX and B. WENDROFF, *Systems of conservation laws*, Comm. Pure Appl. Math., **13**, 217–237, 1960.

21. R. J. LEVEQUE, *Numerical methods for conservation laws*, Birkhäuser, 1992.

22. V. NARAYANAMURTI and R. C. DYNES, *Observation of second sound in bismuth*, Phys. Rev. Lett., **28**, 1401, 1972.

23. W. NOWACKI, *Thermoelasticity* [in Polish], Ossolineum, Wrocław, Warszawa, Kraków, Gdańsk 1972.

24. B. D. COLEMAN, M. FABRIZIO and D. R. OWEN, *On the thermodynamics of second sound in dielectric crystals*, Arch. Rat. Mech. Anal., **80**, 135, 1982.

DEPARTMENT OF MATHEMATICS
UNIVERSITY OF ROSTOCK
18051 Rostock, Germany
e-mail: kurt@sun2.math.uni-rostock.de
and
DEPARTMENT OF MATHEMATICS
UNIVERSITY OF BASILICATA
85100 Potenza, Italy
e-mail: Cimmelli@unibas.it

Received January 30, 1998.

Arch. Mech., 50, 4, pp. 715–730, Warszawa 1998
FIFTY YEARS OF THE ARCHIVES OF MECHANICS

Magnetohydrodynamic stability of streaming liquid cylinder with doubly perturbed interfaces having a streaming fluid mantle jet

AHMED E. RADWAN (CAIRO)

THE MAGNETOHYDRODYNAMIC (MHD) stability of streaming liquid cylinder with doubly perturbed interfaces coaxial with a streaming fluid mantle jet has been developed. A general dispersion relation is derived, discussed and some reported works are described. The analytical results are confirmed numerically and interpreted physically. The streaming is purely destabilizing while the capillary force is such as for small axisymmetric perturbations only. The magnetic field has a strong stabilizing influence and it gives a measure of rigidity in the fluids. The radii (liquid-fluid) ratio plays an essential role in increasing the MHD stabilizing domains. The densities (liquid-fluid) ratio have a very small stabilizing effect. If the magnetic field strength is so strong that the Alfvèn wave velocity is much greater than the streaming speed, the capillary and streaming destabilizing character is completely suppressed and stability sets in. The present results are in good agreement with the experimental results of Kendall (1986) since we neglect here both the magnetic field influence and the inertia force of the interior fluid jet.

1. Introduction

THE CAPILLARY instability of a full liquid jet in a vacuum has received a considerable attention since a long time ago for its important applications in several domains of science. See PLATEAU [1], RAYLEIGH [2] and CHANDRASEKHAR [3]. The last author [3], Nobel prize winner (1986), summarized the previous reported works and made several extensions for studying the stability of different models. The effect of non-linearities on the capillary instability of a liquid jet has been examined by YUEN [4], WANG [5], NAYFEH [6], NAYFEH and HASSAN [7], and the complete analysis has been carried out by KAKUTANI *et al.* [8].

In the present era (especially in the last decade), the scientific province has turned out for investigating more applicable models than the naive one of a full liquid jet in vacuum. KENDALL [9] made very interesting experiments with modern equipment for different amplitudes and various wavelengths in studying the capillary instability of a fluid jet surrounding a gas cylinder (of negligible inertia), i.e. the annular gas jet. The inertia force of the fluid is considered to be greater than that of the gas mantle jet. KENDALL [9] explained clearly the importance and possible applications of the annular jet in astronomy. Moreover, he [9] did attract our attention to the analytical investigation of stability of such

a model. Indeed, the principle and basic physics of the new type of liquid-in-air jet are due to HERTZ and HERMANRUD [10]. The stability of a liquid column with a thin shell endowed with surface tension was studied by PETRYANOV and SHUTOV [11] and SHUTOV [12]. The hydrodynamic and MHD stability of a gas jet (of negligible inertia) immersed in an infinite fluid, i.e. hollow jet, has been elaborated by RADWAN [13]. CHENG [14] has investigated the capillary instability of a streaming gas jet embedded in an infinite liquid, taking into account the inertia forces of both the gas and the liquid media. However, one has to mention here that the results given by CHENG [9], in Eqs. (4) and (5) there, are incorrect in the third term. In fact, the quantity $(1-s^2-k^2a^2)$ must be in the numerator, as it is clear from Eq. (3) derived there. See also Eqs. (3.1) – (3.13) in the present work and Chandrasekhar's results [3], pages 538 – 540 (Eqs. (147) and (155)).

The object of the present work is to study the MHD stability of streaming liquid cylinder with doubly perturbed interfaces having a streaming fluid mantle jet. This instability has been regarded to be important for the origin of the breaking-up of the fluid layers resulting in the appearance of condensation within astronomical objects. Also such a phenomenon of coaxial differently perturbed fluids may be of interest during geological drillings in the crust of the earth, in the case in which we have a fluid column surrounded by a dense gas jet. The present results reduce to those of Refs. [9, 13, 14] under appropriate simplifications.

2. Formulation and eigenvalue relation

We shall consider a fluid cylinder of radius R^i concentric and coaxial with an exterior liquid cylinder of radius R^e with $R^e > R^i$. The fluid and liquid media are assumed to be inviscid, incompressible and perfectly conducting, and the coaxial cylinders are surrounded by vacuum. The model is acting upon the combined effect of inertia, pressure gradient, capillary and electromagnetic forces. The capillary force along the fluid-liquid interface is assumed to be greater than that along the liquid-vacuum interface, and so we shall neglect the latter temporarily in our study here. Both the fluid and liquid are assumed to be streaming with velocity

$$\mathbf{u}_0 = (0,\ 0,\ U_0)\ . \tag{2.1}$$

The interior fluid and exterior liquid are subjected to the magnetic fields

$$\mathbf{H}_0^i = (0,\ 0,\ \alpha,\ H_0), \qquad \alpha \geq 1,$$

$$\mathbf{H}_0^e = (0,\ 0,\ \beta\, H_0), \qquad \beta \geq 1\ , \tag{2.2}$$

while the vacuum surrounding the coaxial cylinders is assumed to be penetrated by

$$\mathbf{H}_0^{\text{vac}} = (0,\ 0,\ H_0)\ . \tag{2.2}'$$

The components of $\mathbf{u}_0$, $\mathbf{H}_0^i$, and $\mathbf{H}_0^{\text{vac}}$ are written in cylindrical polar coordinates (r, ϕ, z) with the z-axis coinciding with the axis of the coaxial cylinders.

The fundamental MHD equations are derived by combining the ordinary hydrodynamic equations and electrodynamic Maxwell's equations. For the problem at hand, the basic equations in the fluid and liquid media could be written in the form

$$\rho^{i,e}\frac{d\mathbf{u}^{i,e}}{dt} = -\nabla p^{i,e} + \mu^{i,e}(\nabla \wedge \mathbf{H}^{i,e}) \wedge \mathbf{H}^{i,e}\ , \tag{2.3}$$

$$\nabla \cdot \mathbf{u}^{i,e} = 0, \tag{2.4}$$

$$\nabla \cdot \mathbf{H}^{i,e} = 0\ , \tag{2.5}$$

$$\frac{\partial \mathbf{H}^{i,e}}{\partial t} = \nabla \wedge (\mathbf{u} \wedge \mathbf{H})^{i,e}\ , \tag{2.6}$$

and along the fluid-liquid interface

$$p_s = T(\nabla \cdot \hat{\mathbf{n}}_s)\ , \tag{2.7}$$

where the superscipts i and e are pertaining the interior fluid and exterior liquid. Here ρ^i, $\mathbf{u}^i$ and p^i are the fluid mass density, velocity vector and kinetic pressure, μ^i is the magnetic field permeability coefficient, $\mathbf{H}^i$ is the magnetic field intensity; and similarly for the liquid variables with superscript e. p_s is the surface pressure due to the capillary force, T is the surface tension coefficient, and $\hat{\mathbf{n}}_s$ (parallel to the coordinate r) is a unit outward normal vector to the fluid-liquid interface.

In the vacuum (medium of negligible inertia) surrounding the coaxial cylinders, the basic equations are

$$\nabla \wedge \mathbf{H}^{\text{vac}} = 0 \tag{2.8}$$

$$\nabla \cdot \mathbf{H}^{\text{vac}} = 0\ . \tag{2.9}$$

The initial unperturbed state is studied. The balance of the (surface, magnetic and kinetic) pressure across the fluid-liquid interface at $r = R^i$, yields

$$p_0^i = p_0^e + (T/R^i) + (H_0^2/2)(\mu^i\alpha - \mu^e\beta)\ . \tag{2.10}$$

Here the unperturbed quantities are those with index 0, and later on the perturbed quantities will be with index 1. It is found more appropriate to take $\alpha = \beta$ from now on, so the jump of $\mathbf{H}_0$ will be zero at the fluid-liquid interface.

Linearization of Eqs. (2.3) – (2.9) is accomplished by substituting the expansion

$$Q^{i,e} = Q_0^{i,e} + \varepsilon(t) Q_1^{i,e} , \tag{2.11}$$

and retaining only the first order terms, in the small fluctuating variable Q_1. The variable Q stands for $\mathbf{u}$, p, $\mathbf{H}$, $\mathbf{n}_s$ and for the perturbed radii of the fluid and liquid cylinders. $\varepsilon(t)$ is the amplitude of perturbation, given by

$$\varepsilon(t) = \varepsilon_0 \exp(\sigma t) , \tag{2.12}$$

where $\varepsilon_0 (= \varepsilon \text{ at } t = 0)$ is the initial amplitude and σ is the growth rate. If $\sigma = i\omega$, $i = (-1)^{1/2}$ is imaginary then $\omega/2\pi$ is the wave oscillation frequency. By considering a simple sinusoidal disturbance waves in z and ϕ, the radii of the fluid and liquid cylinders due to perturbation are

$$r^i = R^i + \varepsilon(t)\eta^i , \tag{2.13}$$

$$r^e = R^e + \varepsilon(t)\eta^e . \tag{2.14}$$

Here

$$\eta^i = R^i \exp\left(i(kz + m\phi)\right), \tag{2.15}$$

$$\eta^e = R^e \exp\left(i(kz + m\phi)\right) \tag{2.16}$$

are the elevations of the perturbed surfaces wave measured from the initial position, where m (an integer) is the azimuthal wavenumber and k (a real number) is the longitudinal wavenumber. In view of the expansion (2.11), the linearized perturbation equations of the fluid media are given by:

$$\rho^j \left(\frac{\partial}{\partial t} + U_0 \frac{\partial}{\partial z}\right) \mathbf{u}_1^j = -\nabla p_1^j + \mu^j (\nabla \wedge \mathbf{H}_1^j) \wedge \mathbf{H}_0^j, \tag{2.17}$$

$$\nabla \cdot \mathbf{u}_1^j = 0, \tag{2.18}$$

$$\nabla \cdot \mathbf{H}_1^j = 0, \tag{2.19}$$

$$\frac{\partial \mathbf{H}_1^j}{\partial t} = \nabla \wedge (\mathbf{u}_1^j \wedge \mathbf{H}_0^j) + \nabla \wedge (\mathbf{u}_0^j \wedge \mathbf{H}_1^j), \tag{2.20}$$

with $j = i, e$.

Along the fluid-liquid interface, at $r = R^i$,

$$p_{1s} = \frac{T}{(R^i)^2} \left(\eta^i + \frac{\partial^2 \eta^i}{\partial \phi^2} + R^{i^2} \frac{\partial^2 \eta^i}{\partial z^2}\right) \tag{2.21}$$

and in the region surrounding the coaxial cylinders

$$\nabla \wedge \mathbf{H}_1^{\text{vac}} = 0, \tag{2.22}$$

$$\nabla \cdot \mathbf{H}_1^{\text{vac}} = 0. \tag{2.23}$$

By taking the divergence of Eq. (2.17), we get

$$\left(\mathbf{H}_0^j \cdot \nabla\right)\left(\nabla \cdot \mathbf{H}_1^j\right) - \rho^j \left(\frac{\partial}{\partial t} + U_0 \frac{\partial}{\partial z}\right)\left(\nabla \cdot \mathbf{u}_1^j\right) = \nabla^2 \Pi_1^j \,, \tag{2.24}$$

where Π_1 is the total MHD pressure which is the sum of magnetic and fluid kinetic pressures given by

$$\Pi_1 = (\mu/2)(\mathbf{H} \cdot \mathbf{H}) + p_1. \tag{2.25}$$

Equation (2.24), upon using Eqs. (2.18) and (2.19), yields

$$\nabla^2 \Pi_1^j = 0 \,. \tag{2.26}$$

Equation (2.22) means that the perturbed magnetic field $\mathbf{H}^{\text{vac}}$ in the vacuum region could be derived from a scalar magnetic potential Ψ_1

$$\mathbf{H}_1^{\text{vac}} = \nabla \Psi_1 \,. \tag{2.27}$$

By combining Eqs. (2.23) and (2.27) we get

$$\nabla^2 \Psi_1 = 0 \,. \tag{2.28}$$

Following the surfaces deformation (2.13) – (2.16), as usual for the stability problems of cylindrical models whether with a single perturbed interface or not, and basing on the linear perturbation technique, we assume that any perturbed quantity can be expressed as $\varepsilon(t)\exp i(kz + m\phi)$ times an amplitude function of r. Henceforth, the non-singular solutions of the relevant perturbation equations (2.17) – (2.23) are given by

$$\Pi_1^i = A\varepsilon(t) I_m(kr) \exp\left(i(kz + m\phi)\right) \,, \tag{2.29}$$

$$\mathbf{u}_1^i = \frac{-(\sigma + ikU_0)}{((\sigma + ikU_0)^2 + (\Omega_A^i)^2)} \nabla \Pi_1^i \,, \tag{2.30}$$

$$\mathbf{H}_1^i = \frac{ikH_0}{(\sigma + ikU_0)} \mathbf{u}_1^i \,, \tag{2.31}$$

$$p_{1s} = -\varepsilon(t)(T/R^i)(1 - m^2 - k^2 R^{i^2}) \exp\left(i(kz + m\phi)\right) \,, \tag{2.32}$$

$$\Pi_1^e = \varepsilon(t)\{B I_m(kr) + C K_m(kr)\} \exp\left(i(kz + m\phi)\right) \,, \tag{2.33}$$

$$\mathbf{u}_1^e = \frac{-(\sigma + ikU_0)}{((\sigma + ikU_0)^2 + (\Omega_A^e)^2)} \nabla \Pi_1^e \,, \tag{2.34}$$

$$\mathbf{H}_1^e = \frac{ikH_0}{(\sigma + ikU_0)} \mathbf{u}_1^e \,, \tag{2.35}$$

$$\mathbf{H}_1^{\text{vac}} = E\varepsilon(t) \nabla \left\{K_m(kr) \exp\left(i(kz + m\phi)\right)\right\} \,. \tag{2.36}$$

Here A, B, C and E are constants of integration to be determined while I_m and K_m are, respectively, the modified first and second kind Bessel functions of order m, Ω_A^i and Ω_A^e are the Alfvèn wave frequencies of the fluid and liquid cylinders:

$$\Omega_A^i = \left((\mu^i/\rho^i)H_0^2k^2\right)^{1/2} , \tag{2.37}$$

$$\Omega_A^e = \left((\mu^e/\rho^e)H_0^2k^2\right)^{1/2} . \tag{2.38}$$

The solution of the perturbation Eqs. (2.17) – (2.32) given by (2.29) – (2.38) must satisfy apropriate conditions valid at the perturbed interfaces of the fluid-liquid and liquid-vacuum interfaces. Under the present circumstances and for the problem under considerations, these boundary conditions are the folowing.

I. The normal component of the velocity vector of the fluid jet must be compatible with the velocity of the fluid-liquid interface (2.13) at $r = R^i$.

II. The normal component of the velocity $\mathbf{n}\cdot\mathbf{u}^e$ of the (outer) liquid jet must be compatible with the velocity of the free liquid interface (2.14) and simultaneously must comply with the normal component of the velocity $\mathbf{n}\cdot\mathbf{u}^i$ of the fluid at $r = R^e$.

III. The normal component of the magnetic fields $\mathbf{n}\cdot\mathbf{H}^e$ and $\mathbf{n}\cdot\mathbf{H}^i$ must be balanced across the perturbed interface of the fluid-liquid regions described by (2.13), at $r = R^i$.

IV. The normal component of the magnetic fields $\mathbf{n}\cdot\mathbf{H}^{\text{vac}}$ and $\mathbf{n}\cdot\mathbf{H}^e$ must be continuous across the perturbed free surface of the liquid jet (2.14) at $r = R^e$.

By applying the foregoing boundary conditions across the perturbed interfaces (2.13) at $r = R^i$ and (2.14) at $r = R^e$, we get

$$A = -\varepsilon_0 R^{i^2}\left((\sigma + ikU_0)^2 + \Omega_A^{i^2}\right)(xI'_m(x))^{-1} , \tag{2.39}$$

$$B = (Y/M_m)(R^{i^2}yK'_m(y) - R^{e^2}xK'_m(x)) , \tag{2.40}$$

$$C = (Y/M_m)(R^{e^2}xI'_m(x) - R^{i^2}yI'_m(y)) , \tag{2.41}$$

$$E = -ikH_0\left(M_mK'_m(y)\right)^{-1}\left(BI'_m(y) + CK'_m(y)\right) , \tag{2.42}$$

$$Y = \left((\sigma + ikU_0)^2 + \Omega_A^{e^2}\right) , \tag{2.43}$$

$$M_m = xy\left(I'_m(y)K'_m(x) - I'_m(x)K'_m(y)\right) , \tag{2.44}$$

where $x\ (= kR^i)$ and $y(= kR^e)$ are the dimensionless longitudinal wavenumbers.

Finally, we have to apply the compatibility boundary condition which states that the normal component of the stresses (due to the liquid and fluid pressure gradients and the electromagnetic forces acting on the model) must be discontinuous, its jump being equal to the capillary force stresses at $r = R^i$. This condition, at $r = R^i$, is

$$p_{1s} = \rho^i \left(p_1^i + (\mu^i/2)(\mathbf{H}\cdot\mathbf{H})_1^i\right) - \rho^e \left(p_1^e + (\mu^e/2)(\mathbf{H}\cdot\mathbf{H})_1^e\right) + \varepsilon(t)\eta^i\rho^i \frac{\partial}{\partial r}\left(p_0^i + (\mu^i/2)(\mathbf{H}_0\cdot\mathbf{H}_0)^i\right) - \varepsilon(t)\eta^i\rho^e \frac{\partial}{\partial r}\left(p_0^e + (\mu^e/2)(\mathbf{H}_0\cdot\mathbf{H}_0)^e\right). \tag{2.45}$$

Substituting from (2.29) – (2.44) into (2.45) we obtain the following relation:

$$(\sigma + ikU_0)^2 = \frac{T}{\rho^i (R^i)^3} N_m M_m I'_m(x)(1 - m^2 - x^2) - \frac{\mu^i H_0^2}{\rho^i (R^i)^2}\left(y I_m(x) N_m M_m\right) - \frac{\mu^e H_0^2}{\rho^e (R^i)^2}\left(\rho x^2 I'_m(x)(R^2 - y L_y^m) N_m\right) \tag{2.46}$$

with

$$\begin{aligned} R &= R^e/R^i \quad , \qquad \rho = \rho^e/\rho^i, \\ L_y^m &= \left(I'_m(y)K_m(x) - I_m(x)K'_m(y)\right), \\ x(N_m)^{-1} &= \{I_m(x)M_m + \rho x(R - yL_y^m)I'_m(x)\}. \end{aligned} \tag{2.47}$$

3. Discussions of the results

Equation (2.46) is the eigenvalue relation of MHD doubly perturbed liquid cylindrical stream having a fluid mantle jet, accounting for the inertia forces of both the liquid and the fluid regions. By means of this relation, the characteristics of the present model can be determined: one can identify the domains of instability (in particular their critical wavenumbers, maximum growth rate values and the corresponding wavenumbers) and those of stability as well.

The eigenvalue relation (2.46) relates the growth rate σ (or rather the oscillation frequency ω) with the value of $\left(\varepsilon T/\rho^i R^{i^2}\right)$, $\left(\mu^i H_0^2/\rho^i R^{i^2}\right)$ as well as $\left(\mu^e H_0^2/\rho^e R^{e^2}\right)$ as a unit of time, the radii ratio R, the densities ratio ρ and the densities ρ^e and ρ^i, the radii of the cylinders R^i and R^e, the surface tension coefficient T, the modified Bessel functions and their combinations N_m, M_m and L_y^m, and with the magnetic field H_0. The marginal or neutral stability could be obtained from (2.46) at $\sigma = 0$, the unstable states are those when σ is real while the stability states are those when σ is imaginary. The eigenvalue relation (2.46) is in reality a simple linear combination of the eigenvalue relations of concentric-coaxial doubly perturbed liquid-fluid cylinders endowed with surface tension only and those with electromagnetic forces only.

Since this problem is somewhat more general, one can obtain other dispersion relations as limiting cases from the present relation (2.46) under suitable assumptions.

If we assume $U_0 = 0$, $H_0 = 0$, $\rho^e = 0$ and $y \to \infty$, Eq. (2.46) gives

$$\sigma^2 = \frac{T}{\rho^i (R^i)^3} (x I'_m(x)/I_m(x))(1 - m^2 - x^2) \,. \tag{3.1}$$

The relation (3.1) was established by CHANDRASEKHAR [3], see also reference [2] as $m = 0$.

If we set $U_0 = 0$, $\rho^e = 0$ and, at the same time, $y \to \infty$, Eq. (2.46) reduces to

$$\sigma^2 = \frac{T}{\rho^i (R^i)^3} \frac{x I'_m(x)}{I_m(x)} \left(1 - m^2 - x^2\right) + \frac{\mu^i H_0^2}{\rho^i (R^i)^2} \frac{x}{I_m(x) K'_m(x)} \,. \tag{3.2}$$

Equation (3.2) is the MHD eigenvalue of a full liquid jet in vacuum acted on by the electromagnetic Lorentz force and endowed with surface tension. It was CHANDRASEKHAR [3] who derived the simple case of Eq. (3.2) at $m = 0$ of axisymmetric perturbation (Eq. (165), page 545) by means of the energy principle.

If we assume that $\rho^i = 0$, $H_0 = 0$ and $y \to \infty$, the relation (2.46) degenerates to

$$(\sigma + ikU_0)^2 = -\frac{T}{\rho^e (R^i)^3} \frac{x K'_m(x)}{K_m(x)} \left(1 - m^2 - x^2\right) \,. \tag{3.3}$$

This is the eigenvalue relation of a hollow jet (i.e a gas jet of negligible inertia immersed in a streaming liquid which extends radially to infinity), endowed with surface tension. Equation (3.3) coincides with our dispersion relation of the recent result in references [13] as $U_0 = 0$ here and neglecting the viscosity effect there. One has to mention here that for $U_0 = 0$ the relation (2.46) leads to that given by DRAZIN and REID [15]. Also Eq. (2.46) with $m = 0$ and $U_0 = 0$ reduced to that reported by CHANDRASEKHAR [3] (page 540).

If we assume $H_0 = 0$ and $y \to \infty$, Eq. (2.46) reduces to

$$(\sigma + ikU_0)^2 = \frac{T}{\rho^i (R^i)^3} \frac{x(1 - m^2 - x^2) I'_m(x) K_m(x)}{(I_m(x) K'_m(X) - \rho I'_m(x) K_m(x)} \,. \tag{3.4}$$

This relation might be identical with the relation obtained by CHENG [14] in investigating the instability of a streaming gas jet through an infinite liquid region, under the influence of the capillary force and pressure gradient forces, in addition to the inertia forces of both the gas and the liquid.

Other limiting cases may be obtained from the relation (2.46) with other simplifying assumptions:

1) $H_0 \neq 0$, $T = 0$, $U_0 \neq 0$,
2) $H_0 \neq 0$, $T = 0$, $y \to \infty$, $U_0 \neq 0$, and
3) $H_0 = 0$, $T \neq 0$, $U_0 \neq 0$.

In order to clarify the hydrodynamic, magnetodynamic and MHD (in-)stability states of the present problem, we have to remember the behaviour of the modified Bessel functions and their products for different arguments.

Consider now the recurrence relations (see ABRAMOWITZ and STEGUN [16])

$$2I'_m(x) = I_{m-1}(x) + I_{m+1}(x) \tag{3.5}$$

$$2K'_m(x) = -K_{m-1}(x) - K_{m+1}(x) \, . \tag{3.6}$$

It is known that $I_m(x)$ is always positive and monotonically increasing function, and that $K_m(x)$ is monotonically decreasing but never negative for each non-zero real value of x; hence one can observe that $I'_m(x)$ is positive while $K'_m(x)$ is always negative. On the basis of these arguments, we may prove that for $x \neq 0$ and $y \neq 0$

$$I_m(y) > I_m(x) \, , \tag{3.7}$$

$$K_m(y) < K_m(x) \, , \tag{3.8}$$

and that the function

$$L_y^m > 0 \tag{3.9}$$

is positive definite and never changes sing. We may also prove that

$$(I'_m(x)K'_m(x)) < (I'_m(y)K'_m(x)) \tag{3.10}$$

and consequently, for all $x \neq 0$ and $y \neq 0$ we have

$$M_m = xy \left\{ -I'_m(x) \left| K'_m(x) \right| + I'_m(x) \left| K'_m(y) \right| \right\} > 0 \, . \tag{3.11}$$

In a similar manner, on utilizing the inequalities (3.7) – (3.10), we can show that

$$N_m > 0 \tag{3.12}$$

is positive definite and never changing sign for all values of $R > 1$, $\rho \neq 0$, $x \neq 0$, $y \neq 0$ and $m \geq 0$.

3.1. Hydrodynamic stability

In this case we neglect the influence of the electromagnetic forces in each of the fluid, liquid and vacuum regions. The eigenvalue relation of the present case is obtained from the general relation (2.46) as $H_0 = 0$, by

$$(\sigma + ikU_0)^2 = \frac{T}{\rho^i (R^i)^3} \left(1 - m^2 - x^2\right) I'_m(x) M_m N_m \, . \tag{3.13}$$

With the aid of the relations (3.5) and (3.6) together with the inequalities (3.7) – (3.12), the relation (3.13) is investigated and we deduce the following.

The stationary coaxial-concentric cylinders of doubly perturbed interfaces are capillary stable in the non-axisymmetric modes of perturbation $m \geq 1$ for all short and long wavelengths $\lambda (= 2\pi/x, \, x \neq 0)$. In the axisymmetric (sausage)

mode $m = 0$ of the perturbation, the model is capillary unstable in the domain $0 < x < 1$ while it is stable in the neighbouring domains $1 \leq x < \infty$ where the equality corresponds to the marginal stability state. This means that present non-streaming model is unstable only in the axisymmetric mode $m = 0$ if the perturbed wavelength λ_i is longer than the circumference of the fluid cylinder $2\pi R^i$, while it is stable in all the remaining states. The streaming has a destabilizing influence and this influence is independent of the kind of the perturbation ($m = 0$ or/and $m \neq 0$) and the perturbed wavelengths. Therefore, the streaming has the property of increasing the capillary unstable domain ($m = 0$, $0 < x < 1$) and, at the same time, it decreases the stable domains ($m = 0, 1 \leq x < \infty$) and ($m \geq 0$, $0 < x < \infty$). Thus, the streaming liquid cylinder with doubly perturbed interfaces having a fluid cylinder mantle is capillary unstable in axisymmetric mode $m = 0$ and non-axisymmetric modes $m \neq 0$ for all short and long wavelengths.

3.2. Magnetodynamic stability

If the effect of the electromagnetic forces acting in the fluid, liquid and vacuum regions is predominant over that of the capillary forces acting along the fluid-liquid and liquid-vacuum interfaces, the general relation (2.46) degenerates to

$$(\sigma + ikU_0)^2 = \left(\mu^e H_0^2\right) / \left(\rho^e R^{i2}\right) \left\{\rho x^2 I'_m(x) N_m \left(y L_y^m - R^2\right)\right\} - \left(\mu^i H_0^2\right) / \left(\rho^i R^{i2}\right) \left\{y I_m(x) M_m N_m\right\}, \tag{3.14}$$

where ρ, R, N_m and M_m are defined by (2.47) and (2.44).

The influence of the magnetic field in the fluid region is represented by the term associated with the natural quantity $\mu^i H_0^2 / (\rho^i (R^i)^2)$. By the use of the inequalities (3.7) – (3.12), we can show that the magnetic field acting in the interior of the fluid cylinder is stabilizing. That stabilizing effect is valid for all short and long wavelengths, not only in the $m = 0$ mode but also in $m \neq 0$ modes. The influence of the magnetic field acting in the liquid cylinder of doubly perturbed interfaces is represented by the terms associated with the quantity $\mu^e H_o^2 / (\rho^e (R^i)^2)$. In view of the inequalities (3.7) – (3.12) it is clear that $\rho x^2 I'_m(x) N_m$ is positive definite for all non-zero values of ρ, x, y and $m \leq 0$. Therefore the magnetic field in the liquid region is stabilizing in all modes $m \geq 0$ of perturbation if the condition

$$R^2 / y > L_y^m \tag{3.15}$$

is satisfied. On the other hand, if that condition is not satisfied then the electromagnetic force acting in the liquid region is purely destabilizing and moreover, it has no influence at all if $R = y L_y^m$. Therefore, the non-streaming coaxial cylinders are magnetodynamically stable in the $m = 0$ or/and $m \neq 0$ modes according to restrictions (cf. (3.15)).

The streaming has a destabilizing influence. That influence is independent of the kind of perturbation (axisymmetric or non-axisymmetric) and short or long wavelengths. Consequently, the streaming has the property of decreasing the magnetodynamic stable domains and at the same time, it increases those of instability.

We conclude that the streaming coaxial fluid-liquid cylinders are magnetodynamically unstable not only in the axisymmetric mode $m = 0$ but also in the non-axisymmetric modes $m \neq 0$ of perturbation.

3.3. Magnetohydrodynamic stability

In this general case the present model of a liquid cylinder with doubly perturbed interfaces having a fluid jet mantle is acted upon by combined effects of the pressure gradient inertial, capillary and electromagnetic forces. The dispersion relation of this case is given by the relation (2.46) in its general form. With the aid of the discussions and results of the two different cases given above in Subsecs. 3.1 and 3.2, the present general case could be discussed.

As we have seen, streaming has a purely destabilizing influence while the capillary forces have a destabilizing influence only in the axisymmetric mode $m = 0$. The electromagnetic forces have a strong stabilizing influence for all modes $m \geq 0$ of perturbation. The latter plays an important role in stabilizing the present model. When the intensity of the magnetic field is so strong that the Alfvèn wave velocity is greater than the fluid streaming velocity, the capillary instability is suppressed and stability sets in. See the numerical example later on.

The stabilizing influence of the electromagnetic force could be interpreted physically as follows.

Indeed, the stabilizing effects of the magnetic fields in the liquid and fluid regions are due to the presence of the magnetodynamic force $\mu(\nabla \wedge \mathbf{H}) \wedge \mathbf{H}$ in the MHD equations of motion (2.3) and (2.17). This force may be interpreted as following from the action on the fluid of the Maxwell stresses: tension $\mu(\mathbf{H} \cdot \mathbf{H})/2$ per unit area along the magnetic lines of force and an equal pressure acting in all directions in the conducting fluid. Note that the latter is not perpendicular to the magnetic lines of force and acting in all directions since the diffusion terms are neglected in the evolution equation of the magnetic field (2.6). Due to these stresses, the lines of force are able to endow the liquid with a sort of rigidity.

Another important physical explanation may be given here for the stabilizing effects of both magnetic fields in the fluid, liquid and vacuum regions as follows. The magnetic field exerts a strong influence not only on the axisymmetric mode that causes only the bending of the magnetic lines of force, but also on non-axisymmetric modes that leads also to twisting of the lines of force. This is physically plausible since the magnetic fields are conserved (cf. (2.5)) and, in addition, they are uniform, see Eqs. (2.2) and (2.2)′.

In order to clarify the electromagnetic force effect and its influence on the capillary force, it is found more convenient to write down the eigenvalue relation (2.46) in the dimensionless form

$$\frac{(\sigma + ikU_0)^2}{T/\rho^i (R^i)^3} = \left\{ \left(1 - m^2 - x^2\right) M_m - \left(H_0/H_s^i\right)^2 \left(M_m \frac{yI_m(x)}{I'_m(x)} \right) - (H_0/H_s^e)^2 \left(\rho x^2 \left(R^2 - yL_y^m \right) \right) \right\} I'_m(x) N_m, \tag{3.16}$$

where

$$H_s^i = \left(T/\mu^i \rho^i\right)^{1/2}, \tag{3.17}$$

$$H_s^e = (T/\rho^e \mu^e)^{1/2}. \tag{3.18}$$

The relation (3.16) has been analyzed by the computer for the most dangerous mode $m = 0$ and assuming that μ^e is infinitesimally small and tends to zero. The calculations have been carried out for different values of (H_0/H_s), (ρ^i/ρ^e) and (R^e/R^i). For every group of values of the last magnitude, several values of $U(= -ikU_0/(T/\rho^i(R^i)^3)^{1/2})$ are given. The numerical data are classified into two types. The results of the instability states are tabulated and presented for the values of $\sigma/(T/\rho^i(R^i)^3)^{1/2}$ against x while those associated with stability states are illustrated for the values of $\omega/(T/\rho^i(R^i)^3)^{1/2}$ against x. These states are analyzed in various categories as follows.

CATEGORY (i). For $(H_0/H_s,\ \rho^e/\rho^i) = (0.3,\ 0.3)$

As $(R^e/R^i) = 1.3$, corresponding to $U = 0,\ 0.2,\ 0.5,\ 0.7$ and 1.0, it is found that the unstable domains are $0 < x < 0.718$, $0 < x < 0.844$, $0 < x < 1.0911$, $0 < x < 1.2447$ and $0 < x < 1.453$, while those of stability neighbouring the unstable domains are $x \geq 0.718$, $x \geq 0.844$, $x \geq 1.0911$, $x \geq 1.2447$ and $x \geq 1.453$, see Fig. 1.

As $(R^e/R^i) = 1.7$, corresponding to $U = 0,\ 0.2,\ 0.5,\ 0.7$ and 1.0, it is found that the unstable domains are $0 < x < 0.8165$, $0 < x < 0.9101$, $0 < x < 1.1061$, $0 < x < 1.2426$ and $0 < x < 1.4356$ while those of stability are such that $x \geq 0.8165$, $x \geq 0.9101$, $x \geq 1.1061$, $x \geq 1.243$ and $x \geq 1.436$. See Fig 2.

As $(R^e/R^i) = 3.0$, corresponding to $U = 0,\ 0.2,\ 0.5, 07$ and 1.0, it is found that the unstable domains are $0 < x < 0.8768$, $0 < x < 0.936$, $0 < x < 1.111$, $0 < x < 1.242$ and $0 < x < 1.431$ while those of stability are such that $x \geq 0.877$, $x \geq 0.936$, $x \geq 1.1111$, $x \geq 1.242$ and $x \geq 1.431$.

CATEGORY (ii). For $(H_0/H_s, \rho^e/\rho^i) = (0.5,\ 0.3)$

As $(R^e/R^i) = 1.3$, corresponding to $U = 0.2,\ 0.5,\ 0.7$ and 1.0, it is found that the unstable domains are $0 < x < 0.489$, $0 < x < 0.863$, $0 < x < 1.047$ and $0 < x < 1.2823$ while those of stability are $x \geq 0.489$, $x \geq 0.862$, $x \geq 1.047$ and $x \geq 1.282$. Note that there is no unstable domain as $U = 0$. See Fig. 2.

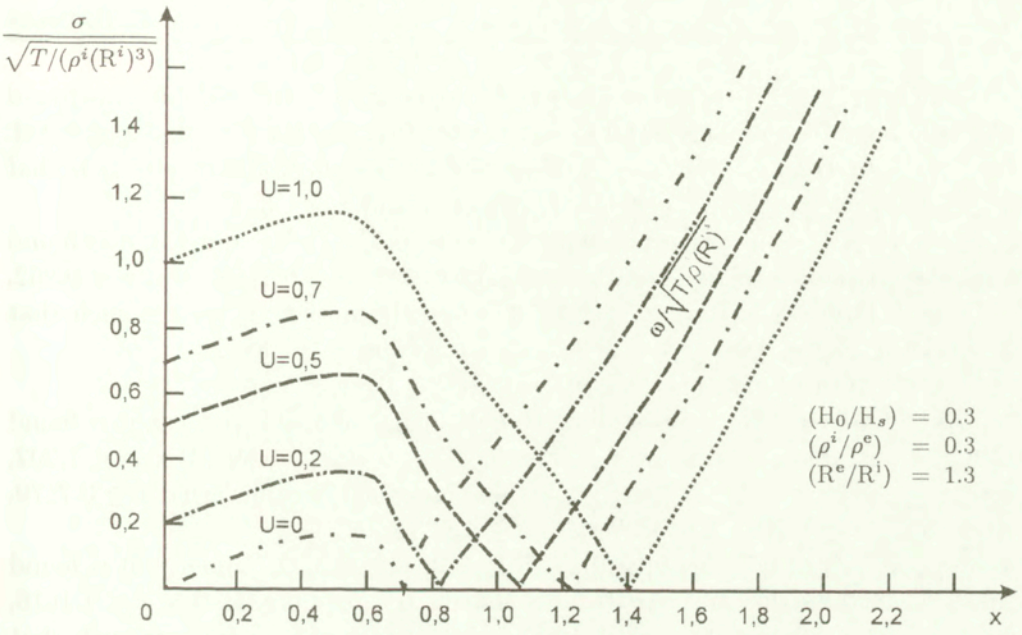

FIG. 1.

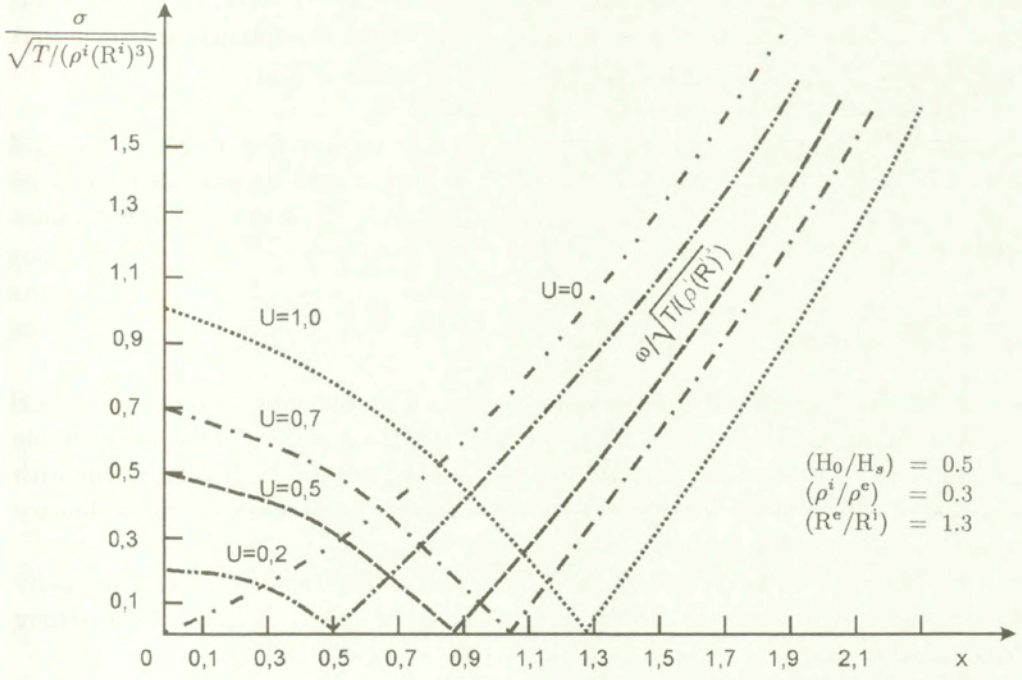

FIG. 2.

As $(R^e/R^i) = 1.7$, corresponding to $U = 0,\ 0.2,\ 0.5,\ 0.7$ and 1.0, it is found that the unstable domains are $0 < x < 0.469,\ 0 < x < 0.6477,\ 0 < x < 0.934,\ 0 < x < 1.0812$ and $0 < x < 1.3045$, while those of stability are such that $x \geq 0.469,\ x \geq 0.6477,\ x \geq 0.934,\ x \geq 1.0812$ and $x \geq 1.3045$.

As $(R^e/R^i) = 3.0$, corresponding to $U = 0,\ 0.2,\ 0.5,\ 0.7$ and 1.0, it is found that the unstable domains are $0 < x < 0.5976,\ 0 < x < 0.7198,\ 0 < x < 0.962,\ 0 < x < 1.1093$ and $0 < x < 1.3112$, while those of stability are such that $x \geq 0.5976,\ x \geq 0.7198,\ x \geq 0.962,\ x \geq 1.1093$ and $x \geq 1.3112$.

CATEGORY (iii). For $(H_0/H_s, \rho^e/\rho^i) = (0.3, 1.0)$

As $(R^e/R^i) = 1.3$, corresponding to $U = 0,\ 0.2,\ 0.5,\ 0.7$ and 1.0, it is found that the unstable domains are $0 < x < 0.7179,\ 0 < x < 0.892,\ 0 < x < 1.202,\ 0 < x < 1.384$ and $0 < x < 1.628$ while those of stability are such that $x \geq 0.7179,\ x \geq 0.892,\ x \geq 1.202,\ x \geq 1.384$ and $x \geq 1.628$.

As $(R^e/R^i) = 1.7$, corresponding to $U = 0,\ 0.2,\ 0.5,\ 0.7$ and 1.0, it is found that the unstable domains are $0 < x < 0.8165,\ 0 < x < 0.927,\ 0 < x < 1.1616,\ 0 < x < 1.3176$ and $0 < x < 1.537$, while those of stability are such that $x \geq 0.8165,\ x \geq 0.927,\ x \geq 1.162,\ x \geq 1.3176$ and $x \geq 1.537$.

As $(R^e/R^i) = 3.0$, corresponding to $U = 0,\ 0.2,\ 0.5,\ 0.7$ and 1.0, it is found that the unstable domains are $0 < x < 0.8769,\ 0 < x < 0.9417,\ 0 < x < 1.1472,\ 0 < x < 1.2959$ and $0 < x < 1.5113$, while those of stability are such that $x \geq 0.8769,\ x \geq 0.9417, \geq 1.1472,\ x \geq 1.2959$ and $x \geq 1.5113$.

CATEGORY (iv). For $(H_0/H_s, \rho^e/\rho^i) = (0.5, 1.0)$

Similar discussions may be presented for the cases with $(R^e/R^i) = 1.3,\ 1.7$ and 3.0 for $U = 0,\ 0.2,\ 0.5,\ 0.7$ and 1.0. See Fig. 3, and similarly for the cases $(H_0/H_s, \rho^e/\rho^i) = (1.0, 1.0), (3.0,\ 3.0), (5,\ 3)$ and $(1,\ 3)$, and for different values of (R^e/R^i) and U.

4. Conclusions

From the foregoing discussions we conclude the following results.

For the same values of H_0/H_s, ρ^e/ρ^i and R^e/R^i, it is found that the unstable domains are increasing and simultaneously those of instability are decreasing with increasing values of U. This means that streaming has a destabilizing influence and this confirms the analytical discussions.

For the same values of (ρ^e/ρ^i), (R^e/R^i) and U, the stable domains are rapidly increasing with increasing H_0/H_s values, i.e. the magnetic fields have strong stabilizing effects.

For the same values of H_0/H_s, U and ρ^e/ρ^i, the stable domains are monotonically increasing with increasing R^e/R^i. This means that the liquid-fluid radii ratio plays an important role in stabilizing the annular fluid jet with doubly perturbed interfaces.

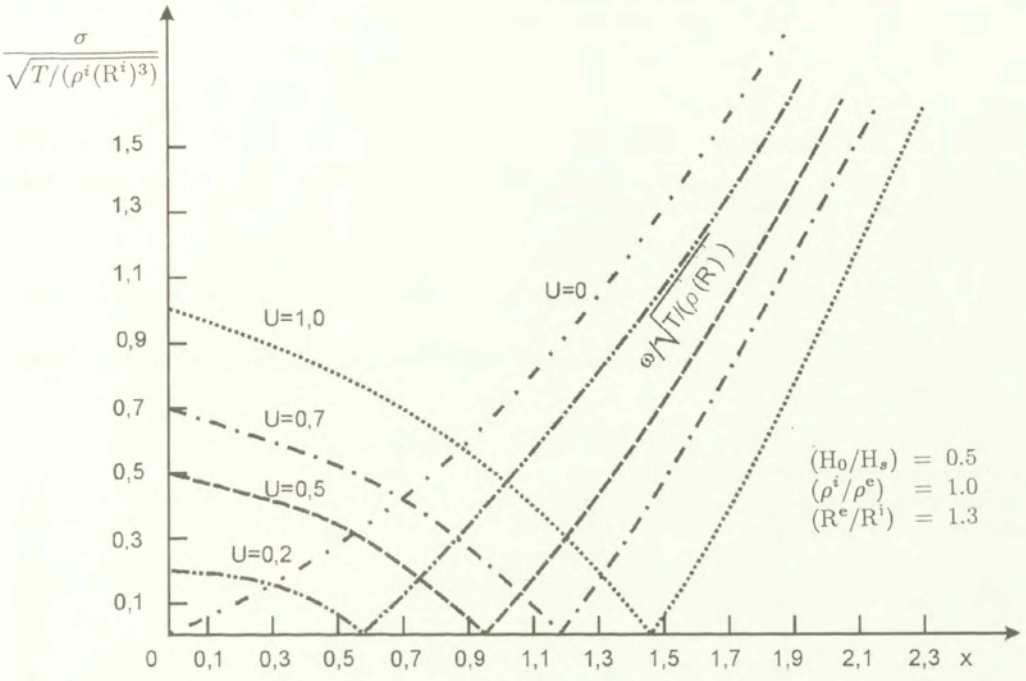

FIG. 3.

For the same values of (H_0/H_s), R^e/R^i and $U(\geq 0)$, the unstable domains are rapidly decreasing with increasing ρ^e/ρ^i values. This means that the liquid-fluid densities ratio is stabilizing.

As $\rho^i = 0, R \to \infty$ and $H_0 = 0$, it is found that the present results are in good agreement with the experimental results of Kendall (1986) that the temporal amplification in the hollow jet is much higher than that appearing in a full liquid jet embedded in a vacuum.

References

1. J. PLATEAU, *Statique experimental et theorique des liquides soumis aux seules forces moleculaires*, Vols. 1 and 2.Gauthier-Villars, Paris.
2. J.W. RAYLEIGH, *The theory of sound*, Dover Publ., New York 1945.
3. S. CHANDRASEKHAR, *Hydrodynamic and magnetohydrodynamic stability*, Dover Publ., New York 1981.
4. M. YUEN, J. Fluid Mech., **33**, 151, 1968.
5. D. WANG, J. Fluid Mech., **34**, 299, 1968.
6. A. NAYFEH, Phys. Fluids, **13**, 841, 1970.
7. A. NAYFEH and S. HASSAN, J. Fluid Mech., **48**, 63, 1971.
8. T. KAKUTANI, Y. INOUE and T. KAN, J. Phys. Soc. Japan, **37**, 529, 1974.

9. J. M. KENDALL, Phys. Fluids, **29**, 2086, 1986.

10. C. H. HERTZ and J. HERMARUD, J. Fluid Mech., **131**, 271, 1983.

11. V. PETRYANOV and A. A. SHUTOV, Sov. Phys. Dokl., **29**, 278, 1984.

12. A. SHUTOV, Fluid Dynamics, **20**, 497, 1985.

13. A. E. RADWAN, J. Magn. Magn. Matrs., **72**, 219, 1988 and **71**, 109, 1992. J. Phys. Soc. Japan, **58**, 1225, 1989.

14. L. Y. CHENG, Phys. Fluids, **28**, 2614, 1985.

15. F. G. DRAZIN and W. H. REID, *Hydrodynamic stability*, Cambridge Univ. Press, London, p. 16, 1981.

16. M. ABRAMOWITZ and I. STEGUN, *Handbook of mathematical functions*, Dover Publ., New York 1965.

DEPARTMENT OF MATHEMATICS
FACULTY OF SCIENCE
AIN-SHAMP UNIVERSITY

Cairo, Egypt

Received December 5, 1997.

Arch. Mech., 50, 4, pp. 731–741, Warszawa 1998
FIFTY YEARS OF THE ARCHIVES OF MECHANICS

On symmetric tensor-valued isotropic functions of a symmetric tensor and a skewsymmetric tensor and related transversely isotropic functions

H. XIAO, O.T. BRUHNS and A. MEYERS (BOCHUM)

A NEW GENERATING set consisting of seven polynomial tensor generators is presented for symmetric second order tensor-valued isotropic functions of a symmetric second order tensor and a skewsymmetric second order tensor. It is smaller than the existing corresponding generating set consisting of eight tensor generators and shown to be minimal in all possible generating sets consisting of homogeneous polynomial tensor generators. This result indicates that the well-known results for isotropic functions may be sharpened. In addition, from the presented result a minimal generating set consisting of six tensor generators is derived for the symmetric second order tensor-valued transversely isotropic functions of a symmetric second order tensor relative to the transverse isotropy group $C_{\infty h}$ consisting of all rotations about a fixed axis.

1. Introduction

IN CONTINUUM MECHANICS, symmetric second order tensor-valued isotropic functions of vectors and second order tensors serve to formulate constitutive relations of isotropic materials, such as stress-deformation relations etc. The isotropy places restrictions on the tensor function forms of constitutive relations. It is important to determine general reduced forms, i.e., representations of the latter under such restrictions. Now general results for isotropic functions of vectors and second order tensors, in the sense of polynomial or nonpolynomial representation, are available and well known (see, e.g., [1 – 7]), and in [1] and [8 – 9] these results are given for use in convenient tabular forms.

To arrive at concise and efficient formulation of complicated material behaviours, representations for constitutive equations of materials should be made as compact as possible. Although the above-mentioned representations for isotropic functions have been proved to be irreducible in the sense of polynomial or nonpolynomial representation, until now it has not been known whether or not each of them is minimal in a suitable sense. Further development requires examining and sharpening the existing results and finally, arriving at minimal representations in a suitable sense. In this paper, we are mainly concerned with symmetric second order tensor-valued isotropic functions of a second order symmetric tensor and a skewsymmetric second order tensor. For such tensor functions, earlier TELEGA [10] made an attempt to find a generating set that is smaller than the existing one (see the end of this section for detail). Although

later this early attempt was shown to be unsuccessful in [5], in this paper we shall show that the expected goal may indeed be arrived at. Specifically, we shall provide a new generating set consisting of seven polynomial tensor generators for the isotropic functions at issue, which is smaller than the existing generating set consisting of eight generators, and furthermore we shall prove that the presented set is a minimal one in all possible generating sets consisting of homogeneous polynomial tensor generators.

It shoud be pointed out that the tensor functions at issue include symmetric second order tensor-valued isotropic functions of an asymmetric second order tensor, since each asymmetric second order tensor has a unique additive decomposition into a symmetric tensor and a skewsymmetric tensor. Moreover, the tensor functions at issue also include symmetric second order tensor-valued transversely isotropic functions of a symmetric second order tensor relative to the transverse isotropy group $C_{\infty h}$, as will be shown in Sec. 3. Accordingly, minimal generating sets for the two types of tensor functions just mentioned can be derived from the presented minimal generating set for the tensor functions at issue. In so doing, by virtue of (1.2) given later, the derivation is direct for the former type of tensor functions. However, the derivation is not so direct for the latter type of tensor functions and will be discussed at the end of Sec. 3.

To facilitate the subsequent account, in what follows we outline some related facts.

A symmetric second order tensor-valued function $\psi(\mathbf{A},\mathbf{W})$ of a symmetric second order tensor $\mathbf{A}$ and a skewsymmetric second order tensor $\mathbf{W}$ is *isotropic* if

$$\psi(\mathbf{Q}\mathbf{A}\mathbf{Q}^{\mathrm{T}},\mathbf{Q}\mathbf{W}\mathbf{Q}) = \mathbf{Q}\psi(\mathbf{A},\mathbf{W})\mathbf{Q}^{\mathrm{T}}, \tag{1.1}$$

for each orthogonal tensor $\mathbf{Q}$. Henceforth, tensor means second order tensor if no confusion arises. Throughout, the superscript T is used to signify the transpose of a tensor.

As mentioned before, each symmetric tensor-valued isotropic function of an asymmetric tensor $\mathbf{B}$ is equivalent to a symmetric tensor-valued isotropic function of a symmetric tensor $\mathbf{A}$ and a skewsymmetric tensor $\mathbf{W}$. Indeed, this can be done just by the replacement

$$\begin{aligned} \mathbf{A} &= \frac{1}{2}(\mathbf{B} + \mathbf{B}^{\mathrm{T}}), \\ \mathbf{W} &= \frac{1}{2}(\mathbf{B} - \mathbf{B}^{\mathrm{T}}). \end{aligned} \tag{1.2}$$

A finite number of symmetric tensor-valued isotropic functions, $\psi_1(\mathbf{A},\mathbf{W})$, $\cdots$, $\psi_r(\mathbf{A},\mathbf{W})$, of a symmetric tensor $\mathbf{A}$ and a skewsymmetric tensor $\mathbf{W}$ form a *generating set* for the symmetric tensor-valued isotropic functions of $\mathbf{A}$ and $\mathbf{W}$

if every symmetric tensor-valued isotropic function $\psi(\mathbf{A}, \mathbf{W})$ is expressible as a linear combination of these tensor functions with invariant coefficients, i.e.

$$\psi(\mathbf{A}, \mathbf{W}) = \mathbf{c}_1\psi_1(\mathbf{A}, \mathbf{W}) + \cdots + \mathbf{c}_r\psi_r(\mathbf{A}, \mathbf{W}), \tag{1.3}$$

where each coefficient $c_i = \bar{c}_i(\mathbf{A}, \mathbf{W})$ is an *isotropic invariant* of the tensors $\mathbf{A}$ and $\mathbf{W}$, and each $\psi_i(\mathbf{A},\mathbf{W})$ is called a *tensor generator*. A generating set is said to be *irreducible* if it contains no redundant tensor generators, i.e. none of its proper subsets is again a generating set.

The following generating set for the isotropic tensor functions at issue is well-known [2 – 3]:

$$\{\mathbf{I}, \mathbf{W}^2, \mathbf{A}, \mathbf{A}^2, \mathbf{AW} - \mathbf{WA}, \mathbf{A}^2\mathbf{W} - \mathbf{WA}^2, \mathbf{WAW}, \mathbf{W}^2\mathbf{AW} - \mathbf{WAW}^2\} . \tag{1.4}$$

Here and hereafter, $\mathbf{I}$ is used to denote the identity tensor. Earlier, it was thought [10] that the generator $\mathbf{WAW}$ could be removed from the above set and hence that a smaller generating set was available. Later, the irreducibility of the above set was proved in [5]. Although the attempt in [10] was unsuccessful, we shall show that we can find a new generating set which is indeed smaller than the above set.

2. A criterion for generating sets

We shall use the following criterion [11] to judge whether a given set of tensor generators is a generating set or not.

Let $\psi_1(\mathbf{A}, \mathbf{W}), \cdots, \psi_r(\mathbf{A}, \mathbf{W})$ be r given symmetric tensor-valued isotropic functions of the symmetric tensor $\mathbf{A}$ and the skewsymmetric tensor $\mathbf{W}$. Then they form a generating set for the symmetric tensor-valued isotropic functions of the tensors $\mathbf{A}$ and $\mathbf{W}$ if and only if

$$\operatorname{rank}\{\psi_1(\mathbf{A}, \mathbf{W}), \cdots, \psi_r(\mathbf{A}, \mathbf{W})\} \geq \dim \operatorname{Sym}(g(\mathbf{A}, \mathbf{W})) \tag{2.1}$$

for any symmetric tensor $\mathbf{A}$ and any skewsymmetric tensor $\mathbf{W}$.

Here and hereafter, the notations rank S and dim L are used to designate the number of the linearly independent elements in any given set S of tensors and the dimension of any given tensor subspace L, respectively. Moreover, for any given symmetric tensor $\mathbf{A}$ and any given skewsymmetric tensor $\mathbf{W}$, the notation $g(\mathbf{A}, \mathbf{W})$ is used to denote the symmetry group of the tensors $\mathbf{A}$ and $\mathbf{W}$, which includes all orthogonal tensors preserving both $\mathbf{A}$ and $\mathbf{W}$, and for any given orthogonal subgroup g, the notation $\operatorname{Sym}(g)$ is used to represent the tensor subspace that is composed of all tensors invariant under the subgroup g. Specifcally,

$$g(\mathbf{A}, \mathbf{W}) = \{\mathbf{Q} \in \operatorname{Orth} \mid \mathbf{QAQ}^{\mathrm{T}} = \mathbf{A}, \mathbf{QWQ}^{\mathrm{T}} = \mathbf{W}\}, \tag{2.2}$$

$$\text{Sym}(g) = \{\mathbf{B} \in \text{Sym} \mid \mathbf{Q}\mathbf{B}\mathbf{Q}^{\mathrm{T}} = \mathbf{B}, \forall \mathbf{Q} \in g\}, \tag{2.3}$$

where Orth and Sym are the full orthogonal group and the space of symmetric tensors, respectively.

To apply the above criterion, it is required to evaluate the dimension dim $\text{Sym}(g(\mathbf{A}, \mathbf{W}))$ for any symmetric tensor $\mathbf{A}$ and any skewsymmetric tensor $\mathbf{W}$. For $\mathbf{W} \neq \mathbf{O}$ and $\mathbf{A} \in$ Sym, we have

$$\dim \text{Sym}(g(\mathbf{A}, \mathbf{W})) \leq \begin{cases} 2 \text{ for } \mathbf{A} = x\mathbf{I} + y\mathbf{w} \otimes \mathbf{w}, \\ 4 \text{ for } \mathbf{w} \times \mathbf{A}\mathbf{w} = \mathbf{0}, \\ 6 \text{ for any } \mathbf{A} \text{ and } \mathbf{W}. \end{cases} \tag{2.4}$$

Here and hereafter, for each skewsymmetric tensor $\mathbf{W}$ we use the following expression

$$\mathbf{W} = \mathbf{E}\mathbf{w}, \tag{2.5}$$

where $\mathbf{w}$ is an axial vector associated with $\mathbf{W}$, determined by

$$\mathbf{w} = \mathbf{E} : \mathbf{W}, \qquad \text{i.e. } w_i = e_{ijk} W_{jk}. \tag{2.6}$$

Here $\mathbf{E}$ is the third-order Livi – Civita tensor and e_{ijk} the permutation symbol.

The proof for (2.4) is as follows. It is evident that $(2.4)_3$ holds, since $\text{Sym}(g(\mathbf{A}, \mathbf{W}))$ is a subspace of the symmetric tensor space Sym for any given tensors $\mathbf{A}$ and $\mathbf{W}$, and moreover dim Sym$= 6$. In what follows we prove that $(2.4)_{1,2}$ hold. Henceforth, $\mathbf{R}^{\theta}_{\mathbf{w}}$ is used to denote the right-handed rotation through the angle θ about an axis in the direction of the vector $\mathbf{w} \neq \mathbf{0}$.

Suppose that $\mathbf{A} = x\mathbf{I} + y\mathbf{w} \otimes \mathbf{w}$. Then we have

$$\mathbf{Q}(\mathbf{E}\mathbf{w})\mathbf{Q}^{\mathrm{T}} = \mathbf{E}\mathbf{w}, \qquad \mathbf{Q}\mathbf{A}\mathbf{Q}^{\mathrm{T}} = \mathbf{A}$$

for any $\mathbf{Q} = \pm\mathbf{R}^{\theta}_{\mathbf{w}}$. Hence

$$C_{\infty h}(\mathbf{w}) \equiv \{\pm\mathbf{R}^{\theta}_{\mathbf{w}} \mid \theta \in R\} \subset g(\mathbf{A}, \mathbf{E}\mathbf{w}). \tag{2.7}$$

From the latter and

$$\text{Sym}(C_{\infty h}(\mathbf{w})) = \text{span}\{\mathbf{I}, \mathbf{w} \otimes \mathbf{w}\}, \tag{2.8}$$

as well as the fact that for two orthogonal subgroups $g_1, g_2 \subset$ Orth,

$$g_1 \subset g_2 \Longrightarrow \text{Sym}(g_2) \subset \text{Sym}(g_1), \tag{2.9}$$

we infer that $(2.4)_1$ holds.

Suppose that $\mathbf{w} \times \mathbf{A}\mathbf{w} = \mathbf{0}$. Then $\mathbf{w} \neq \mathbf{0}$ is an eigenvector of the symmetric tensor $\mathbf{A}$. Let $(\mathbf{w}, \mathbf{e}_1, \mathbf{e}_2)$ be three mutually orthogonal eigenvectors of the symmetric tensor $\mathbf{A}$. Then we have

$$\mathbf{A} = x\mathbf{w} \otimes \mathbf{w} + y\mathbf{e}_1 \otimes \mathbf{e}_1 + z\mathbf{e}_2 \otimes \mathbf{e}_2, \qquad x, y, z \in R\,,$$

and

$$\mathbf{R}_{\mathbf{w}}^{\pi}\mathbf{w} = \mathbf{w}, \qquad \mathbf{R}_{\mathbf{w}}^{\pi}\mathbf{e}_1 = -\mathbf{e}_1,\ \mathbf{R}_{\mathbf{w}}^{\pi}\mathbf{e}_2 = -\mathbf{e}_2$$

Hence, we derive

$$C_2(\mathbf{w}) \equiv \{\mathbf{I}, \mathbf{R}_{\mathbf{w}}^{\pi}\} \subset g(\mathbf{A}, \mathbf{E}\mathbf{w}).$$

From the latter and

$$\mathrm{Sym}(C_2(\mathbf{w})) = \mathrm{span}\{\mathbf{w}\otimes\mathbf{w}, \mathbf{e}_1\otimes\mathbf{e}_1, \mathbf{e}_2\otimes\mathbf{e}_2, \mathbf{e}_1\otimes\mathbf{e}_2 + \mathbf{e}_2\otimes\mathbf{e}_1\}$$

as well as (2.9), we deduce that $(2.4)_2$ holds. *Q. E. D*

3. Smaller generating sets

The main result of this paper is as follows.

THEOREM 1. *The set* $G_0(\mathbf{A}, \mathbf{E}\mathbf{w}) = \{\mathbf{G}_1, \cdots, \mathbf{G}_7\}$ *given by*

$$\begin{aligned}
&\mathbf{G}_1 = \mathbf{I}, \qquad \mathbf{G}_2 = \mathbf{w}\otimes\mathbf{w}, \qquad \mathbf{G}_3 = \mathbf{A}, \qquad \mathbf{G}_4 = \mathbf{A}^2,\\
&\mathbf{G}_5 = \mathbf{A}(\mathbf{E}\mathbf{w}) - (\mathbf{E}\mathbf{w})\mathbf{A}, \mathbf{G}_6 = (\mathbf{w}\times\mathbf{A}\mathbf{w})\otimes(\mathbf{w}\times\mathbf{A}\mathbf{w}),\\
&\mathbf{G}_7 = (\mathbf{w}\times\mathbf{A}\mathbf{w})\otimes(\mathbf{w}\times(\mathbf{w}\times\mathbf{A}\mathbf{w})) + (\mathbf{w}\times(\mathbf{w}\times\mathbf{A}\mathbf{w}))\otimes(\mathbf{w}\times\mathbf{A}\mathbf{w}),
\end{aligned}$$

is a generating set for the symmetric tensor-valued isotropic functions of a symmetric tensor $\mathbf{A}$ *and a skewsymmetric tensor* $\mathbf{W} = \mathbf{E}\mathbf{w}$, *and this set is a minimal one in all possible generating sets consisting of homogeneous polynomial generators.*

In the following, we prove that the set $G_0(\mathbf{A}, \mathbf{E}\mathbf{w})$ given above is a generating set for the isotropic tensor functions at issue. The proof for the minimality of this set will be postponed until the next section.

It can be readily shown that each presented tensor generator $\mathbf{G}_i$ is isotropic with respect to $\mathbf{A}$ and $\mathbf{W} = \mathbf{E}\mathbf{w}$ by means of the facts

$$\begin{aligned}
\mathbf{E} : (\mathbf{Q}\mathbf{W}\mathbf{Q}^{\mathrm{T}}) &= 2(\det\mathbf{Q})\mathbf{Q}\mathbf{w},\\
(\mathbf{Q}\mathbf{e}) \times (\mathbf{Q}\mathbf{e}') &= (\det\mathbf{Q})\mathbf{Q}(\mathbf{e}\times\mathbf{e}'),
\end{aligned}$$

for any skewsymmetric tensor $\mathbf{W}$, any orthogonal tensor $\mathbf{Q}$ and any vectors $\mathbf{e}$ and $\mathbf{e}'$. Note that here $\mathbf{w}$ is the axial vector determined by (2.6). Hence, we need only to prove that the presented set $G_0(\mathbf{A}, \mathbf{E}\mathbf{w})$ obeys the criterion (2.1), i.e.

$$\text{(3.1)} \qquad \mathrm{rank}\, G_0(\mathbf{A}, \mathbf{E}\mathbf{w}) = \mathrm{rank}\,\{\mathbf{G}_1, \cdots, \mathbf{G}_7\} \geq \dim \mathrm{Sym}(g(\mathbf{A}, \mathbf{E}\mathbf{w}))$$

for any symmetric tensor $\mathbf{A}$ and any vector $\mathbf{w}$. Towards this end, four cases will be discussed.

CASE 1. One of the tensor arguments $\mathbf{A}$ and $\mathbf{Ew}$ vanishes

Each tensor generator $\mathbf{G}_i$ for $i = 5, 6, 7$ vanishes. Since the sets $\{\mathbf{I}, \mathbf{w}\otimes\mathbf{w}\}$ and $\{\mathbf{I}, \mathbf{A}, \mathbf{A}^2\}$ provide a generating set for a symmetric tensor $\mathbf{A}$ and a generating set for a skewsymmetric tensor $\mathbf{W} = \mathbf{Ew}$ respectively, the condition (3.1) are satisfied for the case in question.

CASE 2. $\mathbf{w} \times \mathbf{Aw} \neq \mathbf{0}$

Henceforth, for any two vectors $\mathbf{e}$ and $\mathbf{e}'$ the notation $\mathbf{e} \vee \mathbf{e}'$ is used to signify the symmetric tensor defined by

$$\mathbf{e} \vee \mathbf{e}' = \mathbf{e} \otimes \mathbf{e}' + \mathbf{e}' \otimes \mathbf{e} .$$

Let

$$\mathbf{e}_1 = \mathbf{w} \times \mathbf{Aw}, \qquad \mathbf{e}_2 = \mathbf{w} \times \mathbf{e}_1.$$

Then $(\mathbf{w}, \mathbf{e}_1, \mathbf{e}_2)$ is an orthogonal system of vectors. Without loss of generality, we assume that both the vectors $\mathbf{w}$ and $\mathbf{Aw}$ are normalized ones, i.e. $|\mathbf{w}| = |\mathbf{Aw}| = 1$, and therefore that the mentioned system of vectors is an orthonormal one. In terms of this system, the symmetric tensors $\mathbf{I}$ and $\mathbf{A}$ are expressible as

$$\mathbf{I} = \mathbf{w} \otimes \mathbf{w} + \mathbf{e}_1 \otimes \mathbf{e}_1 + \mathbf{e}_2 \otimes \mathbf{e}_2, \tag{3.2}$$

$$\mathbf{A} = a_1\mathbf{e}_1 \otimes \mathbf{e}_1 + a_2\mathbf{e}_2 \otimes \mathbf{e}_2 + a_3\mathbf{w} \otimes \mathbf{w} + a_4\mathbf{e}_1 \vee \mathbf{e}_2 + a_5\mathbf{w} \vee \mathbf{e}_1 + a_6\mathbf{w} \vee \mathbf{e}_2 . \tag{3.3}$$

The condition that $\mathbf{w} \times \mathbf{Aw} \neq \mathbf{0}$ requires

$$(a_5)^2 + (a_6)^2 \neq 0.$$

Hence

$$\mathbf{A}(\mathbf{Ew}) - (\mathbf{Ew})\mathbf{A} = (a_1 - a_2)\mathbf{e}_1 \vee \mathbf{e}_2 - a_4(\mathbf{e}_1 \otimes \mathbf{e}_1 - \mathbf{e}_2 \otimes \mathbf{e}_2) + a_6\mathbf{w} \vee \mathbf{e}_1 - a_5\mathbf{w} \vee \mathbf{e}_2. \tag{3.4}$$

In deriving the above, the identity

$$(\mathbf{Ee})\mathbf{e}' = \mathbf{e} \times \mathbf{e}'$$

for any two vectors $\mathbf{e}$ and $\mathbf{e}'$ is used.

Applying the expressions (3.2) – (3.4), we infer

$$\begin{aligned}
\operatorname{rank} G_0(\mathbf{A}, \mathbf{Ew}) &\geq \operatorname{rank}\{\mathbf{G}_1, \mathbf{G}_2, \mathbf{G}_3, \mathbf{G}_5, \mathbf{G}_6, \mathbf{G}_7\} \\
&= \operatorname{rank}\{\mathbf{w} \otimes \mathbf{w}, \mathbf{e}_1 \otimes \mathbf{e}_1, \mathbf{e}_1 \vee \mathbf{e}_2, \mathbf{I}, \mathbf{A}, \mathbf{A}(\mathbf{Ew}) - (\mathbf{Ew})\mathbf{A}\} \\
&= \operatorname{rank}\{\mathbf{w} \otimes \mathbf{w}, \mathbf{e}_1 \otimes \mathbf{e}_1, \mathbf{e}_1 \vee \mathbf{e}_2, \mathbf{e}_2 \otimes \mathbf{e}_2, \\
&\qquad a_5\mathbf{w} \vee \mathbf{e}_1 + a_6\mathbf{w} \vee \mathbf{e}_2, a_6\mathbf{w} \vee \mathbf{e}_1 - a_5\mathbf{w} \vee \mathbf{e}_2\} \\
&= \operatorname{rank}\{\mathbf{w} \otimes \mathbf{w}, \mathbf{e}_1 \otimes \mathbf{e}_1, \mathbf{e}_1 \vee \mathbf{e}_2, \mathbf{e}_2 \otimes \mathbf{e}_2, \mathbf{w} \vee \mathbf{e}_1, \mathbf{w} \vee \mathbf{e}_2\} \\
&= 6 \geq \operatorname{Sym}(g(\mathbf{A}, \mathbf{Ew}))
\end{aligned}$$

In the last step, $(2.4)_3$ is used.

CASE 3. $\mathbf{w} \times \mathbf{Aw} = \mathbf{0}$ and $\mathbf{A}(\mathbf{Ew}) \neq (\mathbf{Ew})\mathbf{A}$

Let $(\mathbf{w}, \mathbf{e}_1, \mathbf{e}_2)$ be an orthonormal system of vectors, where $\mathbf{e}_1$ may be any unit vector in the $\mathbf{w}$-plane and $\mathbf{e}_2 = \mathbf{w} \times \mathbf{e}_1$. Then the expressions (3.2) – (3.3) remain true. The condition that $\mathbf{w} \times \mathbf{Aw} = \mathbf{0}$ implies that $\mathbf{w} \neq \mathbf{0}$ is an eigenvector of the symmetric tensor $\mathbf{A}$. Hence, in (3.3) we have

$$a_5 = a_6 = 0 \, .$$

Moreover, the condition that $\mathbf{A}(\mathbf{Ew}) \neq (\mathbf{Ew})\mathbf{A}$ yields (cf. (3.4))

$$(a_1 - a_2)^2 + (a_4)^2 \neq 0 \, .$$

Thus, we deduce

$$\begin{aligned} \operatorname{rank} G_0(\mathbf{A}, \mathbf{Ew}) &\geq \operatorname{rank}\{\mathbf{G}_1, \mathbf{G}_2, \mathbf{G}_3, \mathbf{G}_5\} \\ &= \operatorname{rank}\{\mathbf{w} \otimes \mathbf{w}, \mathbf{e}_1 \otimes \mathbf{e}_1 + \mathbf{e}_2 \otimes \mathbf{e}_2, a_1 \mathbf{e}_1 \otimes \mathbf{e}_1 + a_2 \mathbf{e}_2 \otimes \mathbf{e}_2 \\ &\qquad + a_4 \mathbf{e}_1 \vee \mathbf{e}_2, (a_1 - a_2)\mathbf{e}_1 \vee \mathbf{e}_2 - a_4(\mathbf{e}_1 \otimes \mathbf{e}_1 - \mathbf{e}_2 \otimes \mathbf{e}_2)\} \\ &= \operatorname{rank}\{\mathbf{w} \otimes \mathbf{w}, \mathbf{e}_1 \otimes \mathbf{e}_1, \mathbf{e}_2 \otimes \mathbf{e}_2, \mathbf{e}_1 \vee \mathbf{e}_2\} \\ &= 4 \geq \operatorname{Sym}(g(\mathbf{A}, \mathbf{Ew})) \, . \end{aligned}$$

In the last step, $(2.4)_2$ is used. Moreover, we mention that the determinant of the coefficient matrix of the last three tensors in the second equality with respect to the three independent tensors $\mathbf{e}_1 \otimes \mathbf{e}_1$, $\mathbf{e}_2 \otimes \mathbf{e}_2$ and $\mathbf{e}_1 \vee \mathbf{e}_2$ is given by

$$\Delta = \begin{vmatrix} 1 & 1 & 0 \\ a_1 & a_2 & a_4 \\ -a_4 & a_4 & a_1 - a_2 \end{vmatrix} = -(a_1 - a_2)^2 - 2(a_4)^2 \neq 0,$$

and therefore, that the two sets of three tensors just mentioned are equivalent.

CASE 4. $\mathbf{w} \times \mathbf{Aw} = \mathbf{0}$ and $\mathbf{A}(\mathbf{Ew}) = (\mathbf{Ew})\mathbf{A}$, i.e. $\mathbf{A} = x\mathbf{I} + y\mathbf{w} \otimes \mathbf{w}$

From $(2.4)_1$, it is evident that

$$\operatorname{rank} G_0(\mathbf{A}, \mathbf{Ew}) \geq \operatorname{rank}\{\mathbf{I}, \mathbf{w} \otimes \mathbf{w}\} = 2 \geq \dim \operatorname{Sym}(g(\mathbf{A}, \mathbf{Ew})).$$

Finally, combining the above four cases, we conclude that the presented set $G_0(\mathbf{A}, \mathbf{Ew})$ obeys (3.1) for any tensors $\mathbf{A}$ and $\mathbf{W} = \mathbf{Ew}$, and hence it is a generating set for the symmetric tensor-valued isotropic functions of the symmetric tensor $\mathbf{A}$ and the antisymmetric tensor $\mathbf{W} = \mathbf{Ew}$. *Q. E. D.*

From the proof given above, it can be seen that the tensor generator $\mathbf{G}_4 = \mathbf{A}^2$ comes into play only when $\mathbf{W} = \mathbf{O}$, i.e. $\mathbf{w} = \mathbf{0}$. This fact leads to the following result.

COROLLARY 1. The set

$$G_+(\mathbf{A},\mathbf{w}) = \{\mathbf{G}_1, \mathbf{G}_2, \mathbf{G}_3, \mathbf{G}_5, \mathbf{G}_6, \mathbf{G}_7\} \tag{3.5}$$

is a generating set for the symmetric tensor-valued isotropic functions of the symmetric tensor $\mathbf{A}$ and the nonvanishing antisymmetric tensor $\mathbf{W} = \mathbf{Ew} \neq \mathbf{O}$, and this set is a minimal one in all possible generating sets for the isotropic tensor functions at issue.

According to [12], a generating set for the symmetric tensor-valued isotropic functions of the symmetric tensor $\mathbf{A}$ and the antisymmetric tensor $\mathbf{En}$, where $\mathbf{n}$ is a fixed unit vector, furnishes a generating set for the symmetric tensor-valued transversely isotropic functions of the symmetric tensor $\mathbf{A}$ relative to the transverse isotropy group $C_{\infty h}(\mathbf{n})$ (cf. (2.7)). Thus, by assuming the vector $\mathbf{w}$ as a fixed unit vector $\mathbf{n}$ in (3.5), from the above corollary we derive a generating set for the symmetric tensor-valued transversely isotropic functions of the symmetric tensor $\mathbf{A}$ relative to the transverse isotropy group $C_{\infty h}(\mathbf{n})$ as follows:

$$\begin{aligned} G_0(\mathbf{A}) = \{&\mathbf{I}, \mathbf{n} \otimes \mathbf{n}, \mathbf{A}, \mathbf{A}(\mathbf{En}) - (\mathbf{En})\mathbf{A}, \\ &(\mathbf{n} \times \mathbf{An}) \otimes (\mathbf{n} \times \mathbf{An}), (\mathbf{n} \times \mathbf{An}) \vee (\mathbf{n} \times (\mathbf{n} \times \mathbf{An}))\}. \end{aligned} \tag{3.6}$$

This generating set, which is composed of six tensor generators only, is smaller than the existing corresponding generating sets (cf. [13, 14]), each of the latter being composed of eight generators. Furthermore, the generating set given by (3.6) is the smallest possible (cf. Theorem 4 given in [15]). In fact, it is equivalent to the corresponding minimal generating set given in [15].

4. The minimality of the generating set $G_0(\mathbf{A}, \mathbf{Ew})$

In forming the generating sets, homogeneous polynomial generators are commonly used (see, e.g., [1 – 9]). Each such generator except the constant vectors and constant tensors is of the property: it vanishes when one of its variables vanishes. Thus, for the tensor functions concerned, each generating sets is of the form

$$G(\mathbf{A}, \mathbf{Ew}) = G_0 \cup G'(\mathbf{A}) \cup G'(\mathbf{Ew}) \cup G'(\mathbf{A}, \mathbf{Ew}), \tag{4.1}$$

where G_0 is a set consisting of constant tensors, $G'(\mathbf{A})$ and $G'(\mathbf{Ew})$ are two sets consisting of tensor generators depending on a single variable $\mathbf{A}$ or $\mathbf{Ew}$ respectively, and $G'(\mathbf{A}, \mathbf{Ew})$ is a set consisting of tensor generators depending on the two tensor variables $\mathbf{A}$ and $\mathbf{Ew}$. Each set given above is assumed to fulfil the properties:

$$\begin{aligned} &\psi_0(\mathbf{O}) = \mathbf{O}, \ \forall \psi_0(\mathbf{B}) \in G'(\mathbf{A}) \cup G'(\mathbf{Ew}), \\ &\psi(\mathbf{A}, \mathbf{O}) = \psi(\mathbf{O}, \mathbf{Ew}) = \mathbf{O}, \ \forall \psi(\mathbf{A}, \mathbf{Ew}) \in G'(\mathbf{A}, \mathbf{Ew}) \ . \end{aligned} \tag{4.2}$$

The main objective of this section is to verify that the generating set $G_0(\mathbf{A}, \mathbf{W})$ given in the last section is minimal in all possible generating sets of the form just stated. To this end, we prove that each generating set of the above-mentioned form must include at least seven tensor generators.

First, by (4.2) we infer that any given generating set $G(\mathbf{A}, \mathbf{Ew})$ in question has the property

$$G(\mathbf{A}, \mathbf{O}) = G_0 \cup G'(\mathbf{A}) \cup \{\mathbf{O}\}, \qquad G(\mathbf{O}, \mathbf{Ew}) = G_0 \cup G'(\mathbf{Ew}) \cup \{\mathbf{O}\} .$$

These indicate that the set $G_0 \cup G'(\mathbf{A})$ (resp. $G_0 \cup G(\mathbf{Ew})$) must be a generating set for the symmetric tensor-valued isotropic functions of a symmetric (resp. skewsymmetric) tensor $\mathbf{A}$ (resp. $\mathbf{Ew}$). According to Theorem 4 given in [15], the set $G_0 \cup G'(\mathbf{A})$ must include at least three generators. Moreover, it is easily understood that the set $G_0 \cup G'(\mathbf{Ew})$ must include at least two generators, such as $\mathbf{I}$ and $\mathbf{w} \otimes \mathbf{w}$ etc. Finally, the set G_0 must include at least one nonvanishing constant tensor, such as $\mathbf{I}$ etc., or else the criterion (2.1) will be violated when $\mathbf{A} = \mathbf{W} = \mathbf{O}$. Thus, by combining these facts we know that the set $G_0 \cup G'(\mathbf{A}) \cup G'(\mathbf{Ew})$ must include at least four generators.

Next, let

$$\mathbf{A}_0 = (\mathbf{n} + \mathbf{e}) \otimes (\mathbf{n} + \mathbf{e}) ,$$

where $\mathbf{e}$ and $\mathbf{n}$ are two orthonormal vectors, i.e.

$$\mathbf{n} \cdot \mathbf{e} = 0, \quad \mathbf{e} \cdot \mathbf{e} = \mathbf{n} \cdot \mathbf{n} = 1 .$$

Then we have

$$\mathbf{Q}(\mathbf{n} + \mathbf{e}) \neq \pm(\mathbf{n} + \mathbf{e})$$

for each $\mathbf{Q} = \pm\mathbf{R}_{\mathbf{n}}^{\theta}$, $\theta \neq 2k\pi$. Hence we infer

$$\mathbf{Q} = \pm\mathbf{R}_{\mathbf{n}}^{\theta} \quad \text{and} \quad \theta \neq 2k\pi \Longrightarrow \mathbf{Q}\mathbf{A}_0\mathbf{Q}^{\mathrm{T}} \neq \mathbf{A}_0.$$

From the latter and the fact (cf. [12])

$$\mathbf{Q}(\mathbf{En})\mathbf{Q}^{\mathrm{T}} = \mathbf{En} \Longleftrightarrow \mathbf{Q} = \pm\mathbf{R}_{\mathbf{n}}^{\theta} \in C_{\infty h}(\mathbf{n}) ,$$

we deduce that

$$g(\mathbf{A}_0, \mathbf{En}) = \{\pm\mathbf{I}\} .$$

Hence,

$$\dim \mathrm{Sym}(g(\mathbf{A}_0, \mathbf{En})) = \dim \mathrm{Sym} = 6 . \tag{4.3}$$

On the other hand, since

$$C_{\infty h}(\mathbf{n} + \mathbf{e}) \subset g(\mathbf{A}_0, \mathbf{O}), \quad C_{\infty h}(\mathbf{n}) = g(\mathbf{O}, \mathbf{En}),$$

we have (cf. (2.7) – (2.9))

$$\mathrm{Sym}(g(\mathbf{A}_0, \mathbf{O})) \subset \mathrm{span}\{\mathbf{I}, \mathbf{A}_0\}, \qquad \mathrm{Sym}(g(\mathbf{O}, \mathbf{En})) = \mathrm{span}\{\mathbf{I}, \mathbf{n} \otimes \mathbf{n}\}\,.$$

From the latter and the following fact (cf. (1.1) and (2.2) – (2.3); see also Theorem 2.2 given in [11]):

$$\psi_0(\mathbf{B}) \in \mathrm{Sym}(\mathbf{A}, \mathbf{O}) \cup \mathrm{Sym}(\mathbf{O}, \mathbf{Ew}), \quad \forall \psi_0(\mathbf{B}) \in G_0 \cup G'(\mathbf{A}) \cup G'(\mathbf{Ew}),$$

we derive

$$\mathrm{rank}(G_0 \cup G'(\mathbf{A}_0) \cup G'(\mathbf{En})) \leq \dim(\mathrm{Sym}(g(\mathbf{A}_0, \mathbf{O})) + \mathrm{Sym}(g(\mathbf{O}, \mathbf{En}))) = 3. \tag{4.4}$$

Finally, applying the criterion (2.1) with the tensors $(\mathbf{A}_0, \mathbf{En})$ given and using (4.3) – (4.4), for each generating set $G(\mathbf{A}, \mathbf{Ew})$ in question we deduce

$$\begin{aligned} \dim \mathrm{Sym}(g(\mathbf{A}_0, \mathbf{En})) = 6 &\leq \mathrm{rank} G(\mathbf{A}_0, \mathbf{En}) \\ &\leq \mathrm{rank}(G_0 \cup G'(\mathbf{A}_0) \cup G'(\mathbf{En})) + \mathrm{rank} G'(\mathbf{A}_0, \mathbf{En}), \end{aligned}$$

i.e.

$$\mathrm{rank} G'(\mathbf{A}_0, \mathbf{En}) \geq 6 - \mathrm{rank}(G_0 \cup G'(\mathbf{A}_0) \cup G'(\mathbf{En})) = 3.$$

The latter shows that in each generating set $G(\mathbf{A}, \mathbf{Ew})$ (cf. (4.1)) with the property (4.2), the set $G'(\mathbf{A}, \mathbf{Ew})$ consisting of generators depending on the two variables $\mathbf{A}$ and $\mathbf{En}$ must include at least three generators.

Finally, from the fact just-proved and the fact proved before we conclude that each generating set $G(\mathbf{A}, \mathbf{Ew})$ at issue (cf. (4.2) – (4.3)) must include at least seven generators.

Thus, the presented generating set $G_0(\mathbf{A}, \mathbf{Ew})$, which is exactly composed of seven tensor generators, is a minimal one in all possible generating sets $G(\mathbf{A}, \mathbf{Ew})$ with the properties (4.1) and (4.2). *Q. E. D.*

5. Conclusions

Although the well-known general results for isotropic functions have been proved to be irreducible, the results given in the previous sections show that some of them could be sharpened. The same is true for the results for transversely isotropic functions and orthotropic functions etc. (cf. Theorem 5 in [15] for the latter). Further considerations require examining the existing results, sharpening some of them and finally arriving at general results that are minimal in a suitable sense. The results will be reported elsewhere [16 – 17].

Acknowledgement

The first author is much obliged to Alexander von Humboldt Foundation for the grant of a research fellowship.

References

1. A.J.M. SPENCER, *Theory of invariants*, [in:] Continuum Physics, A.C. Eringen [Ed.], Vol. 1, Academic Press, New York 1971.
2. C.C. WANG, *A new representation theorem for isotropic functions. Parts I and II*, Arch. Rat. Mech. Anal., **36**, 166–223, 1970; ibid **43**, 392–395, 1971.
3. G.F. SMITH, *On isotropic functions of symmetric tensors, skewsymmetric tensors and vectors*, Int. J. Engng. Sci., **9**, 899–916, 1971.
4. J.P. BOEHLER, *On irreducible representations of isotropic scalar functions*, Zeits. Angew. Math. Mech., **57**, 323–327, 1977.
5. S. PENNISI and M. TROVATO, *On irreducibility of Professor G.F. Smith's representations for isotropic functions*, Int. J. Engng. Sci., **25**, 1059–1065, 1987.
6. J. KORSGAARD, *On the representation of symmetric tensor-valued isotropic functions*. Int. J. Engng. Sci., **28**, 1331–1346, 1990.
7. Q.S. ZHENG, *On the representations for isotropic vector-valued, symmetric tensor-valued and skewsymmetric tensor-valued functions*, Int. J. Engng. Sci., **31**, 1013–1024, 1993.
8. A.C. ERINGEN, *Continumm mechanics*, 2nd enlarged edition, Krieger, New York 1980.
9. G.F. SMITH, *Constitutive equations for anisotropic and isotropic materials*, Elsevier, New York 1994.
10. J. J. TELEGA, *Some aspects of invariant theory in plasticity. Part I. New results relative to representation of isotropic and anisotropic tensor functions*, Arch. Mech., **36**, 147–162, 1984.
11. H. XIAO, *Two general representation theorems for arbitrary-order-tensor-valued isotropic and anisotropic tensor functions of vectors and second order tensors*, Zeits. Angew. Math. Mech., **76**, 155–165, 1996.
12. I. S. LIU, *On representations of anisotropic invariants*, Int. J. Engng. Sci., **20**, 1099–1109, 1982.
13. Q.S. ZHENG, *On transversely isotropic, orthotropic and relative isotropic functions of symmetric tensors, skewsymmetric tensors and vectors. Part I-V*, Int. J. Engng. Sci., **31**, 1899–1453, 1993.
14. H. XIAO, *General irreducible representations for constitutive equations of elastic crystals and transversely isotropic solids*, J. Elasticity, **39**, 47–73, 1995.
15. H. XIAO, *On minimal representations for constitutive equations of anisotropic elastic materials*, J. Elasticity, **45**, 13–32, 1996.
16. H. XIAO, O.T. BRUHNS and A. MEYERS, *On minimality of generating sets for symmetric second order tensor-valued transversely isotropic functions of vectors and second order tensors*, Zeits. Angew. Math. Mech. [to appear].
17. H. XIAO, O.T. BRUHNS and A. MEYERS, *On minimality of representations for vector-valued and second order tensor-valued isotropic functions* [to be published].

INSTITUTE OF MECHANICS
Ruhr-University Bochum
D-44780 Bochum, Germany

Received October 24, 1997.

Arch. Mech., 50, 4, pp. 743–755, Warszawa 1998
FIFTY YEARS OF THE ARCHIVES OF MECHANICS

Receding contact between an orthotropic layer and an orthotropic half-space

P. K. CHAUDHURI and SUBHANKAR RAY (CALCUTTA)

THE PROBLEM of smooth receding contact between an orthotropic layer and an orthotropic half-space has been considered in this papaer. The paper includes a generalization of the results of the paper by L. M. KEER, J. DUNDURS, K. C. TSAI [4] concerning receding contact between an isotropic layer and an isotropic half-space. It is observed that the task of finding the extent of contact in the loaded configuration can be reduced to an eigenvalue problem of a homogenous Fredholm integral equation. The kernel of the Fredholm integral equation is found to be dependent on the elastic constants of the layer but is independent of the elastic constants of the half-space below, which is in contrast to the study for the isotropic materials, where the kernel is independent of the elastic constants. Finally some numerical results have been presented in graphs in order to compare the results of interest for isotropic and orthotropic materials.

1. Introduction

WHEN TWO ELASTIC media are in contact, the determination of the state of stress in the media has been the subject of study in literature for many years, and the problems are usually termed as contact problems. Usually the contact problems are of two types:

(a) the bodies in contact are bonded together and consequently, the contact regions are known *a priori*, and the main task is to determine the stress distribution in the media;

(b) the bodies are in contact without bond so that the region of contact is not known. In such class of problems determination of the contact region (which depends upon geometric features of the bodies as well as upon the load distribution on the system) becomes an additional task barring the stress distribution in the system. In 1970, (DUNDURS and STIPPES [2]) observed the role of elastic constants in unbonded frictionless contact of two elastically isotropic bodies. They classified the contact between two bodies into three categories, viz. (i) receding contact, (ii) stationary contact, (iii) advancing contact. Clearly, in a contact problem of two unbonded media, the initial region of contact does not always remain the same when deformation occurs in the body. If R' represents the contact region which was initially R, then the contact is receding if $R' \subset R$, stationary if $R' = R$ and advancing if $R' \supset R$. It has been observed that in linear elastostatics, the problems of receding contact have several simplifying features

compared to the advancing contacts. The most important fact is that the extent of receding contact is independent of the level of loading, which implies, in turn, that if uplift is to occur, the change from initial contact to the contact in the loaded configuration takes place discontinuously. Among the studies of receding contact between two bodies recorded in literature, mention may be made of the works of WEITSMAN [8], PU and HUSSAIN [7], WILSON and GOREE [9], KEER, DUNDURS and TSAI [4] and more recently of LI and DEMPSEY [6]. In all the above papers the discussion is limited to isotropic media only.

The aim of the present paper is to study the properties of smooth receding contact when an orthotropic layer is resting unbonded on an orthotropic half-space and to provide information regarding the extent of the contact region. As in [4], it is observed that the task of finding the extent of contact in the loaded configuration can be reduced to an eigenvalue problem of a homogeneous Fredholm integral equation which may be solved numerically to any desired degree of accuracy, when loading intervals are not very large in comparison to the thickness of the layer.

One notable feature in the present study is that the kernel of the Fredholm integral equations is dependent on the elastic constants of the layer but is independent of the elastic constants of the half-space below, whereas in the isotropic media the kernel is totally independent of the elastic constants. Finally, all the results for the isotropic media can be obtained from the corresponding results of our discussion by assigning limiting values to the elastic parameters.

2. The basic equations

For an orthotropic elastic medium, we choose the Cartesian coordinate axes to coincide with the principal material axes and define the plane strain state by

$$u_x = u(x,z), \quad u_y = 0, \quad u_z = w(x,z)\,, \tag{2.1}$$

where u_x, u_y, u_z are the displacements along x, y and z directions, respectively. The stress-displacement relations are

$$\begin{aligned} \sigma_{xx} &= A_{11}\frac{\partial_x}{\partial x} + A_{13}\frac{\partial u_z}{\partial z}, \\ \sigma_{zz} &= A_{13}\frac{\partial u_x}{\partial x} + A_{33}\frac{\partial u_z}{\partial z}, \\ \sigma_{xz} &= A_{55}\left(\frac{\partial u_x}{\partial z} + \frac{\partial u_z}{\partial x}\right), \\ \sigma_{yz} &= 0 = \sigma_{xy}. \end{aligned} \tag{2.2}$$

where A_{ij} are anisotropic constants of the orthotropic material. In terms of the displacement components the equations of equilibrium are

$$
\begin{aligned}
&A_{11}\frac{\partial^2 u_x}{\partial x^2} + A_{55}\frac{\partial^2 u_x}{\partial z^2} + (A_{13}+A_{55})\frac{\partial^2 u_z}{\partial x \partial z} = 0,\\
&A_{55}\frac{\partial^2 u_z}{\partial x^2} + A_{33}\frac{\partial^2 u_z}{\partial z^2} + (A_{55}+A_{13})\frac{\partial^2 u_x}{\partial x \partial z} = 0.
\end{aligned}
\tag{2.3}
$$

At this stage we decide to represent the solution u_x, u_z of Eqs. (2.3) in terms of potential functions. Obviously, the usual potential representation of displacement components in isotropic medium will not be suitable here. However, we can employ the method discussed in LEKHNITSKII [5] to represent u_x, u_z in terms of potential functions as follows:

Let us seek a solution of Eqs. (2.3) in the form

$$
u_x = \frac{\partial \phi_0}{\partial x}, \qquad u_z = \lambda \frac{\partial \phi_0}{\partial z}, \tag{2.4}
$$

where λ is a constant and $\phi_0 \equiv \phi_0(x,z)$. Equations (2.3) are satisfied if

$$
\frac{A_{55}+\lambda(A_{13}+A_{55})}{A_{11}} = \frac{\lambda A_{33}}{\lambda A_{55}+A_{13}+A_{55}} = \delta^2, \tag{2.5}
$$

where δ^2 is another constant.

From the relation (2.5) we get two quadratic equations, one in λ and the other in δ^2. If λ_1, λ_2 and δ_1^2, δ_2^2 are the roots of the quadratic equations

$$
\begin{aligned}
&\lambda^2 A_{55}(A_{13}+A_{55}) + \lambda\left[A_{13}+A_{55})^2 + A_{55}^2 - A_{11}A_{33}\right]\\
&\qquad + A_{55}(A_{13}+A_{55}) = 0,
\end{aligned}
\tag{2.6}
$$

$$
\delta^4 A_{11}A_{55} + \delta^2\left[(A_{13}+A_{55})^2 - A_{55}^2 - A_{11}A_{33}\right] + A_{33}A_{55} = 0, \tag{2.7}
$$

respectively, then we have two potential functions $\phi(x,z)$ and $\psi(x,z)$ satisfying the differential equations

$$
\begin{aligned}
&\frac{\partial^2 \phi}{\partial x^2} + \frac{\partial^2 \phi}{\partial z_1^2} = 0,\\
&\frac{\partial^2 \psi}{\partial x^2} + \frac{\partial^2 \psi}{\partial z_2^2} = 0,
\end{aligned}
\tag{2.8}
$$

where

$$
z_1 = z/\delta_1, \qquad z_2 = z/\delta_2. \tag{2.9}
$$

Hence the displacements and stresses can be expressed in terms of ϕ and ψ as

$$u_x = \frac{\partial \phi}{\partial x} + \frac{\partial \psi}{\partial x},$$

$$u_z = \frac{\lambda_1}{\delta_1}\frac{\partial \phi}{\partial z_1} + \frac{\lambda_2}{\delta_2}\frac{\partial \psi}{\partial z_2}, \tag{2.10}$$

$$\frac{\sigma_{xx}}{A_{55}} = \frac{1+\lambda_1}{\delta_1^2}\frac{\partial^2 \phi}{\partial x^2} + \frac{1+\lambda_2}{\delta_2^2}\frac{\partial^2 \psi}{\partial x^2},$$

$$\frac{\sigma_{zz}}{A_{55}} = (1+\lambda_1)\frac{\partial^2 \phi}{\partial z_z^2} + (1+\lambda_2)\frac{\partial^2 \psi}{\partial z_2^2}, \tag{2.11}$$

$$\frac{\sigma_{xz}}{A_{55}} = \frac{1+\lambda_1}{\delta_1}\frac{\partial^2 \phi}{\partial x \partial z_1} + \frac{1+\lambda_2}{\delta_2}\frac{\partial^2 \psi}{\partial x \partial z_2}.$$

3. Formulation and solution of the problem

We consider the plane elastostatic problem in which an unbonded layer of thickness h is in smooth contact with a semi-infinite base. The coordinate system used in relation to the two bodies is shown in Fig. 1. The layer is pressed against the base by normal tractions distributed over the segment $-a \leq x \leq a$ on the top surface of the layer, while the rest of the surface is free from tractions. The layer is in contact with the base below over the segment $-c \leq x \leq c$ in the deformed state while separation takes place outside this interval.

For simplicity, we consider only the case where the applied normal tractions are symmetric with respect to the centre of the loaded segment. Integral solutions of Eq. (2.8) which will be appropriate for the present problem can be written in the following forms:

$$\phi^{(1)} = \int_0^\infty \left[A(\xi)\mathrm{sh}\left\{\xi(z+h)/\delta_1^{(1)}\right\} + B(\xi)\mathrm{ch}\left\{\xi(z+h)/\delta_1^{(1)}\right\}\right]\cos \xi x \, d\xi \,, \tag{3.1}$$

$$\psi^{(1)} = \int_0^\infty \xi^{-1}\left[C(\xi)\mathrm{sh}\left\{\xi(z+h)/\delta_2^{(1)}\right\} + D(\xi)\mathrm{ch}\left\{\xi(z+h)/\delta_2^{(1)}\right\}\right] \cdot \cos \xi x \, d\xi, \qquad -h \leq z \leq 0 \,, \tag{3.2}$$

and

$$\phi^{(2)} = \int_0^\infty E(\xi) e^{-\xi z/\delta_1^{(2)}} \cos \xi x \, d\xi \,, \tag{3.3}$$

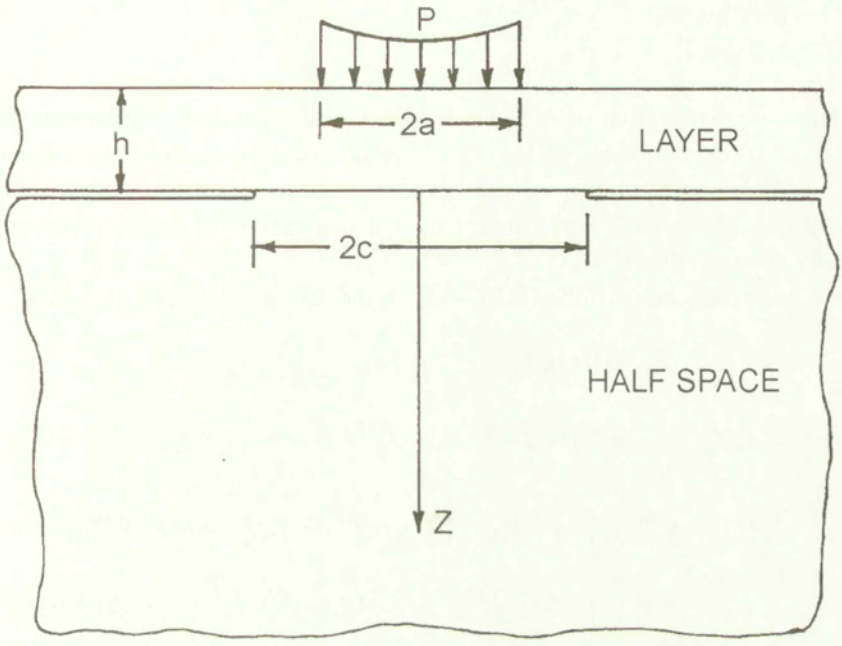

FIG. 1. Layer pressed against a half space.

$$\psi^{(2)} = \int_0^\infty F(\xi)\xi^{-1}e^{-\xi z/\delta_2^{(2)}}\cos\xi x\, d\xi, \qquad z \geq 0, \tag{3.4}$$

where $A(\xi)$, $B(\xi)$, $C(\xi)$, $D(\xi)$, $E(\xi)$ and $F(\xi)$ are arbitrary functions, to be determined from the boundary conditions.

The boundary conditions for the problem are

$$\sigma_{xz}^{(1)}(x, -h) = 0, \qquad 0 \leq |x| < \infty\ ; \tag{3.5}$$

$$\sigma_{zz}^{(1)}(x, -h) = \begin{cases} -p(x) = -\dfrac{P}{\pi}f(x), & 0 \leq |x| \leq a\ , \\ 0, & a < |x| < \infty; \end{cases} \tag{3.6}$$

$$\sigma_{xz}^{(1)}(x, 0) = 0, \qquad 0 \leq |x| < \infty; \tag{3.7}$$

$$\sigma_{xz}^{(2)}(x, 0) = 0, \qquad 0 \leq |x| < \infty\ ; \tag{3.8}$$

$$\sigma_{zz}^{(1)}(x, 0) = \sigma_{zz}^{(2)}(x, 0) \leq 0, \qquad 0 \leq |x| < \infty; \tag{3.9}$$

$$\sigma_{zz}^{(2)}(x, 0) = 0, \qquad c < |x| < \infty; \tag{3.10}$$

$$\frac{\partial u_z^{(1)}(x,0)}{\partial x} = \frac{\partial u_z^{(2)}(x,0)}{\partial x}, \quad 0 \le |x| < c \,, \tag{3.11}$$

where the uknown length of contact between the layer and the base is $2c$. The superscripts 1 and 2 in Eqs. (3.1) – (3.11) refer to the layer and base, respectively. As the normal displacements in the contact region are continuous, we write the boundary condition (3.11) in the form of a derivative to avoid involvement of rigid body displacements.

From boundary conditions (3.5) – (3.9) and using (2.11), (3.1) – (3.4), we get

$$\xi A(\xi)\ (1+\lambda_1^{(1)})/\delta_1^{(1)} = -C(\xi)\ (1+\lambda_2^{(1)})/\delta_2^{(1)}, \tag{3.12}$$

$$\xi B(\xi)\ (1+\lambda_1^{(1)}) + D(\xi)\ (1+\lambda_2^{(1)}) = -\frac{1}{\xi A_{55}^{(1)}}\hat{p}(\xi), \tag{3.13}$$

$$\left\{\xi(1+\lambda_1^{(1)})/\delta_1^{(1)}\right\}\left[A(\xi)\ \mathrm{ch}(\xi h/\delta_1^{(1)}) + B(\xi)\ \mathrm{sh}(\xi h/\delta_1^{(1)})\right] = -\left\{(1+\lambda_2^{(1)})/\delta_2^{(1)}\right\}\left[C(\xi)\ \mathrm{ch}(\xi h/\delta_2^{(1)}) + D(\xi)\ \mathrm{sh}(\xi h/\delta_2^{(1)})\right], \tag{3.14}$$

$$\xi E(\xi)(1+\lambda_1^{(2)})/\delta_1^{(2)} = -F(\xi)\ (1+\lambda_2^{(2)})/\delta_2^{(2)}\,, \tag{3.15}$$

$$\xi\left[(1+\lambda_1^{(1)})\left\{A(\xi)\ \mathrm{sh}(\xi h/\delta_1^{(1)}) + B(\xi)\ \mathrm{ch}(\xi h/\delta_1^{(1)})\right\} - \zeta(1+\lambda_1^{(2)})E(\xi)\right] = -(1+\lambda_2^{(1)})\left\{C(\xi)\ \mathrm{sh}(\xi h/\delta_2^{(1)}) + D(\xi)\ \mathrm{ch}(\xi h/\delta_2^{(1)})\right\} + \zeta(1+\lambda_2^{(2)})F(\xi), \tag{3.16}$$

where

$$\hat{p}(\xi) = (2/\pi)\int_0^a p(x)\ \cos\xi x\ dx\,, \tag{3.17}$$

$$\zeta = A_{55}^{(2)}/A_{55}^{(1)}\,. \tag{3.18}$$

Equation (3.17) is the Fourier cosine transform of the normal tractions acting on the top surface of the layer. Using Eqs. (3.12), (3.13), (3,15) we get from (3.14) and (3.16)

$$A(\xi) = \left\{\delta_1^{(1)}/L_1(\xi)\right\}\left[\left\{\hat{p}(\xi)\ \mathrm{sh}(\xi h/\delta_2^{(1)})\right\} / \left\{\xi^2 A_{55}^{(1)}\delta_2^{(1)}(1+\lambda_1^{(1)})\right\} + B(\xi)L_2(\xi)\right], \tag{3.19}$$

$$B(\xi) = \frac{1}{(1+\lambda_1^{(1)})L_3(\xi)}\left[\zeta\eta_1(1+\lambda_1^{(2)})E(\xi)L_1(\xi) + \frac{\hat{p}(\xi)L_4(\xi)}{\xi^2 A_{55}^{(1)}}\right], \tag{3.20}$$

where

$$L_1(\xi) = \operatorname{ch}(\xi h/\delta_1^{(1)}) - \operatorname{ch}(\xi h/\delta_2^{(1)}), \tag{3.21}$$

$$L_2(\xi) = (1/\delta_2^{(1)})\operatorname{sh}(\xi h/\delta_2^{(1)}) - (1/\delta_1^{(1)})\operatorname{sh}(\xi h/\delta_1^{(1)}), \tag{3.22}$$

$$L_3(\xi) = 2 - 2\operatorname{ch}(\xi h/\delta_1^{(1)})\operatorname{ch}(\xi h/\delta_2^{(1)}) + (\delta_1^{(1)}/\delta_2^{(1)} + \delta_2^{(1)}/\delta_1^{(1)})\operatorname{sh}(\xi h/\delta_1^{(1)})\operatorname{sh}(\xi h//\sigma_2^{(1)}), \tag{3.23}$$

$$L_4(\xi) = \operatorname{ch}(\xi h/\delta_1^{(1)})\operatorname{ch}(\xi h/\delta_2^{(1)}) - (\delta_1^{(1)}/\delta_2^{(1)})\operatorname{sh}(\xi h/\delta_1^{(1)})\operatorname{sh}(\xi h/\delta_2^{(1)}) - 1, \tag{3.24}$$

$$\eta_1 = 1 - (\delta_2^{(2)}/\delta_1^{(2)}). \tag{3.25}$$

From boundary condition (3.10) and Eq. (3.15), we obtain

$$\int_0^\infty \xi^2 E(\xi) \cos \xi x \, d\xi = 0, \qquad c < |x| < \infty \, . \tag{3.26}$$

Using the result [3]

$$\int_0^\infty J_0(\xi t) \cos \xi x \, d\xi = \begin{cases} 0, & 0 < t < x, \\ 1/\sqrt{t^2 - x^2}, & 0 < x < t \end{cases} \tag{3.27}$$

Eq. (3.26) is identically satisfied if we take

$$E(\xi) = -\xi^{-2} \int_0^c M(t) J_0(\xi t) \, dt, \tag{3.28}$$

where $M(t)$ is an unknown function which will be determined so as to satisfy the last boundary condition (3.11). Using Eqs. (3.12), (3.13), (3.15), (3.19), (3.20) and (3.28), the boundary condition (3.11) reduces, after some calculations, to

$$\int_0^c M(t) \int_0^\infty T_1(\xi) J_0(\xi t) \sin \xi x \, d\xi \, dt = \eta_2 \int_0^\infty T_2(\xi) \, \hat{p}(\xi) \sin \xi x \, d\xi \, , \tag{3.29}$$

where

$$\eta_2 = \frac{\left(\lambda_1^{(1)}/\delta_1^{(1)}\right) - \left[\left\{\lambda_2^{(1)}(1+\lambda_1^{(1)})\right\} / \left\{\delta_1^{(1)}(1+\lambda_2^{(1)})\right\}\right]}{(\lambda_1^{(2)}/\delta_1^{(2)}) - \left[\left\{\lambda_2^{(2)}(1+\lambda_1^{(2)})\right\} / \left\{\delta_1^{(2)}(1+\lambda_2^{(2)})\right\}\right]}, \tag{3.30}$$

$$T_1(\xi) = 1 + \frac{\zeta\eta_1\eta_2(1+\lambda_1^{(2)})}{(1+\lambda_1^{(1)})L_3(\xi)} \left[\left(\delta_1^{(1)}/\delta_2^{(1)}\right) \mathrm{sh}\left(\xi h/\delta_2^{(1)}\right) \mathrm{ch}\left(\xi h/\delta_1^{(1)}\right) - \mathrm{sh}(\xi h/\delta_1^{(1)})\mathrm{ch}(\xi h/\delta_2^{(1)}) \right] , \tag{3.31}$$

$$T_2(\xi) = \left\{\delta_1^{(1)} L_2(\xi)\right\} / \left\{A_{55}^{(1)}\left(1+\lambda_1^{(1)}\right) L_3(\xi)\right\} . \tag{3.32}$$

We observe that the integrals in Eq. (3.29) have singularities at $\xi = 0$ which poses the convergence problem for the integrals. This difficulty can be eliminated by taking advantage of the fact that the load applied over the interval $|x| \leq c$ on the top surface of the layer is balanced by the contact pressure acting over $|x| < c$ on the bottom surface. So from Eq. (2.11) and using (3.28), we get

$$\frac{\sigma_{zz}^{(2)}(x,\ 0)}{A_{55}^{(2)}} = -\eta_1\left(1+\lambda_1^{(2)}\right) \int_0^c M(t) \int_0^\infty J_0(\xi t)\ \cos\ \xi x\ d\xi\ dt\ . \tag{3.33}$$

Using (3.27), Eq. (3.33) reduced to

$$\frac{\sigma_{zz}^{(2)}(x,\ 0)}{A_{55}^{(2)}} = -\eta_1\left(1+\lambda_1^{(2)}\right) \int_x^c \frac{M(t)}{\sqrt{t^2-x^2}}\ dt, \quad 0 \leq x < c\ . \tag{3.34}$$

From Eq. (3.34) it is clear that if $M(t)$ is finite in $[0, c]$, the contact pressure vanishes as $x \to c$.

The condition of equilibrium is given by

$$\int_0^c \sigma_{zz}^{(2)}(x,\ 0)\mathrm{d}x = -\int_0^a p(x)\ \mathrm{d}x = -\frac{1}{2}P\ . \tag{3.35}$$

Substituting Eq. (3.34) into (3.35) we get

$$\eta_1 A_{55}^{(2)}\left(1+\lambda_1^{(2)}\right) \int_0^c M(t)dt = \frac{2}{\pi}\int_0^a p(x)\ dx = \hat{p}(0) = \frac{P}{\pi}\hat{f}(0). \tag{3.36}$$

Rewrite Eq. (3.29) in the form

$$(1+\eta_3\eta_4) \int_0^c M(t) \int_0^\infty J_0(\xi t)\ \sin\ \xi x\ d\xi\ dt\ d\xi + \frac{\zeta\eta_1\eta_2\left(1+\lambda_1^{(2)}\right)}{\left(1+\lambda_1^{(1)}\right)} \cdot \int_0^c M(t) \int_0^\infty [\{L_5(\xi)/L_3(\xi)\} - \eta_3]\, J_0(\xi t) \times \sin\ \xi x\ d\xi\ dt - \eta_2 \int_0^\infty T_2(\xi)\hat{p}(\xi)\ \sin\xi x\ dx\ d\xi = 0, \tag{3.37}$$

where

$$\eta_3 = \left\{1 - \left(\delta_2^{(1)}/\delta_1^{(1)}\right)\right\}^{-1}, \tag{3.38}$$

$$\eta_4 = \zeta\eta_1\eta_2\left(1+\lambda_1^{(2)}\right)/\left(1+\lambda_1^{(1)}\right), \tag{3.39}$$

$$L_5(\xi) = \left(\delta_1^{(1)}/\delta_2^{(1)}\right) \operatorname{sh}\left(\xi h/\delta_2^{(1)}\right) \operatorname{ch}\left(\xi h/\delta_1^{(1)}\right) - \operatorname{sh}\left(\xi h/\delta_1^{(1)}\right) \operatorname{ch}\left(\xi h/\delta_2^{(1)}\right). \tag{3.40}$$

Using Eq. (3.36) and the result [3]

$$\int_0^\infty J_0(\xi t)\, \sin\xi x\, d\xi = \begin{cases} \dfrac{1}{\sqrt{x^2-t^2}}, & 0<t<x\,, \\ 0, & 0<x<t \end{cases} \tag{3.41}$$

the integral equation (3.37) reduces to

$$(1+\eta_3\eta_4)\int_0^x \frac{M(t)\,dt}{\sqrt{x^2-t^2}} + \frac{\zeta\eta_1\eta_2\left(1+\lambda_1^{(2)}\right)}{\left(1+\lambda_1^{(1)}\right)}\int_0^c M(t)\int_0^\infty \frac{1}{L_3(\xi)} \cdot \left[\left\{L_5(\xi)-\eta_3 L_3(\xi)\right\} J_0(\xi t) - \delta_1^{(1)} L_2(\xi)\hat{f}(\xi)\right] \sin\,\xi x\, d\xi\, dt = 0\,. \tag{3.42}$$

Although the second integral in Eq. (3.42) is an unknown function of x, considering Eq. (3.42) as an Abel's integral equation and solving for $M(t)$, we get a homogeneous Fredholm integral equation of the second kind of the form

$$\int_0^c U(s,t)\, M(t)\, dt = \frac{2}{1+\alpha} M(s)\,, \tag{3.43}$$

where

$$U(s,t) = \frac{S}{\eta_3}\int_0^\infty \frac{1}{L_3(\xi)}\left[\delta_1^{(1)} L_2(\xi)\, \hat{f}(\xi) - \left\{L_5(\xi)-\eta_3 L_3(\xi)\right\} J_0(\xi t)\right] \xi J_0(\xi s)\, d\xi, \tag{3.44}$$

$$\alpha = (Q_2 - Q_1)/(Q_2+Q_1)\,, \tag{3.45}$$

$$(3.46) \qquad Q_1 = A_{11}^{(2)} A_{55}^{(1)} \left(A_{13}^{(1)} + A_{55}^{(1)}\right) \left(1 + \lambda_1^{(1)}\right) \left(1 + \lambda_2^{(1)}\right) \left(\delta_1^{(2)} + \delta_2^{(2)}\right),$$

$$(3.47) \qquad Q_2 = A_{11}^{(1)} A_{55}^{(2)} \left(A_{13}^{(2)} + A_{55}^{(2)}\right) \left(1 + \lambda_1^{(2)}\right) \left(1 + \lambda_2^{(2)}\right) \left(\delta_1^{(1)} + \delta_2^{(1)}\right).$$

It is evident from Eqs. (3.45), (3.46), (3.47) that the parameter α depends on the elastic constants of both the media. For a given combination of materials, α is known and hence Eq. (3.43) determines the extent of contact between the bodies. But it would be more convenient from the mathematical point of view to consider Eq. (3.43) as an eigenvalue problem for the eigenfunction $M(t)$. This may be done by considering c as specified and determining the eigenvalue $2/(1+\alpha)$ of the homogeneous integral equation (3.43) for which the extent of contact c is realized. Eigenvalues are determined by considering physically possible values of α, and then the corresponding eigenfunction $M(t)$ determines the pressure in the contact zone from Eq. (3.34).

From Eq. (3.43) it is observed that in contrast to isotropic materials, the contact region and contact pressure are not functions of a single parameter depending on the elastic constants of the two media, and even if the layer and the half-space are of the same orthotropic material, the contact region and the contact pressure are not completely independent of the elastic parameters, which was predicted by the general results for isotropic medium in [2], and was verified later in [4].

4. Numerical results

To determine the eigenfunction $M(t)$ corresponding to the eigenvalue $2/(1+\alpha)$ of Eq. (3.43), we discretise the integral to get a system of linear homogeneous equations in $M(t_1)$. For a specified value of c, the determination of $M(t_1)$ demands nonvanishing of the coefficient determinant. This in turn requires choosing appropriate values of α such that the coefficient determinant should be nonzero and the value of α should be acceptable on physical grounds. It may be observed that on physical grounds, α should satisfy the inequality $-1 \leq \alpha \leq 1$. Moreover, it is necessary that the corresponding eigenvector $M(t_1)$ should yield purely compressive tractions in the zone of contact. In all cases the components of the eigenvector associated with an admissible value of α are of the same sign. In this problem, the results have been computed for the concentrated force for which $\hat{f}(\xi) = 1$. During the numerical computations for orthotropic materials we have used the values 2.862 and 0.047 for $\delta_1^{(1)^2}$ and $\delta_2^{(1)^2}$, respectively, for boron-epoxy composite material as given in [1]. The curves of c/h versus α for orthotropic and isotropic materials are shown in Fig. 2. The contact tractions may be calculated from Eq. (3.43) and are shown in Fig. 3 and Fig. 4 for orthotropic and isotropic cases, respectively.

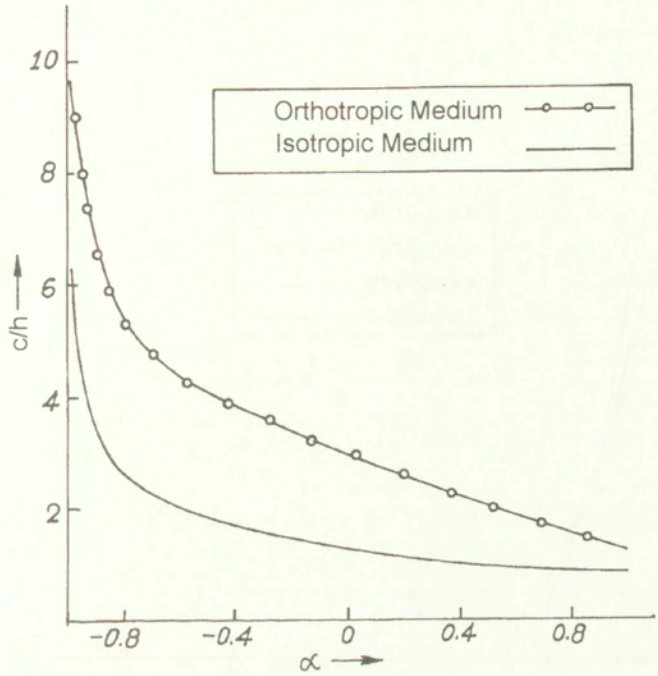

FIG. 2. Extent of contact for loading by a concentrated force in plane problem.

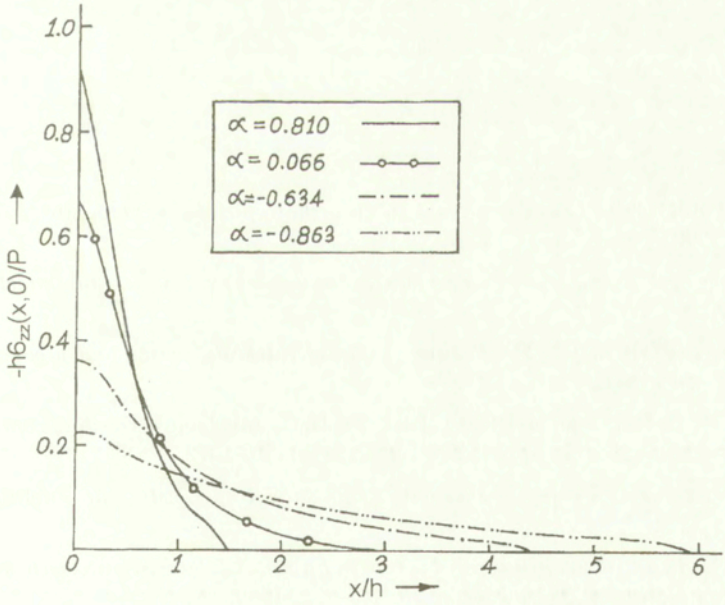

FIG. 3. Contact pressure for loading by a concentrated force in plane problem for orthotropic medium.

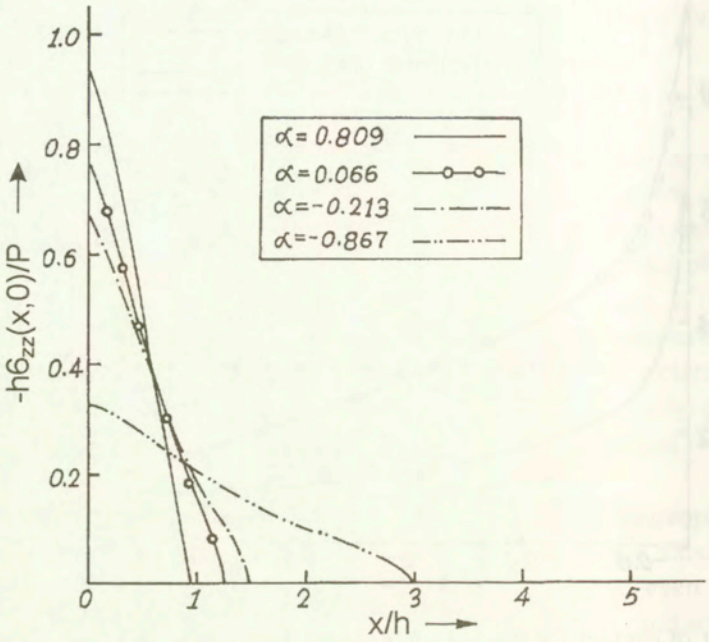

FIG. 4. Contact pressure for loading by a concentrated force in plane problem for isotropic medium.

References

1. J. DE and B. PATRA, *Cruciform crack in an orthotropic elastic plane*, Int. J. Fracture, **53**, 387–397, 1992.

2. J. DUNDURS and M. STIPPES, *Role of elastic constants in certain contact problems*, J. Appl. Mech., **37**, 965–970, 1970.

3. I. S. GRADSHTEYN and I. M. RYZHIK, *Table of integrals, series and products*, Academic Press, Inc., New York 731.

4. L. M. KEER, J. DUNDURS and K. C. TSAI, *Problems involving a receding contact between a layer and a half-space*, J. Appl. Mech., **39**, 1115–1120, 1972.

5. S. G. LEKHNITSKII, *Theory of elasticity of an anisotropic body*, Mir Publishers, Moscow 1963.

6. H. LI and J. P. DEMPSEY, *Unbonded contact of a square plate on an elastic half-space or a Winkler foundation*, J. Appl. Mech., **55**, 430–435, 1988.

7. S. l. PU and M. A. HUSSAIN, *Note on the unbonded contact between plates and an elastic half-space*, J. Appl. Mech., **37**, 859–861, 1970.

8. Y. WEITSMAN, *On the unbonded contact between plates and an elastic half-space*, J. Appl. Mech., **36**, 198–202, 1969.

9. H. B. WILSON, Jr., and J. G. GOREE, *Axisymmetric contact stresses about a smooth elastic sphere in an infinite solid stressed uniformly at infinity*, J. Appl. Mech., **34**, 960–966, 1967.

DEPARTMENT OF APPLIED MATHEMATICS
UNIVERSITY COLLEGE OF SCIENCE

92, Acharya Prafulla Chandra Road,
Calcutta – 700 009, India

Received February 20, 1997; new version March 13, 1998

Arch. Mech., 50, 4, pp. 757–789, Warszawa 1998
FIFTY YEARS OF THE ARCHIVES OF MECHANICS

Plastic inclusion with moving boundary. Application to dislocation cell structures

X. LEMOINE, H. SABAR, M. BERVEILLER (METZ)
and J. MORREALE (FLORANGE)

BASED ON THE DETERMINATION of the Helmholtz free energy and the dissipation of an elastoplastic solid containing moving surfaces of plastic strain discontinuity, a micromechanical approach is developed to study the formation of dislocation cell structure and their effects on the mechanical behavior of metals. The results are applied to an evolutive two-phase microstructure representing the dislocation cell structure induced during plastic straining. The internal variables are reduced to the plastic strain of each mechanical phase, the volume fraction and the morphology of the ellipsoidal inclusion describing the cell structure. We obtain the conjugate forces according to the formalism of irreversible thermodynamics. Complementary relations describing the evolution of these internal variables are introduced in order to obtain the constitutive equation for the grain, the evolution of the microstructure as well as the hardening of the two phases. Preliminary results are presented and discussed in the case of a simplified situation.

1. Introduction

THE MODELLING of the elastoplastic behavior of metals and alloys from physical mechanisms (motion, storage and annihilation of dislocations) and the polycrystalline microstructure of the volume element (texture, grain boundaries) constitutes a difficult task requiring the introduction of different scales of description as well as scale transition methods. Classical meso-macro models (TAYLOR [1], SACHS [2], Self-consistent [3, 4]) taking into account the granular structure of the polycrystal, are based on the hypothesis of homogeneous multiple slip at the intragranular scale and a perfect intergranular interface (no debonding). Thus, using a self-consistent model formulated for large plastic strains [5, 6], the results obtained are by many aspects in good agreement with experiments, both for the overall behavior and the evolution of the internal state corresponding to texture, internal stresses and stored energy.

This description shows, however, its limits when applied to the description of the hardening during complex loading, studied experimentaly by HU and TEODOSIU [7]. It appears clearly that refining of the meso-macro transition has no sense except the case when the description of the intracrystalline behavior is improved to take into account the intragranular heterogeneization of the plastic deformation corresponding to the formation of dislocation cells.

The heterogeneity of the intragranular plastic strain field results from different mechanisms:

- the subdivision of a grain into zones with homogeneous single or multiple slip, related mainly to the discrete nature of the neighbouring grains [8];
- the formation of micro-shear bands corresponds to an intense localized shear [9, 10];
- the development of dislocation cells results from selforganization of the microstructure simultaneously due to the long range stress field, junction reactions between dislocations and mechanisms of annihilation related to the nature of the dislocations [11, 12].

The essential characteristics of the cellular structure may be summarized as follows:

- the formation of cells corresponds to a heterogeneous plastic strain field, weak inside walls and large in the cell interior;
- their topological and morphological aspects depend strongly on the macroscopic loading [13, 14];
- high dislocations density leads to a large hardening corresponding to a pronounced nonlocal effect, since plastic strain inside the cells increases the hardening in the walls where the dislocations are stored [15];
- finally, during sequential loading, the partial dissolution of the microstructure built during the first loading path is accompanied often by the formation of a new microstructure characteristic of the second loading path.

The current models describing the formation of dislocation cells can be cla ssified in three groups:

- Using numerical techniques based on cellular automatons [16, 18], discrete dislocations motion, multiplication and annihilation as well as storage can be described. Besides the huge memory and important CPU time required, these models are based on very specific boundary conditions and the dislocations move individually in a sequential manner so that collective behavior is absent.
- Considering plasticity described by the crystallographic slip mechanisms, AIFANTIS [19] and other authors have added a second gradient to the constitutive equation, to introduce a characteristic length and to reproduce the development of cells. Models using the concept of nonlocal hardening [20, 21] have also been introduced to describe the formation of cells and the intragranular plastic heterogeneization. The concept is indoubtedly correct, nevertheless it remains to ensure the validity of the introduced differential or integral operator which constitutes a difficult task.
- The first attempt for the description of dislocation cells, proposed by MUGHRABI and ESSMANN [11] is based on the representation of the cellular structure by a two-phase mechanical structure where the morphology of cells is *a priori* imposed, neglecting the effect of the external loading.

The aim of this paper is to formulate a model for the formation and evolution of the dislocation cells structure in the classical framework of crystal-plasticity (slip mechanism). In classical micromechanical description of the polycrystal, the discrete motion, interaction and storage of dislocations at grain boundaries are described using the slip rate as an average process variable. Continuity of displacement, velocity of particles and stress vector are required at grain boundaries. According to that, only (second order) long-range internal stresses are taken into account; pile ups at grain boundaries and discrete slip lines are neglected. One follows the same scheme of simplification for the intragranular heterogeneization corresponding to the formation of cell structures (Fig. 2). Dislocations are supposed to move inside the cells and walls and are stored in internal boundaries. It is worthwhile to notice that these walls are free surfaces, contrary to the grain boundaries, so that their morphological characteristics (shape, orientation) become new variables. Therefore, as in classical micromechanical plasticity, the plastification is still represented by slip rate inside the cells and the walls which are assumed to be moving boundaries. In such a way, one loses the precise description of the microstructure inside the walls but the (third order) long-range internal stresses are taken into account. For mobile boundaries, continuity of displacement and stress vector are always needed but the motion of the free surface allows some discontinuity in the particle velocity leading to a more complex problem.

In order to reduce the number of parameters describing the microstructure, one assumes that the cells may be considered as ellipsoidal inclusions with moving boundaries. This last assumption makes the model different from the previous one (Mughrabi) which assumes a fixed boundary.

In the second part, we determine the dissipation of an elastoplastic single crystal containing moving surfaces of plastic discontinuity from the evolution of the Helmholtz free energy and the power of external load. The results are applied in part 3 to an evolutive two-phase microstructure representing the dislocation cells structure inside the grain. In this way, the internal state and process variables reduce to the plastic strain of each phase, the volume fraction and the morphology of the ellipsoidal inclusion inside the grains of the polycrystal.

Complementary laws are introduced in order to obtain the constitutive equation for the grains, the evolution of the microstructure as well as the hardening of the two intragranular phases.

The transition from the grain level to the polycrystal is achieved by a classical elastoplastic self-consistent model described in [4, 5, 6].

Prelininary results are presented and discussed in the situation where the proportion of phases are treated as material parameters [13] and the concept of "Low Energy Dislocations Structures" (LEDS) [22, 23] is adopted to define the morphology of the microstructure.

2. Thermomechanical approach of mobile surface with plastic discontinuity

In this part the kinematical and thermodynamical aspects of a solid containing mobile surface discontinuities of plastic strain are developed. From the Helmholtz free energy, the intrinsic dissipation associated with the progress of the plastic deformation and the motion of surface discontinuities is given.

2.1. The kinematical description

Let us consider a solid with volume V bounded by an external surface ∂V. The reference configuration is assumed to be stress-free. The current configuration corresponds to V loaded by the displacement u^d on the boundary ∂V. We denote by $u(r)$ the total compatible displacement field of a point $r(x_1, x_2, x_3)$ from the reference configuration to the current one. The total distortion field $\beta(r)$ is given from the displacement gradient:

$$\beta(r) = \nabla \oplus u(r), \quad (\beta_{ij} = u_{i,j}) \,. \tag{2.1}$$

This total distortion results from:

- an elastic part $\beta^e(r)$, and
- a plastic part $\beta^p(r)$ with some discontinuity along surfaces S separating the volumes occupied by the plastic phases so that, in the small perturbation hypothesis, one obtains:

$$\beta(r) = \beta^e(r) + \beta^p(r). \tag{2.2}$$

Two fundamental tensors are derived from (2.1), the strain tensor being the symmetrical part of $\beta(r)$:

$$\varepsilon(r) = \frac{1}{2}(\beta(r) + {}^t\beta(r)) \tag{2.3}$$

and, the spin being its antisymmetrical part,

$$\omega(r) = \frac{1}{2}(\beta(r) - {}^t\beta(r)). \tag{2.4}$$

Combining (2.2), (2.3) and (2.4), the following expressions are obtained:

$$\begin{aligned} \beta(r) &= \varepsilon(r) + \omega(r), \\ \beta^e(r) &= \varepsilon^e(r) + \omega^e(r), \\ \beta^p(r) &= \varepsilon^p(r) + \omega^p(r) \,. \end{aligned} \tag{2.5}$$

When the solid is submitted to homogeneous distortion boundary conditions $u_i^d(r) = B_{ij}x_j$, the average B over V of the internal distorsion field β is given by

$$B = \frac{1}{V}\int_V \beta(r)dV = \frac{1}{V}\int_V (\beta^e(r) + \beta^p(r)dV. \tag{2.6}$$

For homogeneous elastic behavior, Eq. (2.6) leads to:

$$B = B^e + B^p, \tag{2.7}$$

where B^e and B^p are, respectively, the macroscopic elastic and plastic parts of the overall distorsion. They are defined by

$$\begin{aligned} B^e &= \frac{1}{V}\int_V \beta^e(r)dV, \\ B^p &= \frac{1}{V}\int_V \beta^p(r)dV. \end{aligned} \tag{2.8}$$

Decomposition (2.5) is also applied to macroscopic quantities:

$$\begin{aligned} B &= E + \Omega, \\ B^e &= E^e + \Omega^e\,, \\ B^p &= E^p + \Omega^p\,. \end{aligned} \tag{2.9}$$

The time evolution of B^p is related with an evolution of $\beta^p(r)$ and a motion of internal surfaces S.

The first step consists in taking the time derivative of $(2.8)_2$ where the local plastic distortion $\beta^p(r)$ is discontinuous across the surface S; S moves with time because the evolution of $\beta^p(r)$ is accompanied by a geometrical extension of the plastic phases. The time derivative of a volume integral containing a discontinuous integrand through a moving surface is given for instance in GERMAIN [24], and leads to

$$\dot{B}^p = \frac{d}{dt}\left[\frac{1}{V}\int_V \beta^p(r)dV\right] = \frac{1}{V}\int_V \dot{\beta}^p(r)dV - \frac{1}{V}\int_S [\beta^p(r)]w_\alpha n_\alpha dS. \tag{2.10}$$

In this equation $\dot{\beta}^p = \partial\beta^p/\partial t$ is the plastic distortion rate in all different plastic phases, $[\beta^p(r)] = \beta^{p^+} - \beta^{p^-}$ denotes the jump of $\beta^p(r)$ when crossing S, n_i is the unit normal to S taken from the negative to positive side, and w_α is the velocity of S (Fig. 1). $\dot{\beta}^p$ is the macroscopic plastic distortion rate, containing the evolution of the microstructure. It is difficult to get $\dot{\beta}^p$ for any distribution of

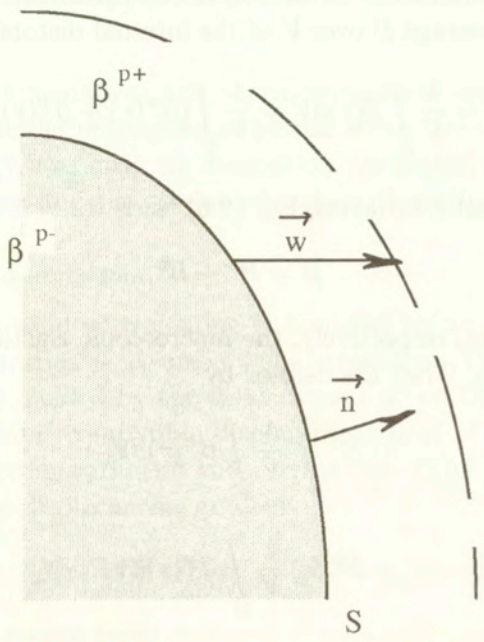

FIG. 1. Jump of plastic distorsion across a moving surface S.

plastic heterogeneity. To account for the cell dislocation structure, a two-phase approximation seems to be well adapted.

Case of a two-phase material

In this case, one assumes that the solid V consists of the assembly of two phases with respective volumes V^1 and V^2. The boundary between phases is given by mobile surface S. One notes that the unit normal n_i to S and the velocity w_α of S are directed into V^2.

If one assumes that the intra-phase heterogeneities are weak in comparison with the interphase one, $(2.8)_2$ becomes, for the two-phase material:

$$B^p = f\beta^{p_1} + (1-f)\beta^{p_2}, \tag{2.11}$$

where $f = V^1/V$ and $1 - f = V^2/V$ are, respectively, the volume fraction of phases 1 and 2. β^{p_1} and β^{p_2} are, respectively, the mean plastic distortions in V^1 and V^2 defined by:

$$\beta^{p_\alpha} = \frac{1}{V_\alpha}\int_{V\alpha} \beta^p(r)dV, \qquad (\alpha = 1, 2).$$

During the evolution, two contributions can be distinguished in (2.10):

• The first one corresponds to the volumic variation of plastic distortion and is written in this case:

$$\frac{1}{V}\int_V \dot{\beta}(r)dV = f\dot{\beta}^{p_1} + (1-f)\dot{\beta}^{p_2}.$$

• The second one is the contribution due to the motion of surface S. Assuming that $[\beta^p(r)]$ is uniform over the surface S and equal to $\beta^{p_2} - \beta^{p_1}$ and taking into account the obvious relation $\dot{f} = \frac{1}{V}\int_S w_\alpha n_\alpha dS$, one obtains

$$\frac{1}{V}\int_S [\beta^p(r)] w_\alpha n_\alpha dS = [\beta^p]\dot{f}.$$

With these expressions, (2.10) is reduced to

$$\dot{B}^p = f\dot{\beta}^{p_1} + (1-f)\dot{\beta}^{p_2} - [\beta^p]\dot{f}. \tag{2.12}$$

Equations (2.10) and (2.12) indicate the nature of internal variables describing the inelastic behavior of the solid:

• plastic flow in the two phases,

• the motion of surface between these phases or the evolution of the voluminal fraction f.

The evolution of these internal variables are deduced from a thermodynamic analysis giving the thermodynamical forces in the internal variables.

2.2. The thermomechanical description

The evolution of a thermodynamical system with irreversible processes is derived generally from the maximal dissipation principe [25, 26]. In the case of quasi-static and isothermal approximation, the dissipation is given by the difference between the external power and the variation of the Helmholtz free energy.

In the following, one calculates successively the free energy, its time derivative, the external power and the intrinsic dissipation for a solid containing mobile discontinuity surfaces.

2.2.1. Helmholtz free energy. In case of isothermal approximation, the Helmholtz free energy density reduces to elastic energy:

$$w(r) = \frac{1}{2}\sigma(r) : \varepsilon^e(r).$$

For a volume V, we have:

$$W = \int_V w(r)dV. \tag{2.13}$$

The stress tensor $\sigma(r)$ and elastic strain $\varepsilon^e(r)$ are related by the usual constitutive relations:

$$\sigma(r) = C : \varepsilon^e(r), \tag{2.14}$$

where the homogeneous elastic moduli C exhibit the usual symmetries:

$$C_{ijkl} = C_{jikl} = C_{ijlk} = C_{klij}. \tag{2.15}$$

Using (2.2), (2.3) and (2.5)

$$\varepsilon(r) = \varepsilon^e(r) + \varepsilon^p(r), \tag{2.16}$$

the Helmholtz free energy (2.13) is written as

$$W = \frac{1}{2}\int_V \sigma(r) : (\varepsilon(r) - \varepsilon^p(r))\, dV. \tag{2.17}$$

2.2.2. Evolution of the Helmholtz free energy. For a load variation, the evolution of the Helmholtz free energy results from the progress of plastic strain $\varepsilon^p(r)$ and the propagation of discontinuity surface S. The jump of $\varepsilon^p(r)$ across S implies the discontinuities of $\varepsilon(r)$, $\sigma(r)$ and $w(r)$. By time differentiation of (2.13), the evolution of Helmholtz free energy of the system is given by

$$\dot{W} = \int_V \dot{w}(r)dV - \int_S [w(r)]w_\alpha n_\alpha dS. \tag{2.18}$$

Due to the symmetry of C and using (2.14) and (2.16), the first integral is transformed into

$$\int_V \dot{w}(r)dV = \int_V \sigma(r) : (\dot{\varepsilon}(r) - \dot{\varepsilon}^p(r))dV. \tag{2.19}$$

Assuming uniform elasticity, $[w]$ is expressed by

$$[w] = \frac{1}{2}\left\{\sigma^+(r) : (\varepsilon^+(r) - \varepsilon^{p+}(r)) - \sigma^-(r) : (\varepsilon^-(r) - \varepsilon^{p-}(r))\right\} \tag{2.20}$$

or

$$[w] = \frac{1}{2}\left\{\sigma^+(r) + \sigma^-(r)\right\} : [\varepsilon(r) - \varepsilon^p(r)]. \tag{2.21}$$

From (2.19) and (2.21), (2.18) is given by

$$\dot{W} = \int_V \sigma(r) : (\dot{\varepsilon}(r) - \dot{\varepsilon}^p(r))dV - \frac{1}{2}\int_S \{\sigma^+(r) + \sigma^-(r)\} : [\varepsilon(r) - \varepsilon^p(r)]w_\alpha n_\alpha dS\,. \tag{2.22}$$

2.2.3. External power. The power $\mathcal{P}_{\text{ext}}$ developed by the forces $T_i = \sigma_{ij} n_j$ applied to the external surface S^{ex} of volume V associated with the particle velocity $\nu_i (= \dot{u}_i)$ is defined by

$$\mathcal{P}_{\text{est}} = \int_{S^{\text{ex}}} T_i \nu_i dS^{\text{ex}} = \int_{S^{\text{ex}}} \sigma_{ij} n_j \nu_i dS^{\text{ex}}. \tag{2.23}$$

Using the divergence theorem, when the volume V contains a discontinuity surface S, the surface integral (2.23) is transformed to a volume integral:

$$\mathcal{P}_{\text{ext}} = \int_V (\sigma_{ij} \nu_i)_{,j} \, dV + \int_S [\sigma_{ij} n_j \nu_i] dS. \tag{2.24}$$

The conditions of continuity of the displacement and the interfacial traction across S yield

$$[u_i] = 0 \tag{2.25}$$

and

$$[\sigma_{ij} n_j] = 0. \tag{2.26}$$

During the propagation of the surface S, these conditions hold at any time t. Thus the jump in the components of material velocity ν_i is determined by taking the time derivative of (2.25). One gets the compatibility equation of HADAMARD [27]:

$$[\nu_i] = -[u_{i,j}] n_j w_\alpha n_\alpha. \tag{2.27}$$

From (2.25) and (2.26) and the equilibrium equation, in the absence of volumic forces ($\sigma_{ij,j} = 0$), the power $\mathcal{P}_{\text{ext}}$ becomes:

$$\mathcal{P}_{\text{ext}} = \int_V \sigma_{ij} \nu_{i,j} dV - \int_S \sigma_{ij} n_j [u_{i,k}] n_k w_\alpha n_\alpha dS. \tag{2.28}$$

The continuity of displacement along the surface S imposes the relation on the jump of displacement gradient:

$$[u_{i,j}] = \lambda_i n_j, \tag{2.29}$$

where λ is an arbitrary vector function of position.

The term $\sigma_{ij} n_j [u_{i,k}] n_k$ is also equal to $\sigma_{ij} [u_{i,j}]$ from compatibility conditions (2.25) and (2.26) along the surface S, so that

$$\sigma_{ij} n_j [u_{i,k}] n_k = \sigma_{ij} [\varepsilon_{ij}] = \frac{1}{2} \left\{ \sigma_{ij}^+ + \sigma_{ij}^- \right\} [\varepsilon_{ij}]. \tag{2.30}$$

Using (2.30), the external power is written as

$$\mathcal{P}_{\text{ext}} = \int_V \sigma(r) : \dot{\varepsilon}(r) dV - \frac{1}{2} \int_S \{\sigma^+(r) + \sigma^-(r)\} : [\varepsilon(r)] w_\alpha n_\alpha dS. \tag{2.31}$$

2.2.4. Analysis of the intrinsic dissipation. During the evolution of the system, the intrinsic dissipation is given by

$$\mathcal{D} = \mathcal{P}_{\text{ext}} - \dot{W}. \tag{2.32}$$

Using (2.22) and (2.31), the intrinsic dissipation is finally given by

$$\mathcal{D} = \int_V \sigma(r) : \dot{\varepsilon}^p(r) dV - \frac{1}{2} \int_S \{\sigma^+(r) + \sigma^-(r)\} : [\varepsilon^p(r)] w_\alpha n_\alpha dS. \tag{2.33}$$

The first term in (2.33) is the volume dissipation due to the evolution of plastic strain. The second one is due to the propagation of surface between the phases.

Two quantities appear: the energy release rate $-\frac{1}{2}\{\sigma^+(r) + \sigma^-(r)\} : [\varepsilon^p(r)]$ which corresponds to the thermodynamic force associated with the normal velocity $w_\alpha n_\alpha$ of the surface S, and the thermodynamic force σ associated with the plastic strain rate $\dot{\varepsilon}^p(r)$.

For any microstructure, the determination of the intrinsic dissipation is difficult because the variables describing this internal structure are complex. In the next section, an application of this approach is developed in the case of a two-phase material with ellipsoidal microstructure.

3. Two phase model for a crystal with evolution of microstructure

3.1. Representation of the intragranular microstructure

During plastic strain of a metal, dislocation cells are formed leading to high dislocation density gradients which allows us to describe the cell structure as a two-phase composite, the cell interiors (zones with a low dislocation density) and the walls (zones with a high dislocation density) represented, respectively, by soft (s) and hard (h) phases. This partition of the volume V of a grain into two domains V^s (s = soft) and V^h (h = hard) implies for a macroscopic variable M described as a voluminal average of the corresponding local variable m in V,

$$M = \frac{1}{V} \int_V m(r) dV \tag{3.1}$$

which can be simplified by

$$M = f m^s + (1 - f) m^h, \tag{3.2}$$

where $f = V^s/V$ and $1 - f = V^h/V$ are respectively the volume fraction of soft and hard phases. The average values m^s and m^h are defined by

$$m^\alpha = \frac{1}{V^\alpha} \int_{V^\alpha} m(r)dV, \qquad (\alpha = h, s). \tag{3.3}$$

TEM results show that the dislocation cell shape may be approximated by ellipsoids [13, 28]. This allows us to consider only an averaged description of the cell structure where the cell shape is an ellipsoid with semi-axes $a_i (i = 1, 2, 3)$ and Euler angles $\alpha_i (i = 1, 2, 3)$ describing the orientation of the ellipsoid principal reference frame versus the crystalline lattice. On the other hand, the cell with its dislocation wall is described as a coated inclusion. Thus, the cell is represented by two similar and concentric ellipsoids.

The topology of the coated inclusion problem assumes that an inclusion (interior cell) with plastic strain ε^{P_s} and volume V^s is surrounded by a thin coating of the second phase (wall) with plastic strain ε^{P_h} and volume V^h. The coating is bounded at its outer boundary by a surrounding homogenous material (matrix) whose plastic strain is E^P (Fig. 2). V^e denotes the volume of the composite inclusion (inclusion + coating). If N is the number of cells inside V, one has

$$V = Nv^e = N(v^h + v^s). \tag{3.4}$$

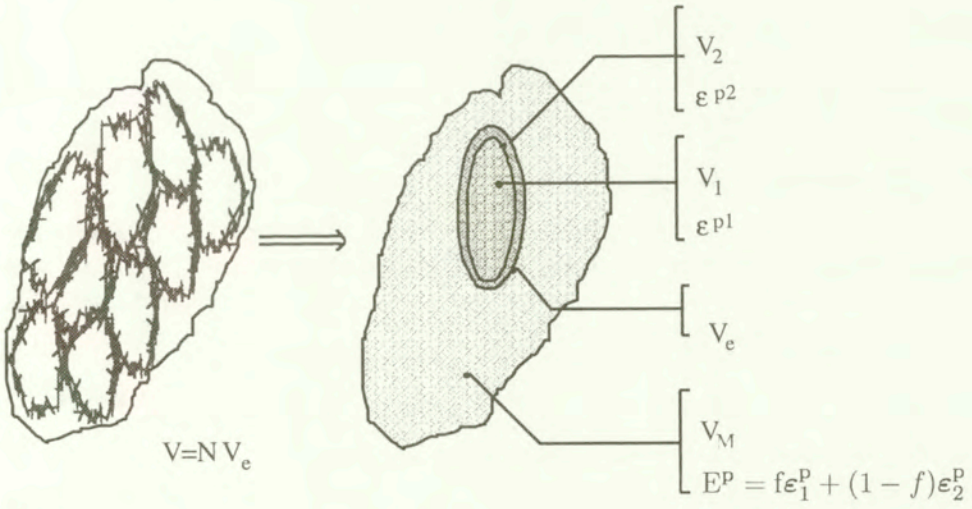

FIG. 2. Simplified representation of the microstructure of dislocation cells by a two-phase material with coated inclusions.

The proportion of the phase h in the grain is supposed to be the same as in the composite inclusion. Thus, the volume fraction of the two phases are given by

$$f = \frac{Nv^s}{V} = \frac{V^S}{V} = \frac{v^S}{v^e}, \tag{3.5}$$

$$1 - f = \frac{Nv^h}{V} = \frac{V^h}{V} = \frac{v^h}{v^e} \,. \tag{3.6}$$

An Eshelby-Kröner-type approximation is used to account for the interactions between the coated inclusions. This approximation assumes that each coated inclusion is embedded in an infinitely extended medium (matrix) having macroscopic plastic strain E^P equal to volume average of the local plastic strain $\varepsilon^p(r)$ on V.

This representation implies that there is no creation of new composite inclusion during the evolution of the system: $\dot{N} = 0$. Thus, with (3.4) and $\dot{V} = 0$ one gets

$$\dot{v}^e = 0. \tag{3.7}$$

Finally, the internal variables describing the microstructure of the grain and the field $\varepsilon^p(r)$ are:

- the plastic strain ε^{P_s} inside the cells,
- the plastic strain ε^{P_h} inside the walls,
- the volume fraction f of cells,
- the morphology of the internal inclusion a_p and α_p described by a tensor $A(a_p, \alpha_p)$ defined by

$$A_{ij} x_i x_j = 1. \tag{3.8}$$

The components A_{ij} can be deduced from the variables a_p and α_p (see Appendix B).

3.2. Calculation of the dissipation

For the simplified representation (Fig. 2) of the microstructure, the dissipation $\mathcal{D}$ resulting from the plastic strain rate $\dot{\varepsilon}^p(r)$ and the motion $w_\alpha n_\alpha$ of surfaces S^1 and S^e surrounding, respectively, v^1 and v^e is calculated. From (2.33), this dissipation is expressed by

$$\mathcal{D} = \int_v \sigma(r) : \dot{\varepsilon}^p(r) dV - \frac{N}{2} \int_{S^1} \left\{ \sigma^{+1}(r) + \sigma^{-1}(r) \right\} : [\varepsilon^p(r)]^1 w_\alpha^1 n_\alpha^1 dS^1 \tag{3.9}$$

$$- \frac{N}{2} \int_{S^e} \left\{ \sigma^{+e}(r) + \sigma^{-e}(r) \right\} : [\varepsilon^p(r)]^e w_\alpha^e n_\alpha^e dS^e$$

or $\mathcal{D} = \mathcal{D}^1 + \mathcal{D}^2 + \mathcal{D}^3$ where $[\varepsilon^p(r)]^e$ and $[\varepsilon^p(r)]^1$ are respectively, the jumps of plastic strain across S^e and S^1. In case of two phases, the plastic strain rate is given by

$$\begin{aligned} \dot{\varepsilon}^p(r) &= \dot{\varepsilon}^{p_s}, \quad r \in V^s, \\ \dot{\varepsilon}^p(r) &= \dot{\varepsilon}^{p_h}, \quad r \in V^h. \end{aligned} \tag{3.10}$$

Consequently, it is possible to evaluate the first integral $\mathcal{D}^1$ in (3.9):

$$\mathcal{D}^1 = N\sigma^s : \dot{\varepsilon}^{p_s} v^s + N v^h \sigma^h : \dot{\varepsilon}^{p_h}, \tag{3.11}$$

where σ^s and σ^h are the mean stress in each phase defined by (3.3).
For the evaluation of the surface integrals in (3.9), an enlargement of the zones near the surfaces S^1 and S^e allows us to determine the interfacial stresses (Fig. 3).

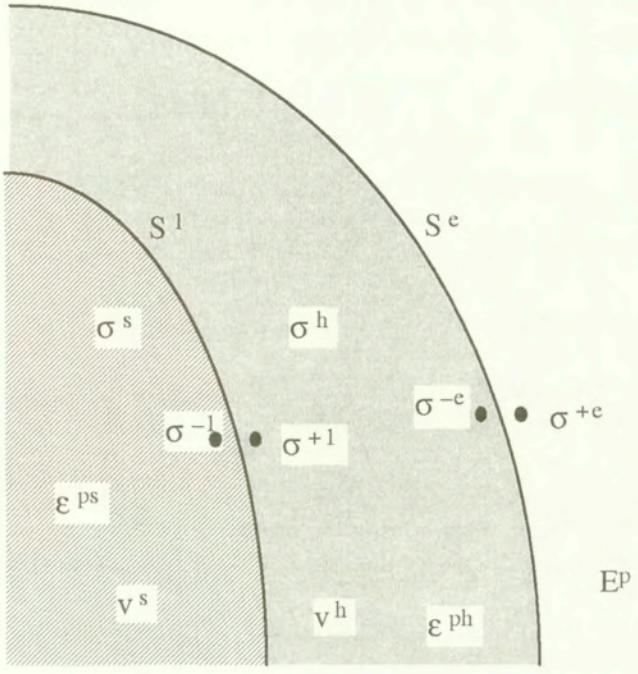

FIG. 3. Definition of stresses near surface S^1 and S^e.

In the second surface integral $\mathcal{D}^2$ in (3.9), the stress σ^{-1} inside the ellipsoid v^1 is uniform and equal to σ^s . This stress is obtained through the Eshelby-Kröner formula [30, 31], namely

$$\sigma^s = \Sigma - (1-f)C : (I - S^E) : \Delta\varepsilon^P, \tag{3.12}$$

where Σ is the macroscopic stress given by (3.1), S^E is the Eshelby tensor for the inclusion v^1 (see Appendix B), I is the fourth order unit tensor, and $\Delta\varepsilon^p = \varepsilon^{p_s} - \varepsilon^{p_h}$. The stress σ^h is deduced from (3.3) and given by

$$\sigma^h = \Sigma + fC : (I - S^E) : \Delta\varepsilon^P. \tag{3.13}$$

Using the interfacial operators [29], the stress σ^{+1} is linked to the stress σ^{-1} by

$$\sigma^{+1} = \sigma^{-1} - Q^1 : [\varepsilon^p]^1 \tag{3.14}$$

with $[\varepsilon^p]^1 = \varepsilon^{p_h} - \varepsilon^{p_s} = -\Delta\varepsilon^p$ and the interfacial operator Q^1 is defined in Appendix A. Due to (3.12) and (3.14), the second surface integral $\mathcal{D}^2$ in (3.9) becomes

$$\mathcal{D}^2 = \frac{N}{2}\sigma^s : \Delta\varepsilon^p \int_{S^1} w_\alpha^1 n_\alpha^1 dS^1 + \frac{N}{2}\Delta\varepsilon^p : \int_{S^1} Q^1 w_\alpha^1 n_\alpha^1 dS^1 : \Delta\varepsilon^p. \tag{3.15}$$

The first surface integral in (3.15) describes the evolution of the volume v^1 bounded by S^1. The solution of the integral J defined by

$$J^1 = \int_{S^1} Q^1 w_\alpha^1 n_\alpha^1 dS^1$$

is given in Appendix A,

$$J^1 = C : (I - S^E)\dot{v}^1 + C : (S^2 : \dot{A})v^1, \tag{3.16}$$

and (3.15) is reduced to

$$\mathcal{D}^2 = N\sigma^S : \Delta\varepsilon^p \dot{v}^S + \frac{N}{2}\Delta\varepsilon^p : C : (I - S^E) : \Delta\varepsilon^p \dot{v}^S + \frac{N}{2}\Delta\varepsilon^p : C : (S^2 : \dot{A}) : \Delta\varepsilon^p v^S \tag{3.17}$$

where $S^2 = \partial S^E / \partial A$ (see Appendix B).

A similar step for the evaluation of the surface integral $\mathcal{D}^3$ in (3.9) leads to

$$\mathcal{D}^3 = -\frac{N}{2} \int_{S^e} \{\sigma^{+e}(r) + \sigma^{-e}(r)\} : [\varepsilon^p(r)]^e w_\alpha^e n_\alpha^e dS^e, \tag{3.18}$$

where $\sigma^{+e} = \sigma^{-e} - Q^e : [\varepsilon^p]^e$ and $[\varepsilon^p]^e = E^P - \varepsilon^{ph} = f\Delta\varepsilon^p$.

Since $[\varepsilon^p]^e$ is assumed to be uniform along S^e, $\mathcal{D}^3$ is given by

$$D^3 = -Nf\Delta\varepsilon^p : \int_{S^e} \sigma^{-e} w_\alpha^e n_\alpha^e dS^e + \frac{Nf^2}{2}\Delta\varepsilon^p : \int_{S^e} Q^e w_\alpha^e n_\alpha^e dS^e : \Delta\varepsilon^p. \tag{3.19}$$

Contrary to the relation (3.12), σ^{-e} is not uniform along S^e. A time derivative of the mean value σ^h over the volume v^h allows us to account for the first surface integral I in (3.19). Indeed, the volume integral defining σ^h is

$$v^h \sigma^h = \int_{v^h} \sigma(r) dV. \tag{3.20}$$

The volume v^h is bounded by the surfaces S^1 and S^e and the stress in v^h is equal to σ^{+1} and σ^{-e}, respectively, near S^1 and S^e.

During the evolution of v^h, one has

$$\frac{d}{dt}(v^h\sigma^h) = \int_{v^h} \dot{\sigma}(r)dV + \int_{S^e} \sigma^{-e}(r)w_\alpha^e n_\alpha^e dS^e - \int_{S^1} \sigma^{+1}(r)w_\alpha^1 n_\alpha^1 dS^1. \tag{3.21}$$

The first term in (3.21) is

$$\frac{d}{dt}(v^h\sigma^h) = \dot{v}^h\sigma^h + v^h\dot{\sigma}^h. \tag{3.22}$$

From (3.21) and (3.22), the surface integral I in (3.19) is equal to

$$I = \int_{S^e} \sigma^{-e}(r)w_\alpha^e n_\alpha^e dS^e = \dot{v}^h\sigma^h + \int_{S^1} \sigma^{+1}(r)w_\alpha^1 n_\alpha^1 dS^1. \tag{3.23}$$

According to (3.22), (3.23) and (3.16), I is written as

$$I = \sigma^h\dot{v}^h + C : (I - S^E) : \Delta\varepsilon^p\dot{v}^s + C : (S^2 : \dot{A}) : \Delta\varepsilon^p v^s. \tag{3.24}$$

Due to (3.4) to (3.7) and using the expressions (3.12) and (3.13), I reduces to

$$I = C : (S^2 : \dot{A}) : \Delta\varepsilon^p v^s. \tag{3.25}$$

The calculation of the second surface integral J^2 in (3.19) is identical to the surface integral J^2 in (3.15) if S^1 and v^1 are replaced, respectively, by S^e and v^e. In the case of homothetic coated inclusions, the Eshelby tensors corresponding to the ellipsoids v^1 and v^e are equal. Thus, with the condition (3.7), J^2 is given by

$$J^2 = \int_{S^e} Q^e w_\alpha^e n_\alpha^e dS^e = C : (S^2 : \dot{A})v^e. \tag{3.26}$$

With these results, (3.19) becomes:

$$D^3 = -Nf\Delta\varepsilon^p : C : (S^2 : \dot{A}) : \Delta\varepsilon^p v^s + \frac{1}{2}Nf^2\Delta\varepsilon^p : C(S^2 : \dot{A}) : \Delta\varepsilon^p v^e. \tag{3.27}$$

Finally, with (3.4) to (3.6) and the solutions of the integrals $\mathcal{D}^1$, $\mathcal{D}^2$ and $\mathcal{D}^3$, the dissipation $\mathcal{D}$ per unit volume is expressed by

$$\frac{\mathcal{D}}{V} = f\sigma^s : \dot{\varepsilon}^{p_s} + (1-f)\sigma^h : \dot{\varepsilon}^{p_h} + \frac{1}{2}f(1-f)\Delta\varepsilon^p : C : (S^2 : \dot{A}) : \Delta\varepsilon^p \tag{3.28}$$

$$+\dot{f}\left\{\sum : \Delta\varepsilon^p - \frac{1}{2}(1-2f)\Delta\varepsilon^p : C : (I - S^E) : \Delta\varepsilon^p\right\}.$$

Generally the dissipation is expressed in the following manner:

$$\frac{\mathcal{D}}{V} = F_i(\Sigma, X)\dot{X}_i \tag{3.29}$$

where X_i are the internal variables of the thermodynamical system, and F_i are the thermodynamical forces acting on X_i. Here, the thermodynamical forces associated with the internal variables $\varepsilon^{p_s}, \varepsilon^{p_h}$, f and A are given by:

$$\begin{aligned} F_{\varepsilon^{Ps}} &= \sigma^S, \\ F_{\varepsilon^{Ph}} &= \sigma^h, \\ F_f &= \Sigma : \Delta\varepsilon^p - \frac{1}{2}(1-2f)\Delta\varepsilon^p : C : (I - S^E) : \Delta\varepsilon^p, \\ F_A &= \frac{1}{2}f(1-f)\Delta\varepsilon^p : C : S^2 : \Delta\varepsilon^p. \end{aligned} \tag{3.30}$$

Contrary to the kinematical analysis (Sec. 2.1) where the internal variables are reduced to $\varepsilon^{P_s}, \varepsilon^{p_s}$ and f, the analysis of the dissipation shows an additionnal internal variable corresponding to the morphology (shape and orientation) of the cell structure described by A.

To complete the study, complementary equations describing the evolution of these internal variables have to be introduced.

3.3. Complementary relations and global behavior

The analysis developed in Secs. 2 and 3 allows us to relate internal variables describing possible evolution of the microstructure with the mechanical state. In the case of reversible processes, the thermodynamical forces have to be taken equal to zero. This provides additional equations for the internal variables. For thermodynamical irreversible processes like in the classical plasticity approach, critical forces $F_i^c(X)$ are introduced. In this case the evolution $\dot{X}_i$ of internal variables X_i is given by

$$\begin{aligned} \dot{X}_i = 0 \quad \text{if} \quad & \begin{cases} F_i(\Sigma, X) < F_i^c(X), \\ \forall \dot{F}_i(\Sigma, X); \end{cases} \\ \dot{X}_i = 0 \quad \text{if} \quad & \begin{cases} F_i(\Sigma, X) = F_i^c(X), \\ \dot{F}_i(\Sigma, X) \leq \dot{F}_i^c(X); \end{cases} \\ \dot{X}_i \neq 0 \quad \text{if} \quad & \begin{cases} F_i(\Sigma, X) = F_i^c(X), \\ \dot{F}_i(\Sigma, X) = \dot{F}_i^c(X). \end{cases} \end{aligned} \tag{3.31}$$

Using the consistency rule,

$$\dot{F}_i(\Sigma, X) = \dot{F}_i^c(X) \,, \tag{3.32}$$

the following system with unknows $\dot{X}_i$

$$\left(\frac{\partial F_i^c}{\partial X_j}(X) - \frac{\partial F_i}{\partial X_j}(\Sigma, X)\right)\dot{X}_j = \frac{\partial F_i}{\partial \Sigma}(\Sigma, X) : \dot{\Sigma} \tag{3.33}$$

or, formally

$$\dot{X} = K : \dot{\Sigma} \,, \tag{3.34}$$

gives the evolution of the internal variables as a function of the loading parameter $\dot{\Sigma}$.

From

$$\dot{\Sigma} = C : (\dot{E} - \dot{E}^p) \tag{3.35}$$

and

$$\dot{E}^p = f\dot{\varepsilon}^p + (1-f)\dot{\varepsilon}^{p_h} + \dot{f}\Delta\varepsilon^p \tag{3.36}$$

or, formally

$$\dot{E}^p = M \cdot \dot{X} \,, \tag{3.37}$$

we have for a given $\dot{E}$:

$$\dot{X} = (I + K : C : M)^{-1} : K : C : \dot{E}$$

and

$$\dot{E}^p = M : (I + K : C : M)^{-1} : K : C : \dot{E}.$$

So, the overall behavior of the grain is written as:

$$\dot{\Sigma} = L : \dot{E}, \tag{3.38}$$

where L is the instantaneous elastoplastic modulus of the grain given by

$$L = C : (I - M : (I + K : C : M)^{-1} : K : C). \tag{3.39}$$

In the case of crystalline metals, dislocations are restricted to move on the crystallographic slip systems. As a first approximation, the walls are considered

as a crystallographic part of the grain, in spite of their high defect density. Furthermore the slip planes are assumed to remain continuous through the walls. Thus the plastic glide γ is introduced such as

$$\dot{\varepsilon}_{ij}^{p_\alpha} = R_{ij}^g \dot{\gamma}_\alpha^g, \qquad (\alpha = s, h), \tag{3.40}$$

where the Schmid tensor R_{ij}^g for the system g is given by

$$R_{ij}^g = \frac{1}{2}(m_i^g n_j^g + m_j^g n_i^g). \tag{3.41}$$

n_i is the unit normal to the slip plane and m_i is the slip direction. In order to obtain the tangent moduli (3.39), the critical forces $F_i^c(X)$ are introduced.

In case of time-independent plasticity, the evolution of these critical forces as a function of internal variables X_i is generally given by:

$$\dot{F}_i^c = \mathcal{H}^{ij} \dot{X}_j; \tag{3.42}$$

$\mathcal{H}^{ij} = \partial F_i^c / \partial X_j$ is the interaction matrix between the different internal variables X_i. According to different types of internal variables, (3.42) is explicitly written in the form

$$\begin{pmatrix} \dot{F}^c_{\gamma_S^i} \\ \dot{F}^c_{\gamma_h^i} \\ \dot{F}^c_f \\ \dot{F}^c_{a_i} \\ \dot{F}^c_{\alpha_i} \end{pmatrix} = \begin{pmatrix} \mathcal{H}^{ij}_{ss} & \mathcal{H}^{ij}_{hs} & \mathcal{H}^{ij}_{sf} & \mathcal{H}^{ij}_{sa} & \mathcal{H}^{ij}_{s\alpha} \\ \mathcal{H}^{ij}_{hs} & \mathcal{H}^{ij}_{hh} & \mathcal{H}^{ij}_{hf} & \mathcal{H}^{ij}_{ha} & \mathcal{H}^{ij}_{h\alpha} \\ \mathcal{H}^{ij}_{fs} & \mathcal{H}^{ij}_{fh} & \mathcal{H}^{ij}_{ff} & \mathcal{H}^{ij}_{fa} & \mathcal{H}^{ij}_{f\alpha} \\ \mathcal{H}^{ij}_{as} & \mathcal{H}^{ij}_{ah} & \mathcal{H}^{ij}_{af} & \mathcal{H}^{ij}_{aa} & \mathcal{H}^{ij}_{a\alpha} \\ \mathcal{H}^{ij}_{\alpha s} & \mathcal{H}^{ij}_{\alpha h} & \mathcal{H}^{ij}_{\alpha f} & \mathcal{H}^{ij}_{\alpha a} & \mathcal{H}^{ij}_{\alpha\alpha} \end{pmatrix} \begin{pmatrix} \dot{\gamma}_s^j \\ \dot{\gamma}_h^j \\ \dot{f} \\ \dot{a}_j \\ \dot{\alpha}_j \end{pmatrix}. \tag{3.43}$$

The submatrices $\begin{pmatrix} \mathcal{H}_{ss} & \mathcal{H}_{sh} \\ \mathcal{H}_{hs} & \mathcal{H}_{hh} \end{pmatrix}$ correspond to the hardening matrices between slip γ of each phase. One finds here the selfhardening, in other words the hardening of a slip system on itself, and the latent hardening defined by the hardening of a system by an other active slip system. The terms $\mathcal{H}_{sh}$ and $\mathcal{H}_{hs}$ determine the hardening of a phase by the other ones (non-local hardening). The components of this submatrix are obtained from dislocation concepts like creation or annihilation [11, 32, 33]:

$$H_{hs}^{gh} = \frac{(1-f)b\mu^2}{\tau_{ch}^g - \tau_{ch}^{0g}} \left(\frac{a_{(g)h}}{L^{(h)}} - y a_{(g)l} \rho_h^l A_{hs}^{(l)h} \right), \quad H_{sh}^{gh} = 0,$$

$$H_{hh}^{gh} = -\frac{(1-f)b\mu^2}{\tau_{ch}^g - \tau_{ch}^{0g}} y a_{(g)l} \rho_H^l A_{hh}^{(l)h}, \quad H_{ss}^{gh} = \frac{f\alpha_{ss}}{\tau_{cs}^g - \tau_{cs}^{0g}} a_{(g)h}, \tag{3.44}$$

where b is the modulus of the Burgers vector, μ the elastic shear modulus, L^g the mean free path of dislocations in cell interiors, y a dislocation annihilation distance, ρ_α^l the dislocation density, $\tau_{c\alpha}^{0g}$ the initial critical shear stress and $a_{(g)h}$ denotes the anisotropy of the dislocation interactions [34].

4. Applications

Despite the fact that interaction matrix $\mathcal{H}^{ij}$ remains partially unknown, some first conclusions can be derived from the micromechanical approach developed in this paper. Numerical applications can be obtained using some additional assumptions. These assumptions reduce the field of validity of the developed model but are consistent with the physical aspects considered. In Secs. 2 and 3, the elastoplastic behavior of the grains was established. For the meso-macro scales transition (from the grains to the polycrystal), a classical elastoplastic self-consistent scheme is used so that the effects of fixed grain boundaries are taken into account (interactions of grains with the surrounding homogenous material). This model is extensively presented and discussed in [3 – 6]. The numerical application is restricted to a uniaxial tensile test.

4.1. Simplifying hypotheses

The analysis of dislocation in cell structures induced during a monotoneous path allows us to assume that the volume fraction f remains practically constant during plastic straining [13]. Therefore one assumes that the volume fraction of cells is no longer an internal variable but becomes a material parameter, so that $\dot{f} = 0$. The concept of Low Energy Dislocation Structure (LEDS) popular in physical metallurgy [22 – 23] allows to assume that the microstructure morphology adapts itself instantaneously to the loading. This second simplifying assumption corresponds to an organisation of cell structure which minimizes the free energy with respect to the corresponding variables. The consequence of this hypothesis gives

$$F_A = 0 \quad \text{and} \quad \dot{F}_A = 0$$

and by (3.37), the thermodynamical force F_A is equal to zero, so that

$$F_A = \frac{1}{2} f(1-f)\Delta\gamma R : C : S^2 : R\Delta\gamma = 0. \tag{4.1}$$

The time derivative of (4.1) gives the evolution of the parameters of the ellipsoid and is a function of the slip rates $\dot{\gamma}$.

4.2. Input data used for the calculation

The calculations are performed for a BCC polycrystal without initial texture (100 grains). Isotropic and homogeneous elasticity ($\mu = 80$ GPa, $\nu = 0.3$) and

slip systems of type $\{110\} < 111 >$ are assumed. The initial critical shear stress is assumed to be identical for all the systems of each phase and equal to 65 MPa. Characteristics of dislocations are: $b = 2.5$ Å, $L = 6.4$ μm, $a = 1.5$ Å, $y = 4.7$, $\alpha_{ss} = 900$ (MPa)^2. Finally the ellipsoid describing the cell shape in each grain is initially nearly spherical: $a_1 = 1$, $a_2 = 1.02$, $a_3 = 0.98$.

4.3. Numerical results

Figure 4a represents the mechanical response (Σ_{11}, E_{11}) in uniaxial tension. The stress distributions in each phase are described for two macroscopic plastic

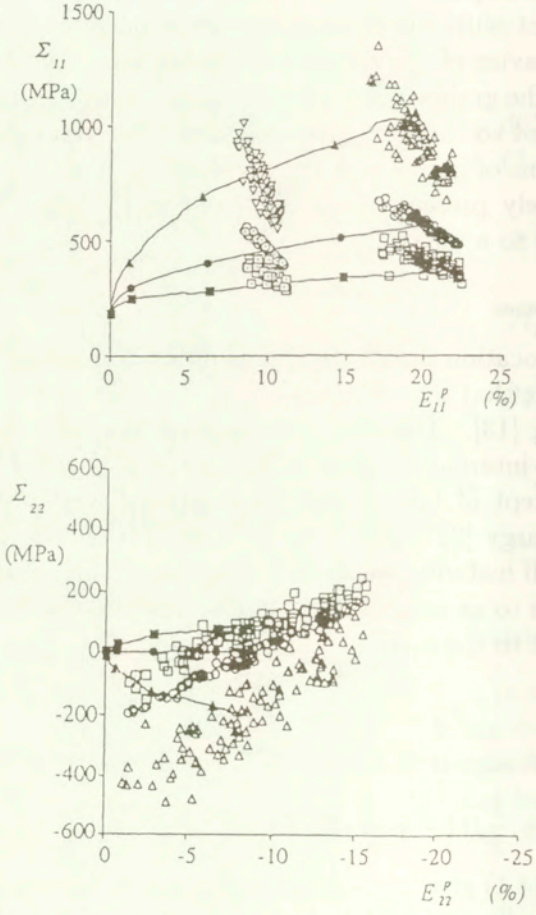

FIG. 4. Mechanical states during an uniaxial tensile test. a) – Macroscopic response of the polycrystal (—●—), mean stresses and strains over the hard phase (—▲—) and soft phase (—■—), mechanical state $(\sigma_{11}, \varepsilon_{11}^P)$ for each grain at: $E_{11}^P = 0.1$ (o) and $E_{11}^P = 0.2$ (o), mechanical state $(\sigma_{11}, \varepsilon_{11}^P)$ for each phase at: $E_{11}^P = 0.1$ (∇, □) and $E_{11}^P = 0.2$ (Δ , □). b) Same as for Fig. 4 a) but for σ_{22} and ε_{22}^P components ($E_{11}^P = 0.2$).

strains 0.1 and 0.2 by clouds of square (s) and triangle (h) points (the third order stresses). The mean stresses in each grain are represented by two clouds of circle points for the same two macroscopic plastic strains. The three curves describe respectively the overall behavior of the polycrystal (first order stresses) and the averaged third order stresses. One finds in the Fig. 4b the same description for the components of the stress tensor. In agreement with experimental measurements by MUGHRABI [35], the cloud of phase (h) is more extented than the cloud of phase (s), and third order internal stresses (inside the hard phase) are twice the overall yield stress for the σ_{11} component. One observes that the fluctuations of components σ_{22} and σ_{33} are more important than those concerning the component σ_{11}.

The corresponding evolution of the cell morphology in each grain is given in Fig. 5 for one grain and Fig. 6 for all the grains. Figure 5 shows the evolution of the two semi-axes ratios of the ellipsoid ($r_1 = a_1/a_2$, $r_2 = a_1/a_3$) during the plastification. After a few percent of plastic strain, a saturation of the cell shape evolution occurs as it was observed on BCC polycrystals by SCHMITT [13]. One can explain this saturation by the stabilisation of the multislip deformation mode. Figure 6 allows to follow the mean evolution of the highest semi-axis ratio of the ellipsoid. Starting from a spherical shape in the reference state, the cells become more and more elongated and reach a stable shape for a few percent of

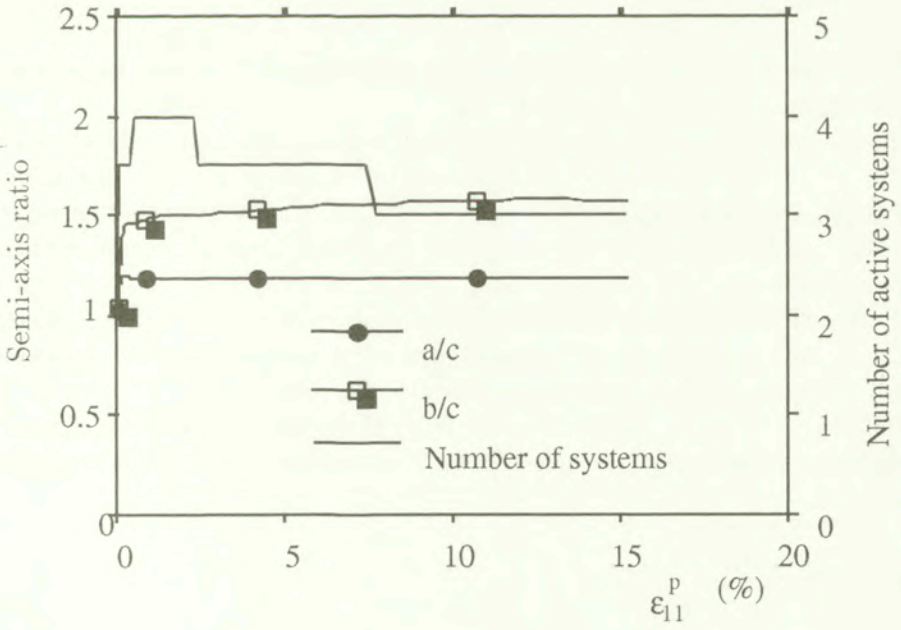

FIG. 5. Evolution of semi-axis ratio in one particular grain of the polycrystal during the loading path.

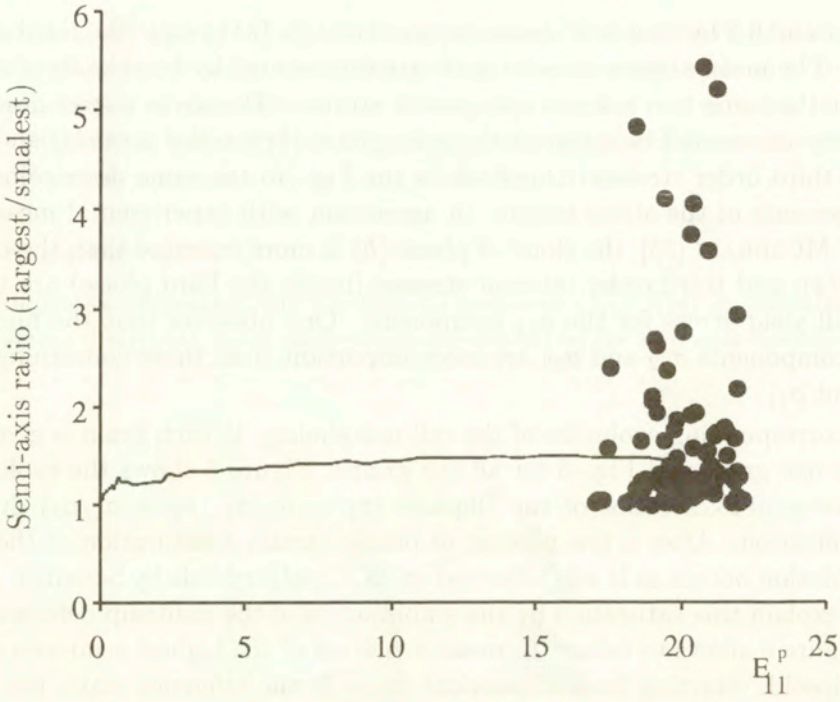

FIG. 6. Evolution of the largest semi-axis ratio in all grains as a function of E_{11}^P.

plastic strain. The cloud of points represents the highest semi-axis ratio in each grain at $E_{11}^P = 0.2$. These remarks (final shape and saturation) have been confirmed experimentally by SCHMITT [13].

In the present applications, the volume fraction f was assumed to be constant so that the results obtained better apply to the formation of stable dislocation cell structures. On the contrary, if the volume fraction is allowed to change, an overall softening is obtained. This softening will be able to produce strain localization as it was shown in [43] and [44]. Thus even if the model is formulated for small elastic-plastic strains, it is well adapted to capture strain localization effect; this is due to the fact that the third order stress fluctuations and the possibility to have a changing microstructure are taken into account.

This way of modelling is different from those used by PIERCE, ASARO and NEEDLEMAN [45] where third order effects are neglected but a large strain formulation is used.

5. Conclusions

Contrary to the grain boundaries, which are stationary with respect to the material, dislocation walls are considered as free surfaces of plastic strain discontinuities similar to a single dislocation which is a linear defect.

Plasticity can be described at various spatial levels. In the common "micro-macro" approach, the local constitutive equations are written in the framework of classical continum mechanics (i. e. with internal variable) and induced dislocation microstructures are not explicity taken into account. The most important physics related with the dislocation walls are the kinematical and the statical boundary conditions which are written here assuming uniform plastic strain inside the cells and the walls. The field fluctuations at the level of the dislocations are lost by the two-phase representation but third order effects (fluctuations at the length scale of cells) are found.

Like in the framework of classical crystal plasticity, some phenomenological parameters and relations describing the hardening and the evolution of the internal state are introduced. Future work has to be done in order to base some phenomenological aspects of the model on a more precise physical description. Applied for complex loading paths, a similar model was able to describe correctly the subsequent behavior [43].

Appendix A

A.1. Interfacial operators [36]

Consider a surface S between two different phases whose plastic strain is denoted by ε^{p_1} and ε^{p_2}, respectively. The stress and strain tensors are discontinuous across S. HILL [36] has explained how their jumps are related together by interfacial operators. The equilibrum equations:

$$[\sigma_{ij} n_j] = (\sigma^2_{ij} - \sigma^1_{ij}) n_j = 0 \tag{A.1}$$

and compatibility conditions:

$$[\varepsilon_{ij}] = \varepsilon^2_{ij} - \varepsilon^1_{ij} = \frac{1}{2}(\lambda_i n_j + \lambda_j n_i), \tag{A.2}$$

where λ_i is a vector determined completely by the condition

$$C_{ijkl}\lambda_k n_l n_j = C_{ijkl}[\varepsilon^p_{kl}] n_j \ , \tag{A.3}$$

lead to the relation:

$$[\varepsilon_{ij}] = P_{ijkl} C_{klmn} [\varepsilon^p_{mn}]. \tag{A.4}$$

P is an interfacial operator depending of the unit normal n_i to the surface S and homogeneous elastic tensor C. The operator P [29] can be written as

$$P_{ijkl} = \frac{1}{4}(C^{-1}_{ik} n_j n_l + C^{-1}_{jl} n_j n_k + C^{-1}_{ik} n_i n_l + C^{-1}_{jl} n_i n_k), \tag{A.5}$$

where C^{-1} denotes the inverse of the Christoffel matrix defined by

$$C_{ik} = C_{ijkl} n_j n_l. \tag{A.6}$$

From (A.3) and (A.4), the stress jump across the surface S is given by

$$[\sigma_{ij}] = -Q_{ijkl}[\varepsilon^p_{kl}], \tag{A.7}$$

where

$$Q_{ijkl} = (I_{ijmn} - C_{ijpq} P_{pqmn}) C_{mnkl}. \tag{A.8}$$

A.2. Determination of the tensor J (Eq. (3.16))

$$J = \int_S Q w_\alpha n_\alpha dS. \tag{A.9}$$

Consider an infinitely extended material with homogeneous elastic tensor C containing an ellipsoidal inclusion V bounded by the surface S. From classical results [37 - 39], the relation between the Green tensor G and the interfacial operator P is given by:

$$\int_V \Gamma(r^+ - r') : C dV' - \int_V \Gamma(r^- - r') : C dV' = P : C \tag{A.10}$$

where

$$\Gamma_{ijkl} = \frac{1}{2}(G_{ik,jl} + G_{jk,il}); \tag{A.11}$$

r' and $r^- \in V$, r^+ is an external point to V and near to S.
Using the definition of the Eshelby tensor [30]

$$S^E = -\int_V \Gamma(r^- - r') : C dV', \tag{A.12}$$

we have

$$\int_V \Gamma(r^+ - r') : C dV' = P : C - S^E. \tag{A.13}$$

On the other hand, the time derivative of S^E (A.12) gives

$$\dot{S}^E = -\int_{S^+} \Gamma(r^- - r^+) : C w_\alpha n_\alpha dS; \tag{A.14}$$

$\dot{S}^E$ is homogeneous inside the ellipsoidal inclusion [40]. Thus, we have

$$\dot{S}^E = \frac{1}{V}\int_V \dot{S}^E dV. \tag{A.15}$$

Applying (A.15) to (A.14) and using (A.13) and the property of Green tensor G

$$\int_V \Gamma(r^- - r'^+)dV' = \int_V \Gamma(r^+ - r'^-)dV', \tag{A.16}$$

we obtain

$$\dot{S}^E v = \int_{S^+} (S^E - P : C)w_\alpha n_\alpha dS. \tag{A.17}$$

By the definition $\dot{V} = \int_{S^+} w_\alpha n_\alpha dS$, we have the integral

$$\int_{S^+} P : C w_\alpha n_\alpha dS = S^E \dot{v} - \dot{S}^E V. \tag{A.18}$$

Using (A.8), the integral J (A.9) is given by

$$J_{ijkl} = C_{ijmn}(I_{mnkl} - S^E_{mnkl})\dot{v} + C_{ijmn}S^2_{mnklpq}\dot{A}_{pq}v \tag{A.19}$$

with $\dot{S}^E = S^2 : \dot{A}$ (see Appendix B).

Appendix B. Determination of the tensors S^E, S^2, and S^3

B.1. Characterization of an ellipsoid and its evolution

The Eshelby tensor S^E is defined by the volume integral (A.12) and its time derivative $\dot{S}^E$ by the surface integral (A.14). Using the divergence theorem, (A.14) becomes:

$$\dot{S}^E = \int_V \Gamma_{,\alpha}(r - r') : C w_\alpha dV' - \int_V \Gamma(r - r')w_{\alpha,\alpha}dV'. \tag{B.1}$$

The time derivative of $\dot{S}^E$ is also given by

$$\text{(B.2)} \qquad \frac{d\dot{S}^E}{dt} = \ddot{S}^E = \int_v \Gamma_{,pq}(r-r') : Cw_p w_q dV' - \int_v \Gamma_{,p}(r-r') : C(w_{p,q}w_q + w_p w_{q,q})dV' - \int_v \Gamma_{,q}(r-r') : Cw_{p,p}w_q dV' - \int_v \Gamma(r-r') : C(w_{p,pq}w_q + w_{p,p}w_{q,q})dV' - \int_v \Gamma_{,p}(r-r') : C\dot{w}_p dV' - \int_v \Gamma(r-r') : C\dot{w}_{p,p}dV' .$$

The evaluation of these volume integrals requires the knowledge of the velocity w_α and its time and spacial derivatives which can be deduced easily from the kinematical evolution of the ellipsoid v.

Indeed, an ellipsoid is described by semi-axes $a_i (i = 1, 2, 3)$ and Euler angles $\alpha_i (i = 1, 2, 3)$ giving the orientation of the ellipsoid principal reference frame versus the crystalline lattice. These parameters can be regrouped in the tensor $A(a_p, \alpha_p)$ defined by

$$\text{(B.3)} \qquad A_{ij}x_i x_j = 1.$$

In the principal axis of the ellipsoid, A takes the following form:

$$\text{(B.4)} \qquad A^e_{ij} = \begin{pmatrix} 1/a_1^2 & 0 & 0 \\ 0 & 1/a_2^2 & 0 \\ 0 & 0 & 1/a_3^2 \end{pmatrix}.$$

A standard coordinate transformation by the orthogonal matrix $b(\alpha_i)$ gives the tensor A in the crystalline lattice as

$$\text{(B.5)} \qquad A_{ij}(a_k, \alpha_l) = b_{im}(\alpha_l)b_{jn}(\alpha_l)A^e_{mn}(a_k).$$

By time derivative of (B.3), we obtain for w_α:

$$\text{(B.6)} \qquad w_i = \dot{x}_i = -\frac{1}{2}A^{-1}_{ik}\dot{A}_{kl}x_l$$

and its time and spatial derivatives

$$w_{i,j} = \dot{x}_{i,j} = -\frac{1}{2}A^{-1}_{ik}\dot{A}_{kj}\,, \qquad w_{i,jk} = 0\,,$$

$$\dot{w}_i = \frac{1}{2}\left\{\frac{3}{2}A^{-1}_{ik}\dot{A}_{kl}A^{-1}_{lm}\dot{A}_{mn}x_n - A^{-1}_{ik}\ddot{A}_{kl}x_l\right\},$$

$$\dot{w}_{i,j} = \frac{1}{2}\left\{A^{-1}_{im}\dot{A}_{mn}A^{-1}_{nk}\dot{A}_{kj} - A^{-1}_{ik}\ddot{A}_{kj}\right\}.$$

For the application of the consistency relation, a second derivative of S^E is also needed so that we have to determine

$$\dot{S}^E_{ijkl} = S^2_{ijklpq}\dot{A}_{pq}\,, \qquad \ddot{S}^E_{ijkl} = S^3_{ijklpqrs}\dot{A}_{pq}\dot{A}_{rs} + S^2_{ijklpq}\ddot{A}_{pq}, \tag{B.8}$$

where the new tensors S^2 and S^3 are defined from to S^E by

$$S^2_{ijklpq} = \frac{\partial S^E_{ijkl}}{\partial A_{pq}}\,, \qquad S^3_{ijklpqrs} = \frac{\partial^2 S^E_{ijkl}}{\partial A_{pq}\partial A_{rs}} \tag{B.9}$$

and given by the following expressions:

$$S^2_{ijklpq} = \frac{1}{2}\left(\overline{S}^2_{ijklpq} + \overline{S}^2_{ijklpqrs}\right)\,, \qquad S^3_{ijklpqrs} = \frac{1}{2}\left(\overline{S}^3_{ijklpqrs} + \overline{S}^3_{ijklpqrs}\right)\,,$$

$$S^E_{ijkl} = \frac{1}{2}\left(\overline{S}^E_{ijkl} + \overline{S}^E_{ijkl}\right) \tag{B.10}$$

with

$$\begin{aligned}
\overline{S}^2_{ijklpq} &= -\frac{1}{4}\left\{T^2_{ijmntp}A^{-1}_{tq} + T^2_{ijmntq}A^{-1}_{tp} - 2T^1_{ijmn}A^{-1}_{pq}\right\}C_{mnkl}\,,\\
\overline{S}^3_{ijklpqrs} &= -\frac{1}{16}\left\{T^3_{ijmntqus}A^{-1}_{tp}A^{-1}_{ur} + T^3_{ijmntpus}A^{-1}_{tq}A^{-1}_{ur}\right.\\
&\qquad \left. + T^3_{ijmntqur}A^{-1}_{tp}A^{-1}_{us} + T^3_{ijmntpur}A^{-1}_{tq}A^{-1}_{us}\right\}C_{mnkl}\\
&\quad + \frac{1}{8}\left\{T^2_{ijmnts}(A^{-1}_{tp}A^{-1}_{qr} + A^{-1}_{tq}A^{-1}_{pr} + A^{-1}_{pq}A^{-1}_{tr}) + T^2_{ijmntr}(A^{-1}_{tp}A^{-1}_{qs}\right.\\
&\quad + A^{-1}_{tq}A^{-1}_{ps} + A^{-1}_{pq}A^{-1}_{ts}) + T^2_{ijmntq}(A^{-1}_{tr}A^{-1}_{sp} + A^{-1}_{ts}A^{-1}_{rp} + A^{-1}_{rs}A^{-1}_{tp})\\
&\qquad \left. + T^2_{ijmntp}(A^{-1}_{tr}A^{-1}_{sq} + A^{-1}_{ts}A^{-1}_{rq} + A^{-1}_{rs}A^{-1}_{tq})\right\}C_{mnkl}\\
&\qquad - \frac{1}{4}T^1_{ijmn}C_{mnkl}\left(A^{-1}_{pq}A^{-1}_{rs} + A^{-1}_{rp}A^{-1}_{qs} + A^{-1}_{rq}A^{-1}_{ps}\right),\\
\overline{S}^E_{ijkl} &= T^1_{ijmn}C_{mnkl}.
\end{aligned}$$

The tensors T^1, T^2 and T^3 are given in the condensed form:

$$\mathcal{T}_{ijkl} = -\frac{D\partial^2}{\partial x_j \partial x_l}\int_V G_{ik}(r - r')f(r')dV'\,, \tag{B.11}$$

where D denotes a differential operator and $f(r')$ is a function such that three choices are possible:

$$\text{(B.12)} \quad \begin{aligned} &D = 1\,, && f(r') = 1 && \forall r' \in v \text{ then } \mathcal{T} = T^1;\\ &D = \frac{\partial}{\partial x_m}, && f(r') = x'_n && \forall r' \in v \text{ then } \mathcal{T} = T^2\,;\\ &D = \frac{\partial^2}{\partial x_m \partial x_p}, && f(r') = x'_n x'_q && \forall r' \in v \text{ then } \mathcal{T} = T^3. \end{aligned}$$

The tensor $\mathcal{T}$ (B.11) can be calculated using Fourier's transformation of the Green tensor G.

B.2. Numerical method by Fourier transformation

The explicit calculation of the Green tensor G from the equation

$$\text{(B.13)} \qquad C_{ijkl} G_{jn,ik}(r) + \delta_{ln}\delta(r) = 0$$

can be accomplished by Fourier's transformation. $\delta(r)$ and δ_{ln} are respectively the distribution of Dirac and Kronecker's symbol. If $\tilde{G}(k)$represents the Fourier transformation of $G(r)$, then

$$\text{(B.14)} \qquad \tilde{G}(k) = \int_v G(r) e^{-ik_s x_s} dV, \quad G(r) = \frac{1}{8\pi^3} \int_{v_k} \tilde{G}(k) e^{ik_s x_s} dV_k$$

so that the transform of (B.13) is

$$\text{(B.15)} \qquad C_{ijkl} \tilde{G}_{jk} k_i k_k = \delta_{ln}.$$

The vector k may be described with the spherical coordinates $\mathbf{k}$, θ, φ by

$$\text{(B.16)} \qquad k_j = \mathbf{k} X_j, \qquad (j = 1, 2, 3),$$

where

$$\text{(B.17)} \qquad X_1 = \sin\theta\cos\varphi, \quad X_2 = \sin\theta\sin\varphi, \quad X_3 = \cos\theta,$$

with $\mathbf{k} \in [0, +\infty]$, $\theta \in [0, \pi]$, $\varphi \in [0, 2\pi]$.
Consequently (B.15) becomes

$$\text{(B.18)} \qquad \mathbf{k}^2 \tilde{G}_{jn}(k) = M^{-1}_{jn}(X),$$

where the matrix M depends on the orientation of the vector k by

$$\text{(B.19)} \qquad M_{jn}(X) = C_{jknl} X_k X_l.$$

Integration with respect to k in (B.14) uses spherical layers $S(X)$ of thickness $d\mathbf{k}$ and mean radius $\mathbf{k}$, and it gives:

$$dV_k = \mathbf{k}^2 d\mathbf{k} dS(X) \quad \text{with} \quad dS(X) = \sin\theta d\theta d\varphi, \tag{B.20}$$

so that with these equations, (B.11) becomes

$$\mathcal{T}_{ijkl} = -\frac{1}{8\pi^3} \frac{D\partial^2}{\partial x_j \partial x_l} \int_S M_{ik}^{-1}(X) dS \int_V f(r') \int_0^\infty e^{i\mathbf{k}X_s(x_s - x_s')} d\mathbf{k} dV'. \tag{B.21}$$

Following FAIVRE [41], only the real part of the integral of $e^{i\mathbf{k}X_s(x_s - x_s')}$ gives a non-zero contribution,

$$Re \int_0^\infty e^{i\mathbf{k}X_s(x_s - x_s')} d\mathbf{k} = \frac{1}{2} \int_{-\infty}^{+\infty} e^{i\mathbf{k}X_s(x_s - x_s')} d\mathbf{k},$$

but in terms of the unidimensional Dirac function δ, we have

$$\int_{-\infty}^{+\infty} e^{i\mathbf{k}\eta} d\mathbf{k} = 2\pi\delta(\eta).$$

Finally (B.21) is rewritten as

$$\mathcal{T}_{ijkl} = -\frac{1}{8\pi^2} \int_S M_{ik}^{-1}(X) \frac{D\partial^2}{\partial x_j \partial x_l} \int_V f(r')\delta(X_s(x_s - x_s')) dV' dS. \tag{B.22}$$

Recalling that function f is zero outside the ellipsoid V, we can extend the integral $\int_v f(r')\delta(X_s(x_s - x_s))dV'$ over the infinite volume. Then, observing that equation

$$\mathbf{X}(\mathbf{r} - \mathbf{r}') = 0$$

represents a plane $\mathcal{P}(\mathbf{r}')$ passing throught point r and with unit normal X, we obtain the case of the Dirac function concentrated on plane $\mathcal{P}(\mathbf{r}')$. Using KECS and TEODORESCU [42], we have:

$$I_f(r) = \int_{-\infty}^{+\infty} f(r')\delta(X_m(x_m - x_m'))dV' = \frac{1}{\chi_\alpha} \int_p f(r')dx_r' dx_s \tag{B.23}$$

with (α, r, s) being equal to any permutation of $(1, 2, 3)$.

$I_f(r)$ is a classical surface integral that gives for a point r **located in the ellipsoid** the following three results:

- first case of (B.12): $f(r') = 1$ then $I_f(r) = \dfrac{a_1 a_2 a_3 \pi}{Z}(1 - H^2)$

with $Z = \sqrt{a_1^2 X_1^2 + a_2^2 X_2^2 + a_3^2 X_3^2}$, $H = \dfrac{X_i x_i}{Z}$;

- second case of (B.12): $f(r') = x_n$ then $I_f(r) =$

$$= a_N^2 X_n \frac{a_1 a_2 a_3 \pi}{Z^2}(1 - H^2)H;$$

- third case of (B.12): $f(r') = x_n x_q$ then $I_f(r) =$

$$= a_N^2 a_Q^2 X_n X_q \frac{a_1 a_2 a_3 \pi}{Z^3}(1 - H^2)H^2.$$

Substituting the three possible choices into (B.22), we obtain by performing the partial differentiations D, $\dfrac{\partial}{\partial x_j}$ and $\dfrac{\partial}{\partial x_l}$:

$$T^1_{ijkl} = \frac{a_1 a_2 a_3}{4\pi} \int_\Omega M^{-1}_{ik}(X) \frac{X_j X_l}{k^3} d\Omega,$$

$$T^2_{ijklmn} = \frac{3 a_1 a_2 a_3 a_N^2}{4\pi} \int_\Omega M^{-1}_{ik}(X) \frac{X_j X_l X_m X_n}{k^5} d\Omega, \tag{B.24}$$

$$T^3_{ijklmnpq} = \frac{3 a_1 a_2 a_3 a_N^2}{\pi} \int_\Omega M^{-1}_{ik}(X) \frac{X_j X_l X_m X_n X_p X_q}{k^5} d\Omega.$$

Let us observe that T^1, T^2 and T^3 do not depend on r for r lying inside the ellipsoid; this result was previously mentioned by Eshelby for T^1.

Calculations of these tensors require the knowledge of M_{ik} given from (B.21); in the general case of an ellipsoidal inclusion and anisotropic material, a numerical method is used. In the next section the case of spherical inclusion and isotropic material is solved analytically.

B.3. Isotropic elasticity – flattening of a sphere into ellipsoid

From the components M_{ik} (B.19) we obtain for isotropic elasticity with shear modulus μ and Poisson's ratio v the result:

$$M^{-1}_{ik}(X) = \frac{1}{\mu}(\delta_{ik} - \frac{1}{2(1-v)} X_i X_k). \tag{B.25}$$

Substituting for a sphere $a_1 = a_2 = a_3$ and (B.25) in (B.24), we obtain tensors T^1, T^2 and T^3:

$$T^1_{ijkl} = \frac{1}{30(1-v)\mu}\left((9 - 10v)\delta_{ik}\delta_{jl} - (\delta_{ij}\delta_{kl} + \delta_{il}\delta_{jk})\right),$$

$$T^2_{ijklmn} = \frac{1}{70(1-v)\mu}\Big((13-14v)\delta_{ik}(\delta_{jl}\delta_{mn} + 2\overline{\Delta}_{jlmn}) - \delta_{ij}\delta_{kl}\delta_{mn}$$
$$-\delta_{il}\delta_{jk}\delta_{mn} - 2\delta_{ij}\overline{\Delta}_{klmn} - 2\delta_{kl}\overline{\Delta}_{ijmn} - 2\delta_{il}\overline{\Delta}_{jkmn} - 2\delta_{im}\overline{\Delta}_{jnkl}$$
$$-2\delta_{in}\overline{\Delta}_{jmkl}\Big),$$

$$T^3_{ijklmnpq} = \frac{2}{315(1-v)\mu}\Big((17-18v)\delta_{ik}(\delta_{jl}\delta_{mn}\delta_{pq} + 2\delta_{jl}\overline{\Delta}_{mnpq}$$
$$+2\delta_{pq}\overline{\Delta}_{jlmn} + 2\delta_{mn}\overline{\Delta}_{jlpq} + 8\overline{\Delta}_{jlmnpq}) - (\delta_{ij}\delta_{kl}\delta_{mn}\delta_{pq} + \delta_{il}\delta_{jk}\delta_{mn}\delta_{pq}$$
$$+2\delta_{ij}\delta_{kl}\overline{\Delta}_{mnpq} + 2\delta_{ij}\delta_{mn}\overline{\Delta}_{klpq} + 2\delta_{ij}\delta_{pq}\overline{\Delta}_{klmn} + 2\delta_{kl}\delta_{mn}\overline{\Delta}_{ijpq}$$
$$+2\delta_{kl}\delta_{pq}\overline{\Delta}_{ijmn} + 2\delta_{il}\delta_{mn}\overline{\Delta}_{jkpq} + 2\delta_{ip}\delta_{mn}\overline{\Delta}_{jqkl} + 2\delta_{iq}\delta_{mn}\overline{\Delta}_{jpkl}$$
$$+2\delta_{il}\delta_{pq}\overline{\Delta}_{jkmn} + 2\delta_{im}\delta_{pq}\overline{\Delta}_{jnkl} + 2\delta_{in}\delta_{pq}\overline{\Delta}_{jmkl} + 2\delta_{il}\delta_{jk}\overline{\Delta}_{mnpq}$$
$$+8\delta_{ij}\overline{\overline{\Delta}}_{klmnpq} + 8\delta_{kl}\overline{\overline{\Delta}}_{ijmnpq} + 8\delta_{il}\overline{\Delta}_{jkmnpq} + 16\overline{\overline{\overline{\nabla}}}_{ijmnklpq}$$
$$+16\overline{\overline{\overline{\nabla}}}_{ijpqklmn} + 4\overline{\Delta}_{ijmn}\overline{\Delta}_{klpq} + 4\overline{\Delta}_{ijpq}\overline{\Delta}_{klmn})\Big),$$

with

$$\overline{\Delta}_{ijkl} = \frac{1}{2}(\delta_{ik}\delta_{jl} + \delta_{il}\delta_{jk}),$$

$$\overline{\overline{\Delta}}_{ijklmn} = \frac{1}{4}(\delta_{ik}\overline{\Delta}_{jlmn} + \delta_{il}\overline{\Delta}_{jkmn} + \delta_{im}\overline{\Delta}_{jnkl} + \delta_{in}\overline{\Delta}_{jmkl}),$$

$$\overline{\overline{\overline{\nabla}}}_{ijklmnpq} = \frac{1}{2}(\delta_{ik}\overline{\overline{\Delta}}_{jlmnpq} + \delta_{il}\overline{\overline{\Delta}}_{jkmnpq}).$$

References

1. G.Y. TAYLOR, *Plastic strain in metals*, J. Inst. Metals., **62**, 307, 1938.
2. G. SACHS, *Zur Ableitung einer Fliessbedingung*, Z. der V.D.I., **72**, 739, 1928.
3. M. BERVEILLER and A. ZAOUI, *Méthodes self-consistentes en mécanique des solides hétérogenes*, Comportements rhéologiques et structures des matériaux, C. HUET and A. ZAOUI [Eds.], 175, 1981.
4. P. LIPINSKI and M. BERVEILLER, *Elastoplasticity of microinhomogeneous metals at large strains*, Int. J. of Plast., **5**, 149, 1989.
5. P. LIPINSKI, J. KRIER and M. BERVEILLER, *Elastoplasticité des métaux en grandes déformations: comportement global et évolution de la structure interne*, Rev. Phys. Appl., **25**, 361, 1990.
6. P. LIPINSKI, M. BERVEILLER, E. REUBREZ and J. MORREALE, *Transition theories of elastic-plastic deformation of metallic polycrystals*, Arch. of Appl. Mech., **95**, 291, 1995.
7. Z. HU, E.F. RAUCH and C. TEODOSIU, *Work-hardening behavior of mild steel under stress reversal at large strains*, Int. J. Plast., **7**, 839, 1992.

8. C. REY, *Effects of grain boundaries on the mechanical behavior of grains in polycrystals*, Revue Phys. Appl., **23**, 491, 1988.

9. A. KORBEL and P. MARTIN, *Microscopic versus macroscopic aspect of shear bands deformation*, Acta Met., **34**, 1905, 1986.

10. S. THUILLIER, *Rhéologie et microstructure associées á un trajet complexe de déformation pour une nuance d'acier doux*, Thése de INPG Grenoble 1992.

11. U. ESSMANN and H. MUGHRABI, *Annihilation of dislocations during tensile and cyclic deformation and limits of dislocation densities*, Phil. Mag., A **40**, 735, 1979.

12. A. LUFT, *Microstructural processes of plastic instabilities in strengthened metals*, Prog. Mater. Sci., **35**, 97, 1991.

13. J. H. SCHMITT, *Contribution á l'étude de la micro-plasticité des aciers*, Thése de INPG Grenoble 1986.

14. X. LEMOINE, D. MULLER and M. BERVEILLER, *Texture of microstructures in BCC metals for various loading paths*, Mat. Science Forum **157–162**, 1821, 1994.

15. D. MULLER, X. LEMOINE and M. BERVEILLER, *Nonlocal behavior of elastoplastic metals : theory and results*, Trans. of the ASME, **116**, 378, 1994.

16. F. B. PRINZ and A. S. ARGON, *Dislocation cell formation during plastic deformation of copper single crystals*, Phys. Stat. Sol., **57**, 741, 1980.

17. L. P. KUBIN and Y. ESTRIN, *Strain nonuniformities and plastic instabilities*, Revue Phys. Appl., **23**, 573, 1988.

18. S. B. GORYACHEV and A. V. SHALENKOV, *Theory and computer simulation of dislocation structure relaxation during annealing*, Solid State Phenomena, **35–36**, 375, 1994.

19. E. C. AIFANTIS, *Higher order gradients and self-organization at nano, micro and macro-scales*, Mat. Science Forum CMDS7, 55, 1993.

20. J. KRATOCHVIL, *Continuum mechanics approach to collective behavior of dislocations*, Solid State Phenomena, **35–36**, 71, 1994.

21. A. FENNAN, *Homogénéisation élastoplastique discréte*, Thèse de l'Ecole Centrale de Lyon 1995.

22. D. KUHLMANN-WILSDORF, LEDS, *Properties and effects of low energy dislocation structure*, Mater. Sci. and Engng., **86**, 53, 1987.

23. D. KUHLMANN-WILSDORF, *Theory of plastic deformation: properties of low energy dislocation structure*, Mater. Sci. and Engng., **A113**, 1, 1989.

24. P. GERMAIN, *Cours de mécanique des milieux continus*, Théorie générale, eds. Masson et Cie, Paris **1**, 1973.

25. J. R. RICE, *Inelastic constitutive relations for solids : an internal-variable theory and its application to metal plasticity*, J. Mech. Phys. Solids, **19**, 433, 1971.

26. G. A. MAUGIN, *The thermodynamics of plasticity and fracture*, Cambridge in Applied mathematics, eds. Cambridge University Press 1992.

27. J. HADAMARD, *Leçons sur la propagation des ondes et les équations de l'hydrodynamique*, Cours du Collége de France, Paris 1903.

28. H. INAGAKI, *Development of microstructures and textures during cold rolling of polycrystalline iron containing an excess amount of dissolved carbon*, Z. Metalkde, 474, 1989.

29. R. HILL, *Interfacial operators in the mechanics of composite media*, J. Mech. Phys. Solids, **31**, 347, 1983.

30. J. D. ESHELBY, *The determination of the elastic field of an ellipsoidal inclusion and related problems*, Proc. Roy. Soc., **A241**, 376, 1957.

31. E. KRÖNER, *Zur plastischen Verformung des Vielkristalls*, Acta Metall., **9**, 155, 1961.

32. D. MULLER, J. KRATOCHVIL and M. BERVEILLER, *Effets des écrouissages couplés de différentes parties d'un métal sur la réponse en traction-compression et sur les contraintes internes*, C. R. Acad. Sci., **316**, 435, 1993.

33. D. MULLER, *Influence de l'écrouissage non local et de l'hétérogénéisation intragranulaire sur le comportement des aciers polycristallins*, Thèse, Université de Metz 1994.

34. P. FRANCIOSI, M. BERVEILLER and A. ZAOUI, *Latent hardening in copper and aluminium single crystal*, Acta Met., **28**, 273, 1980.

35. H. MUGHRABI, *Dislocation clustering and long-range internal stresses in monotically and cyclically deformed metal crystals*, Revue Phys. Appl., **23**, 367, 1988.

36. R. HILL, *An invariant treatment of interfacial discontinuities in elastic composites*, Continuum Mechanics and Related Problems of Analysis, 597, Moscow 1972.

37. M. CHERKAOUI, H. SABAR and M. BERVEILLER, *Micromechanical approach of the coated inclusion problem and applications to composite materials*, Trans. of the ASME, **16**, 274, 1994.

38. M. CHERKAOUI, H. SABAR and M. BERVEILLER, *Elastic composites with coated reinforcements : a micromechanical approach for non homothetic topology*, Int. J. Engng Sci., **33**, 829, 1995.

39. L. J. WALPOLE, *A rotated rigid ellipsoidal inclusion in an elastic medium*, Proc. R. Soc. Lond. **A 433**, 179, 1991.

40. H. SABAR, M. BUISSON and M. BERVEILLER, *The inhomogeneous and plastic inclusion problem with moving boundary*, Int. J. Plast., **7**, 759, 1991.

41. G. FAIVRE, *Hétérogénéités ellipsoidales dans un milieu élastique anisotrope*, J. Physique, **32**, 325, 1971.

42. W. KECS and P. P. TEODORESCU, *Applications of the theory of distributions in mechanics*, Abacus Press, England 1974.

43. I. AUBERT, *Effet de l'hétérogénéisation plastique sur le comportement macroscopique lors de chargements complexes*, Thèse de l'Université de Metz, 1998.

44. M. BERVEILLER, M. CHERKAOUI and I. AUBERT, *Micromechanics of moving inelastic discontinuities and applications*, Proceeding of the IUTAM Symposium Micro and Macrostructural Aspects of Thermoplasticity, Bochum, Germany, 25–29 August 1997.

45. D. PIERCE, R. J. ASARO and NEEDLEMAN, *Material rate-dependence and localized deformation in crystalline solids*, Acta Metall., **31**, 12, pp. 1951–1976, 1983.

LABORATOIRE DE PHYSIQUE ET MECANIQUE DES MATERIAUX
INSTITUT SUPERIEUR DE GENIE MECANIQUE ET PRODUCTIQUE
Metz, France
and
LABORATOIRE D'ETUDES ET DE DEVELOPPEMENT DES PRODUITS PLATS
Sollac, Florange, France

Received December 9, 1997

Arch. Mech., 50, 4, pp. 791–803, Warszawa 1998
FIFTY YEARS OF THE ARCHIVES OF MECHANICS

Existence and uniqueness result for Stokes flows in a half-plane

M. KOHR (CLUJ-NAPOCA)

THIS PAPER is concerned with the study of the two-dimensional Stokes flow past a smooth obstacle near a plane wall. Using the boundary integral formulation, the flow is represented in terms of a combined distribution of a single-layer and a double-layer potentials of Green's functions over the boundary of the obstacle. The problem is formulated as a set of Fredholm integral equations of the second kind for the density of the potentials. The existence and uniqueness results of the solution are obtained. Numerical results are presented in the case of a rigid circular obstacle moving parallel or normal to the plane wall.

1. Introduction

THE MOTION of a body of simple shape, near a plane wall, with small Reynolds number, has a long record in fluid dynamics research. For example, the motion of a rigid sphere parallel to a plane wall was treated by H. FAXEN (see [5]). The author used the method of reflections and determined a scheme of successive iterations, which solved the associated boundary value problem. The problem of a sphere moving perpendicular to a plane rigid wall was solved by H. BRENNER (see [1]). He used the general bipolar coordinate solution. By applying the method of reflections, S. J. WAKIYA (see [8]) determined the motion of a sphere toward a plane wall. H. POWER, G. MIRANDA and R. GONZALES (see [15]) obtained an exact formulation for the slow viscous flow due to the arbitrary motion of a particle of arbitrary shape near a plane wall. This formulation is given in terms of a system of Fredholm integral equations of the first kind. The authors used the Green's function, which is equal to zero on the rigid wall. R. HSU and P. GANTOS (see [9]) determined an integral equation method, based on the Green's integral representation formulae, instead of only a single-layer potential. This method solved the problem of the motion of a rigid body in a viscous fluid bounded by a plane wall. Using the method of second kind integral equations, S. J. KARRILA and S. KIM (see [10]) deduced an elegant solution for the problem of multiple particles in the unbounded flow with an exterior container as the boundary. Karrila and Kim's method was called the Completed Double-Layer Boundary Integral Equation Method, because, it uses the idea of completing the deficient range of the double-layer operator. Also, this method is a deflation procedure needed to give an integral operator with a spectral radius strictly less than one. The author shows that this method is the most efficient one when

the mobility problem is numerically solved. In such a problem the force and the torque acting on each particle are given and the unknown motion of the particle is determined.

A second kind of integral equation formulation was applied by H. POWER and B. F. POWER (see [16]), for the slow motion of an arbitrary particle near a plane wall and in a viscous fluid. Also, Y. TAKAISI (see [8]) gave an analytical solution for the motion of a rigid cylindrical obstacle, parallel to a rigid wall, in the limiting case of large values of the distance between the wall and the center of obstacle.

The goal of this paper is to present an integral formulation based on the theory of double-layer and single-layer potentials, for the slow motion of a cylindrical obstacle near a plane wall.

2. Mathematical model

We consider the problem of the slow motion of a cylindrical rigid obstacle of arbitrary shape, near a plane wall, in a viscous fluid. The cross-section of the obstacle, in the Ox_1x_2 plane, is denoted by Ω^1, having the boundary C of Lyapunov type. We assume that the rigid wall, denoted by L, is given by the equation $x_2 = 0$.

The velocity and pressure fields of the undisturbed fluid flow are denoted by $\mathbf{U}_\infty(U_{1\infty}, U_{2\infty})$ and p_∞. The functions $\mathbf{U}_\infty$ and p_∞ satisfy the continuity equation and the Stokes equations in the half-plane $x_2 > 0$. Additionally, the velocity $\mathbf{U}_\infty$ satisfies the following nonslip boundary condition:

$$\mathbf{U}_\infty(x) = \mathbf{0}, \quad \text{for} \quad x_2 = 0. \tag{2.1}$$

Furthermore, we suppose that the rigid particle Ω^1 has the velocity $\mathbf{U}(U_1, U_2)$. Under this condition, the velocity field $\mathbf{u}$ and the pressure field p of the resulting flow, obtained by the superposition of the undisturbed flow and the presence of the rigid obstacle Ω^1, satisfy, in the first approximation, the following system of equations:

$$\begin{aligned} &\sum_{k=1}^{2} \frac{\partial^2 u_i(x)}{\partial x_k \partial x_k} = \frac{\partial p(x)}{\partial x_i}, \quad x \in \Omega, \\ &\sum_{i=1}^{2} \frac{\partial u_i(x)}{\partial x_i} = 0, \quad x \in \Omega. \end{aligned} \tag{2.2}$$

Here, Ω is the domain above the wall, exterior to the particle and having C and L as boundaries. Also, we suppose that the dynamic viscosity coefficient of the flow

is equal to 1, because the general case can be reduced to this one by a coordinate transformation.

The flow satisfies the nonslip boundary condition on the wall L:

$$u_i(x) = 0, \qquad \text{for} \quad x \in L, \tag{2.3}$$

the following condition on the boundary C:

$$u_i(x) = U_i(x), \qquad \text{for} \quad x \in C, \tag{2.4}$$

and the conditions at infinity:

$$|u_i(x) - U_{i\infty}(x)| \to 0, \qquad |p(x) - p_\infty(x)| \to 0, \qquad \text{as} \qquad |x| \to \infty. \tag{2.5}$$

3. The Green function of the flow

Let $\mathbf{G}(G_{ij})$ and $\mathbf{q}(q_i)$ be the Green's function and the pressure vector, associated with the Stokes equations in the half-plane $x_2 > 0$. These functions correspond to the velocity and pressure fields of a Stokes flow, produced by source point or a pole placed at the point y of the above specified half-plane.

Hence, $\mathbf{G}$ and $\mathbf{q}$ are solutions for the following equations and conditions (see [12, 18]):

$$\sum_{k=1}^{2} \frac{\partial^2 G_{ij}(x,y)}{\partial x_k \partial x_k} - \frac{\partial q_j(x,y)}{\partial x_i} = -4\pi\delta_{ij}\delta(x-y), \quad \text{for} \quad x_2 > 0, \tag{3.1}$$

$$\sum_{i=1}^{2} \frac{\partial G_{ij}(x,y)}{\partial x_i} = 0, \quad \text{for} \quad x_2 > 0, \tag{3.2}$$

$$G_{ij}(x,y) = 0, \quad \text{for} \quad x_2 = 0, \tag{3.3}$$

$$G_{ij}(x,y) \to 0, \quad q_j(x,y) \to 0, \quad \text{as} \quad |x| \to \infty, \tag{3.4}$$

where $y(y_1, y_2)$ is the pole or the source point of the Green's function and δ is the two-dimensional Dirac's distribution.

The function $\mathbf{G}$ is given by (see [17]):

$$\mathbf{G}(x,y) = \mathbf{G}^{ST}(x-y) - \mathbf{G}^{ST}(x-y^{im}) + 2y_2^2\, \mathbf{G}^{D}(x-y^{im}) - 2y_2\, \mathbf{G}^{SD}(x-y^{im}), \tag{3.5}$$

where $y^{im}(y_1, -y_2)$ is the image of the pole with respect to the wall, $\mathbf{G}^{ST}$ is the two-dimensional Stokeslet, having the following components:

$$G_{ij}^{ST}(x) = -\delta_{ij} \ln|x| + \frac{x_i\, x_j}{|x|^2}, \qquad x \in \mathbf{R}^2. \tag{3.6}$$

The matrices $\mathbf{G}^D$ and $\mathbf{G}^{SD}$ contain potential dipoles and Stokeslet doublets, respectively, and are given by (see [18]):

$$G_{ij}^D(x) = \pm\left(\frac{\delta_{ij}}{|x|^2} - 2\frac{x_i\, x_j}{|x|^4}\right), \quad G_{ij}^{SD}(x) = x_2 G_{ij}^D(x) \pm \frac{\delta_{j2}x_i - \delta_{i2}x_j}{|x|^2}, \tag{3.7}$$

with the plus sign for the x_1 direction and the minus sign for the x_2 direction.

The associated pressure vector $\mathbf{q}$ is given by (see [17]):

$$\mathbf{q}(x,y) = \mathbf{q}^{ST}(x-y) - \mathbf{q}^{ST}(x-y^{im}) - 2y_2\mathbf{q}^{SD}(x-y^{im}), \tag{3.8}$$

where

$$q_i^{ST}(x) = 2\frac{x_i}{|x|^2}, \quad \mathbf{q}^{SD}(x) = -\frac{2}{|x|^4}(2x_1x_2, x_1^2 - x_2^2). \tag{3.9}$$

The stress tensor $\mathbf{T}$, associated with the Green's function $\mathbf{G}$, has the following components (see [12, 18]):

$$T_{ijk}(x,y) = -q_j(x,y)\delta_{ik} + \frac{\partial G_{ij}(x,y)}{\partial x_k} + \frac{\partial G_{kj}(x,y)}{\partial x_i}, \quad \text{for } x_2 > 0. \tag{3.10}$$

The relations (3.5) – (3.9) lead to (see [17]):

$$\mathbf{T}(x,y) = \mathbf{T}^{ST} - \mathbf{T}^{ST}(x-y^{im}) + 2y_2^2\,\mathbf{T}^D(x-y^{im}) - 2y_2\mathbf{T}^{SL}(x-y^{im}), \tag{3.11}$$

where

$$\begin{aligned} T_{ijk}^{ST}(x) &= -4\frac{x_i\, x_j\, x_k}{|x|^4}, \qquad T_{ijk}^D(x) = \frac{\partial G_{ij}^D(x)}{\partial x_k} + \frac{\partial G_{kj}^D(x)}{\partial x_i}, \\ T_{ijk}^{SD}(x) &= -q_j^{SD}(x)\delta_{ij} + \frac{\partial G_{ij}^{SD}(x)}{\partial x_k} + \frac{\partial G_{kj}^{SD}(x)}{\partial x_i}. \end{aligned} \tag{3.12}$$

The Green's function $\mathbf{G}$ vanishes over the wall L. When the pole y tends to a point x of L, $\mathbf{G}$ has a singular behaviour and must vanish, because $x \in L$. Then, we obtain the following properties:

$$G_{ij}(x,y) = q_i(x,y) = T_{ijk}(x,y) = 0, \qquad \text{for} \qquad y \in L\ . \tag{3.13}$$

Also, it is easily seen that the Green's function $\mathbf{G}$ satisfies the symmetry property given below:

$$G_{ij}(x,y) = G_{ji}(y,x). \tag{3.14}$$

4. Integral representation of solution

The velocity field of the Stokes flow is represented in the following form:

$$u_i(x) = U_{i\infty}(x) + \int_C T_{jik}(y,x) n_k(y) \varphi_j(y) ds_y + \int_C G_{ij}(x,y) \varphi_j(y) ds_y , \quad x \in \Omega, \tag{4.1}$$

where the unknown density φ is assumed to be a continuous function on C, and the unit normal vector $\mathbf{n}$ is directed outside of Ω^1.

In the following we denote by $\mathcal{P}(y,x)$ the pressure field at the point y, associated with the flow $\mathbf{q}(x,y)$. Indeed, the pressure term $\mathbf{q}(x,y)$ is a solution to the equations of the Stokes flow given by a singularity with the pole at the point x (see [12, 18]). Furthermore, the pressure tensor $\mathbf{P}(x,y)$, associated with the stress tensor $\mathbf{T}(y,x)$, has the following components (for more details, see [18]):

$$T_{ij}(x,y) = -\mathcal{P}(x,y)\delta_{ij} + \frac{\partial q_i(x,y)}{\partial y_j} + \frac{\partial q_j(x,y)}{\partial y_i} . \tag{4.2}$$

By applying the above properties, we use the following integral representation for the pressure field p of the flow:

$$p(x) = p_\infty(x) + \int_C T_{ij}(x,y) n_j(y) \varphi_i(y) ds_y + \int_C q_j(x,y) \varphi_j(y) ds_y , \quad x \in \Omega. \tag{4.3}$$

By a simple computation, it can be shown that the functions $\mathbf{u}$ and p satisfy Eqs. (2.2) of the Stokes flow. Also, from (3.3) and (3.13), we deduce that the boundary condition (2.3) is satisfied.

From the following conditions (see also, [12, 18]):

$$T_{ijk}(y,x) \to 0, \quad T_{ij}(x,y) \to 0, \quad G_{ij}(x,y) \to 0, \quad q_j(x,y) \to 0, \quad \text{as} \quad |x| \to \infty, \tag{4.4}$$

we deduce that the conditions at infinity (2.5) hold.

The double-layer potential of the integral representation (4.1) has the following jump properties(see [12, 18]):

$$\lim_{x' \to x \in C} \int_C T_{jik}(y,x') n_k(y) \varphi_j(y) ds_y = \pm 2\pi \varphi_i(x) + \int_C^{PV} T_{jik}(y,x) n_k(y) \varphi_j(y) ds_y , \tag{4.5}$$

where the plus sign applies to the external side of C, in the direction of the normal vector $\mathbf{n}$, and the minus sign to the internal side. The symbol $\mathcal{P}V$ means that the double-layer integral is evaluated in the principal value sense (i.e. the value of the improper but convergent double-layer integral, when $x \in C$).

By using the boundary conditions (2.4) and the above jump properties, we obtain the following integral equations:

$$2\pi\varphi_i(x) + \mathop{\mathcal{P}V}\int_C T_{jik}(y,x)n_k(y)\varphi_j(y)ds_y + \int_C G_{ij}(x,y)\varphi_j(y)ds_y = U_i(x) - U_{i\infty}(x). \tag{4.6}$$

In what follows, let us suppose that $\mathbf{U}$ is a continuous function on C. Because the contour C is a Lyapunov curve, it follows that the kernel of the single-layer operator $\mathbf{V^1}$, defined by:

$$\left[V^1\boldsymbol{\varphi}\right]_i(x) = \int_C G_{ij}(x,y)\varphi_j(y)ds_y, \quad x \in C, \tag{4.7}$$

is weakly singular (i.e. its singularity has the type $1/(|x-y|^\lambda)$, where $0 \leq \lambda < 1$) (see, for example [13]). Thus, the single-layer operator is a compact operator on the space of continuous functions on C (see also, [13]).

With similar arguments we conclude that the double-layer operator $\mathbf{V^2}$, defined by:

$$\left[V^2\boldsymbol{\varphi}\right]_i(x) = \mathop{\mathcal{P}V}\int_C T_{jik}(y,x)n_k(y)\varphi_j(y)ds_y, \qquad x \in C, \tag{4.8}$$

has the kernel with a weak singularity. Then the double-layer operator is compact in the space of continuous function in C, having the values in the same Banach space (see also, [13]).

These properties show that the integral equations (4.6) determine a Fredholm integral system of the second kind. By using the Fredholm's result (see [13]), we deduce that this system has a unique continuous solution if and only if it can be proved that the associated homogeneous system has only the null solution, in the space of continuous functions on C.

Consider the following homogeneous system:

$$2\pi\varphi_i^0(x) + \mathop{\mathcal{P}V}\int_C T_{jik}(y,x)n_k(y)\varphi_j^0(y)ds_y + \int_C G_{ij}(x,y)\varphi_j^0(y)ds_y = 0, \quad x \in C. \tag{4.9}$$

By using a continuous solution $\boldsymbol{\varphi}^0$ of the above system (4.9), we can define the velocity field $\mathbf{u}^0(u_1^0, u_2^0)$ and the pressure field p^0, given below:

$$u_i^0(x) = \int_C T_{jik}(y,x) n_k(y) \varphi_j^0(y) ds_y + \int_C G_{ij}(x,y) \varphi_j^0(y) ds_y, \qquad x \in \Omega \cup \Omega^1,$$

(4.10)

$$p^0(x) = \int_C T_{ij}(x,y) n_j(y) \varphi_i^0(y) ds_y + \int_C q_j(x,y) \varphi_j^0(y) ds_y, \qquad x \in \Omega \cup \Omega^1.$$

Taking into account the fact that the functions $(\mathbf{G}, \mathbf{q})$ and $(\mathbf{T}, \mathbf{P})$ are solutions of the equations of the Stokes flow, we conclude that the fields $\mathbf{u}^0$ and p^0 determine a Stokes flow in Ω (and Ω^1, respectively), with the zero velocity on the wall L and at infinity. Because the function $\boldsymbol{\varphi}^0$ is a solution of the system (4.9), we deduce that the velocity field $\mathbf{u}^0$ becomes zero on the boundary C. By using the uniqueness result of the Stokes flow in Ω, we obtain the following equalities:

$$\mathbf{u}^0(x) = \mathbf{0}, \qquad p^0(x) = 0, \qquad \text{for all} \quad x \in \Omega. \tag{4.11}$$

On the other hand, the continuity property of the single-layer potential across the boundary C and the jump formulas (4.5) of the double-layer potential, imply:

$$u_i^{0^+}(x) - u_i^{0^-}(x) = 4\pi \varphi_i^0(x), \qquad x \in C\ , \tag{4.12}$$

where

$$u_i^{0^+}(x) = \lim_{\substack{x' \to x \in C \\ x' \in \Omega}} u_i^0(x') \quad \text{and} \quad u_i^{0^-}(x) = \lim_{\substack{x' \to x \in C \\ x' \in \Omega^1}} u_i^0(x')\ .$$

From (4.11) and (4.12), we obtain:

$$u_i^{0^-}(x) = -4\pi \varphi_i^0(x), \qquad x \in C\ , \tag{4.13}$$

$$F_i^{0^+}(x) = \lim_{\substack{x' \to x \in C \\ x' \in \Omega}} \left[-p^0(x)\delta_{ik} + \frac{\partial u_i^0(x')}{\partial x_k'} + \frac{\partial u_k^0(x')}{\partial x_i'} \right] n_k(x) = 0\ , \tag{4.14}$$

where $\mathbf{F}^{0^+}$ denotes the limiting value on C of the stress field $\mathbf{F}^0$, evaluated from the external side of C and corresponding to the flow field $\mathbf{u}^0$. Also, we denote by $\mathbf{F}^{0^-}$ the limiting value of $\mathbf{F}^0$ evaluated from the internal side of C.

By an easy computation, it follows that the stress tensor $\mathbf{S}^1$, given by the single-layer potential $\mathbf{V}^1\boldsymbol{\varphi}^0$, has the following components:

$$S_{ij}^1(x) = \int_C T_{ijk}(x,y) \varphi_j^0(y) ds_y, \qquad x \in \Omega \cup \Omega^1. \tag{4.15}$$

The associated stress field $\mathbf{F}^1$ of $\mathbf{S}^1$ exhibits the following discontinuities across its distribution domain C (see, for example [12, 18]):

$$F_i^{1^+}(x) = \lim_{\substack{x' \to x \in C \\ x' \in \Omega}} S_{ik}^1(x') n_k(x) = -2\pi\varphi_i^0(x) + \int_C^{PV} T_{ijk}(x,y) n_k(x) \varphi_j^0(y) ds_y,$$

(4.16)

$$F_i^{1^-}(x) = \lim_{\substack{x' \to x \in C \\ x' \in \Omega^1}} S_{ik}^1(x') n_k(x) = 2\pi\varphi_i^0(x) + \int_C^{PV} T_{ijk}(x,y) n_k(x) \varphi_j^0(y) ds_y.$$

Therefore, we have:

$$F_i^{1^+}(x) - F_i^{1^-}(x) = -4\pi\varphi_i^0(x), \qquad x \in C. \tag{4.17}$$

From properties (4.11) and (4.16), we deduce that the following limiting value on C exists and is finite:

$$\lim_{\substack{x' \to x \in C \\ x' \in \Omega}} F_i^{2^+}(x') = 2\pi\varphi_i^0(x) - \int_C^{PV} T_{ijk}(x,y) n_k(x) \varphi_j^0(y) ds_y,$$

where $\mathbf{F}^2$ is the stress field associated with the double-layer potentials $\mathbf{V}^2\boldsymbol{\varphi}^0$.

By a Lyapunov result (see [13]), it follows that there exists an analogous limiting value from the domain Ω^1 on C, of the stress field $\mathbf{F}^2$. Additionally, these limiting values are equal (see [12, 18]).

Thus, we obtain the following equalities:

$$\lim_{\substack{x' \to x \in C \\ x' \in \Omega}} F_i^{2^+}(x') = \lim_{\substack{x' \to x \in C \\ x' \in \Omega^1}} F_i^{2^-}(x'), \qquad x \in C\,. \tag{4.18}$$

By using the properties (4.17) and (4.18), we obtain the following jump of the stress field $\mathbf{F}^0$ across C:

$$\mathbf{F}^{0^+}(x) - \mathbf{F}^{0^-}(x) = -4\pi\boldsymbol{\varphi}^0(x), \qquad x \in C\,. \tag{4.19}$$

From (4.14) and (4.19), we deduce:

$$\mathbf{F}^{0^-}(x) = 4\pi\boldsymbol{\varphi}^0(x), \qquad x \in C\,. \tag{4.20}$$

Green's formula, applied in the bounded domain Ω^1 for the flow $(\mathbf{u}^0, p^0)$, implies the following equality:

$$\int_C u_i^{0^-}(x) F_i^{0^-}(x) ds_x = 2 \int_{\Omega^1} e_{ik}^0(x) e_{ik}^0(x) dx \ , \tag{4.21}$$

where $e_{ik}^0 = \frac{1}{2}\left(\frac{\partial u_i^0}{\partial x_k} + \frac{\partial u_k^0}{\partial x_i}\right)$ represents the rate of the deformation tensor.

If we use the relations (4.13), (4.20) and (4.21), we obtain:

$$\int_{\Omega^1} e_{ik}^0(x) e_{ik}^0(x) dx = -8\pi^2 \int_C \varphi_i^0(x) \varphi_i^0(x) ds_x \ . \tag{4.22}$$

Since the above integrals are real and non-negative, we deduce that all integrals in (4.22) become zero. Hence, $\boldsymbol{\varphi}(x) = 0$, for $x \in C$.

Thus, we can formulate the following result.

THEOREM. *The Fredholm integral system* (4.6) *has a unique continuous solution* $\boldsymbol{\varphi}$. *The integral representations* (4.1), (4.3), *with the density* $\boldsymbol{\varphi}$, *provide the Stokes flow due to the slow motion of the rigid obstacle* Ω^1, *in the presence of the wall* L.

It is easy to see that if there exists the limiting value on C of the stress field associated with the double-layer potential $\mathbf{V}^2\boldsymbol{\varphi}$, then its total force and torque on C are zero. By using the jump formulas (4.16) of the surface force due to a single-layer potential, we can easily prove that the total force and torque, exerted on C by the flow $(\mathbf{u}, p)$, are given by the following equalities:

$$\begin{aligned} \mathcal{F}_i &= \int_C F_i(x) ds_x = -4\pi \int_C \varphi_i(x) ds_x \ , \\ \mathbf{M} &= \int_C \mathbf{x} \times \mathbf{F}(x) ds = -4\pi \mathbf{k} \int_C \mathbf{x} \times \boldsymbol{\varphi}(x) ds_x . \end{aligned} \tag{4.23}$$

In the above equalities we have used the notation:

$$F_i(x) = \left[-p(x)\delta_{ik} + \frac{\partial u_i(x)}{\partial x_k} + \frac{\partial u_k(x)}{\partial x_i}\right] n_k(x), \qquad x \in C.$$

Also $\mathbf{x}$ is the position vector of the point x with respect to the orthogonal frame Ox_1x_2 and $\mathbf{k}$ is the unit vector of the Ox_3 axis, which is orthogonal to the plane of the flow.

5. Numerical results

If we use properties (3.1), (3.2) of the functions $\mathbf{G}$ and $\mathbf{q}$, we obtain the following property of the stress tensor $\mathbf{T}$ (see, for example [12, 18]):

$$(5.1) \qquad \overset{PV}{\int_C} T_{jik}(y,x)n_k(y)ds_y = -2\pi\delta_{ij}\,, \qquad x \in C\,,$$

where the unit normal vector $\mathbf{n}$ is directed outwards of C. Considering this property, the integral system (4.6) can be written in the following manner:

$$(5.2) \qquad \int_C T_{jik}(y,x)n_k(y)(\varphi_j(y)-\varphi_j(x))ds_y + \int_C G_{ij}(x,y)\varphi_j(y)ds_y = U_i(x) - U_{i\infty}(x), \quad x \in C.$$

The double-layer integrals of (5.2) are non-singular (i.e. they are regular integrals), hence the singularities of double-layer potential of system (4.6) are removed by means of the above procedure. In order to remove the singularities of single-layer potentials of system (4.6), it is sufficient to isolate these singularities and also, to integrate the singularities over the corresponding boundary element.

In the following, the numerical results are given for the case of a circular rigid obstacle with radius a, moving parallel or normal to the wall L. We solve the integral system (5.2) by means of a standard boundary element method. To this end, we consider a polygonal contour consisting of the segments C_j, $j = 1, ..., n$, and we suppose that on each segment C_j, the functions φ_i, $i = 1, 2$, are constant and equal to their values at the middle point $x_j^*(x_{1j}^*, x_{2j}^*)$ of this segment. These values are denoted by φ_i^j, $i = 1, 2$, $j = 1, .., n$. Now, if we require the discretized form of (5.2) to be satisfied at each point x_m^*, $m = 1, ..., n$, we obtain the algebraic linear system given below:

$$(5.3) \qquad \sum_{p=1}^{n}(\varphi_j^p - \varphi_j^m)\int_{C_p} T_{jik}(y,x_m^*)n_k(y)ds_y + \sum_{p=1}^{n}\varphi_j^p\int_{C_p} G_{ij}(x_m^*,y)ds_y = U_i(x_m^*) - U_{i\infty}(x_m^*).$$

If $p = m$, then we have $(\varphi_j^p - \varphi_j^m)\int_{C_p} T_{jik}(y,x_m^*)n_k(y)ds_y = 0$.

In the case when $p = m$, we use the following decomposition for single-layer potential:

$$\int_{C_p} G_{ij}(x_m^*,y)ds_y = \int_{C_p}(G_{ij}(x_m^*,y) - G_{ij}^{ST}(x_m^*,y))ds_y + \int_{C_p} G_{ij}^{ST}(x_m^*,y)ds_y.$$

In the above equality the first integral is regular and can be numerically determined by a Gaussian quadrature formula. The second integral can be evaluated accurately.

If $p \neq m$, then the double layer integrals and the single layer integrals of the system (5.3) are computed by means of the Gaussian quadrature formula.

Furthemore, after discretization, the total force and torque on C become:

$$\mathcal{F}_i = -4\pi \sum_{m=1}^{n} \varphi_i^m \int_{C_m} ds \,,$$

(5.4)

$$\mathcal{M} = -4\pi \mathbf{k} \sum_{m=1}^{n} \left\{ \varphi_2^m \int_{C_m} y_1 ds - \varphi_1^m \int_{C_m} y_2 ds \right\}.$$

In the sequel we denote by Y_0 the ratio of the distance d, between the center of the circular obstacle and the rigid wall, to the radius a.

Figure 1 illustrates the dependence between the dimensionless drag force F and Y_0, in the case of the circular rigid obstacle moving perpendicular to the rigid wall L (i.e. $\mathbf{U}_\infty = \mathbf{0}$ and $|\mathbf{U}| = 1$).

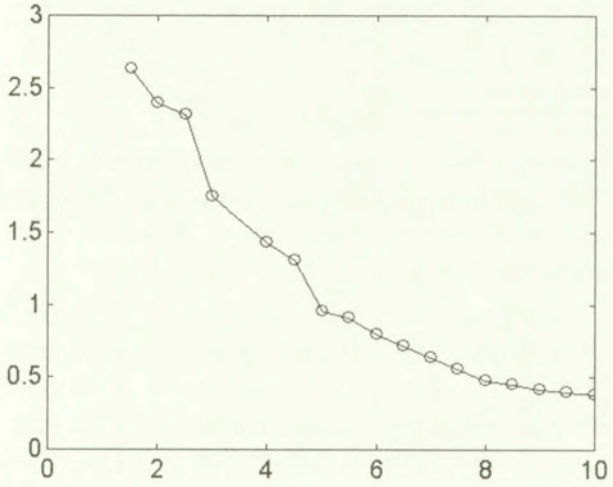

FIG. 1. Dependence of F vs. Y_0 : perpendicular motion.

Note that $F = \mathcal{F}/4\pi U$ and $\mathcal{F}$ is the modulus of the total force $\mathbb{F}$ on C.

Figure 2 presents the dependence between the dimensionless drag force F and Y_0, in the case of the circular obstacle moving parallel to the wall L (i.e. $\mathbf{U}_\infty = \mathbf{0}$ and $\mathbf{U} = (1, 0)$).

Both these results show that F increases when the ratio Y_0 decreases.

The maximum value of N was assumed to be equal to 60.

In the limiting case of large values of Y_0, it follows that the presented numerical results can be compared with the analogous results obtained by Y. TAKAISI (see [8]), where the analytical expression of the dimensionless drag force F_T was equal to

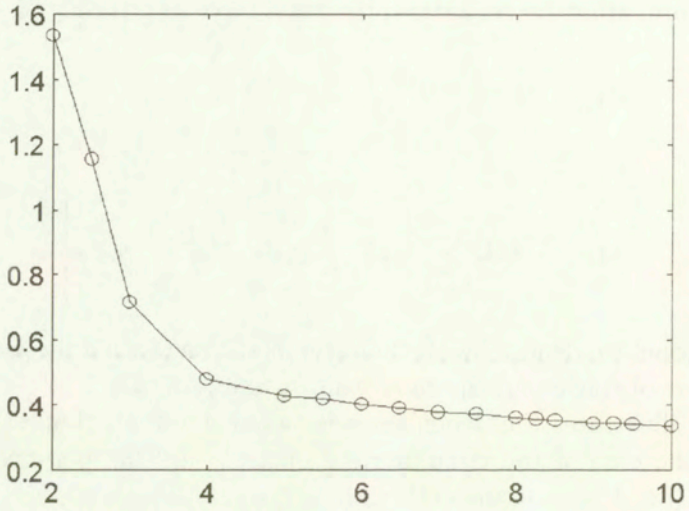

FIG. 2. Dependence of F vs. Y_0 : parallel motion.

$$F_T = \frac{\mathcal{F}_T}{4\pi\mu U} = \frac{1}{\log(2Y_0)},$$

the viscosity coefficient μ and the translational velocity U of circular obstacle in the direction of the wall being equal to 1. Note that $\mathcal{F}_T$ is the modulus of the total force acting on on C and corresponding to Takaisi's method.

For example, we have:

$$\begin{aligned}
Y_0 = 6.0 &\Rightarrow F_T = 0.4024296043, \quad F = 0.40312,\\
Y_0 = 6.5 &\Rightarrow F_T = 0.3898712452, \quad F = 0.39012,\\
Y_0 = 7.0 &\Rightarrow F_T = 0.3789231816, \quad F = 0.37901,\\
Y_0 = 7.5 &\Rightarrow F_T = 0.3692693730, \quad F = 0.37002,\\
Y_0 = 8.0 &\Rightarrow F_T = 0.3606737602, \quad F = 0.36107,\\
Y_0 = 8.5 &\Rightarrow F_T = 0.3529561238, \quad F = 0.35301,\\
Y_0 = 9.0 &\Rightarrow F_T = 0.3459762562, \quad F = 0.34599,\\
Y_0 = 9.5 &\Rightarrow F_T = 0.3396232718, \quad F = 0.33969,\\
Y_0 = 10 &\Rightarrow F_T = 0.3338082006, \quad F = 0.33381.
\end{aligned}$$

References

1. H. BRENNER, *The slow motion of a sphere through a viscous fluid towards a plane surface*, Chem. Engrg. Sci., **16**, 242–251, 1961.

2. L. DRAGOŞ, *Principles of continuous mechanics media* [in Romanian], Ed. Tehnică, Bucharest 1983.

3. L. DRAGOŞ and A. DINU, *A direct boundary integral equations method to subsonic flow with circulation past thin airfoils in ground effect*, Comput. Methods Appl. Mech. Engng., **127**, 357–370, 1995.

4. L. DRAGOŞ and A. DINU, *A direct boundary integral method for the three-dimensional lifting flow*, Comput. Methods Appl. Mech. Engng., **127**, 357–370, 1995.

5. H. FAXEN, *Die Bewegung einer starren Kugel längs der Achse eines mit Flüssigkeit gefüllten Rohres*, Arkiv. Mat. Astron. Fys., **17**, 1–28, 1923.

6. T. M. FISCHER, G. C. HSIAO and W. L. WENDLAND, *On two-dimensional slow viscous flows past obstacles in a half-plane*, Proc. Royal Soc. Edinburgh, **104A**, 205–215, 1986.

7. T. M. FISCHER and R. ROSENBERGER, *A boundary integral method for the numerical computation of the forces exerted on a sphere in viscous incompressible flows near a plane wall*, ZAMP, **38**, 339–365, 1987.

8. J. HAPPEL and H. BRENNER, *Low Reynolds number hydrodynamics*, Martinus Noordhoff, The Netherlands 1973.

9. R. HSU and P. GANATOS, *The motion of a rigid body in viscous fluid bounded by a plane wall*, J. Fluid Mech., **207**, 29–72, 1989.

10. S. J. KARRILA and S. KIM, *Integral equations of the second kind for Stokes flow: Direct solution for physical variables and removal of inherent accuracy limitations*, Chem. Engng. Comm., **82**, 123–161, 1989.

11. S. KIM and S. J. KARRILA, *Microhydrodynamics, principles and selected applications*, Butterworth-Heinemann, 1991.

12. M. KOHR, *The study of some viscous flows by boundary integral methods*, [in Romanian], Cluj University Press, 1997.

13. R. KRESS, *Linear integral equations*, Springer-Verlag, 1989.

14. O. A. LADYZHENSKAYA, *The mathematical theory of viscous incompressible flow*, Gordon Breach, 1963.

15. H. POWER, G. MIRANDA and R. GONZALES, *Integral equation solution for the flow due to the motion of a body of arbitrary shape near a plane wall at small Reynolds number*, Math. Appl. Comput., **4**, 279–296, 1985.

16. H. POWER and B. F. POWER, *Second-kind integral equation formulation for the slow motion of a particle of arbitrary shape near a plane wall in a viscous fluid*, SIAM J. Appl. Math., **53**, 1, 60–70, 1993.

17. C. POZRIKIDIS, *Creeping flow in two-dimensional channels*, J. Fluid Mech., **188**, 495–514, 1987.

18. C. POZRIKIDIS, *Boundary integral and singularity methods for linearized viscous flows*, Cambridge University Press, 1992.

BABEŞ-BOLYAI UNIVERSITY
FACULTY OF MATHEMATICS

1, M. Kogălniceanu Str.
3400 Cluj-Napoca, Romania.
email:mkohr@math.ubbcluj.ro

Received December 16, 1996; new version January 7, 1998.

Arch. Mech., 50, 4, p. 805, Warszawa 1998
FIFTY YEARS OF THE ARCHIVES OF MECHANICS

HONORARY DEGREE

IT IS OUR PLEASURE to inform the Readers of the Archives of Mechanics that our long-time Editor in Chief, Professor WŁADYSLAW FISZDON, world-wide known specialist in Fluid Mechanics, has been elected in april 1998 by the EUROMECH Council to the position of a Honorary Member of the EUROMECH. This has been done in order "to recognize His long and invaluable support of the work in the EUROMECH Comittee and of mechanics in Europe, through His participation in many EUROMECH Colloquia in Western and Eastern Europe, His stimulation of many EUROMECH Colloquia in Western and Eastern Europe, His stimulation of many EUROMECH Colloquia in Poland, and His key role played in providing a bridge between the Eastern and Western scientists during many difficult years".

Editorial Committee
of the Archives of Mechanics

INSTITUTE OF FUNDAMENTAL TECHNOLOGICAL RESEARCH
is publishing the following periodicals:

ARCHIVES OF MECHANICS – bimontly (in English)
ARCHIVES OF ACOUSTICS – quarterly (in English)
ARCHIVES OF CIVIL ENGINEERING – quarterly (in English)
ENGINEERING TRANSACTION – quarterly (in English)
COMPUTER ASSISTED MECHANICS AND ENGINEERING SCIENCES – quarterly (in English)
JOURNAL OF TECHNICAL PHYSICS – quarterly (in English)

Subscription orders for the journals edited by IFTR may be sent directly to the

Editorial Office
Institute of Fundamental Technological Research,
Świętokrzyska 21, p. 508,
00-049 WARSZAWA, Poland.

DIRECTIONS FOR THE AUTHORS

The journal *ARCHIVES OF MECHANICS (ARCHIWUM MECHANIKI STOSOWANEJ)* deals with the printing of original papers which should not appear in other periodicals.

As a rule, the volume of a paper should not exceed 40 000 typographic signs, that is about 20 type-written pages, format: 210×297 mm, leaded. The papers should be submitted in two copies. They must be set in accordance with the norms established by the Editorial Office. Special importance is attached to the following directions:

1. The title of the paper should be as short as possible.

2. The text should be preceded by a brief introduction; it is also desirable that a list of notations used in the paper should be given.

3. The formula number consists of two figures: the first represents the section number and the other the formula number in that section. Thus the division into subsections does not influence the numbering of formulae. Only such formulae should be numbered to which the author refers throughout the paper, and also the resulting formulae. The formula number should be written on the left-hand side of the formula; round brackets are necessary to avoid any misunderstanding. For instance, if the author refers to the third formula of the set (2.1), a subscript should be added to denote the formula, viz. $(2.1)_3$.

4. All the notations should be written very distinctly. Special care must be taken to write small and capital letters as precisely as possible. Semi-bold type should be underlined in black pencil. Explanations should be given on the margin of the manuscript in case of special type face.

5. It has been established to denote vectors by semi-bold type. Trigonometric functions are denoted by sin, cos, tg and ctg, inverse functions – by arc sin, arc cos, arc tg and arc ctg; hyperbolic functions are denoted by sh, ch, th and cth, inverse functions – by Arsh, Arch, Arth and Arcth.

6. Figures in square brackets denote reference titles. Items appearing in the reference list should include the initials of the first name of the author and his surname, also the full title of the paper (in the language of the original paper); moreover;

a) In the case of books, the publisher's name, the place and year of publication should be given, e.g.,

5. S. Ziemba, *Vibration analysis*, PWN, Warszawa 1970;

b) In the case of a periodical, the full title of the periodical, consecutive volume number, current issue number, pp. from ... to ..., year of publication should be mentioned; the annual volume number must be marked in black pencil so as to distinguish it from the current issue number, e.g.,

6. M. Sokołowski, *A thermoelastic problem for a strip with discontinuous boundary conditions*, Arch. Mech., **13**, 3, 337–354, 1961.

7. The authors should enclose a summary of the paper. The volume of the summary is to be about 100 words.

8. The authors are kindly requested to enclose the figures prepared on diskettes (format PCX, BitMap or PostScript).

Upon receipt of the paper, the Editorial Office forwards it to the reviewer. His opinion is the basis for the Editorial Committee to determine whether the paper can be accepted for publication or not.

The printing of the paper completed, the author receives 25 copies of reprints free of charge. The authors wishing to get more copies should advise the Editorial Office accordingly, not later than the date of obtaining the galley proofs.

The papers submitted for publication in the journal should be written in English. No royalty is paid to the authors.

Please send us, in addition to the typescript, the same text prepared on a diskette (flopy disk) 3 1/2″ or 5 1/4″ as an ASCII file, in Dos or Unix format.

EDITORIAL COMMITTEE
ARCHIVES OF MECHANICS
(ARCHIWUM MECHANIKI STOSOWANEJ)

The next number of Archives of Mechanics will contain the following papers:

K. PIECHÓR, *The dependence of dynamic phase transitions on parameters*

Z. A. KOTULSKI, *On efficiency of identification of a stochastic crack propagation model based on Virkler experimental data*

A. GAWĘCKI, *On elastic energy of structures under proportional loading*

J. SZCZEPAŃSKI and Z.A. KOTULSKI, *On two motions of a particle driven by equivalent ergodic and chaotic reflection laws*

L. DIETRICH and Z.L. KOWALEWSKI, *On the cyclic yield surface of some engineering materials under complex stress conditions*

H. GOUIN and W. KOSIŃSKI, *Boundary conditions for a capillary fluid in contact with a wall*

SUDESHNA BANERJEA and C.C. KAR, *On waves due to a line source in front of a vertical wall with a gap*

Archives of Mechanics

cena zł 15.

WARUNKI PRENUMERATY

Wpłaty na prenumeratę przyjmują na okresy półroczne:

na teren kraju

– jednostki kolportażowe RUCH S.A. i wszystkie urzędy pocztowe na terenie całego kraju, właściwe dla miejsca zamieszkania lub siedziby prenumeratora, oraz doręczyciele w miejscowościach, gdzie dostęp do urzędu jest utrudniony;

– od osób zamieszkałych lub instytucji mieszczących się w miejscowościach, w których nie ma jednostek kolportażowych RUCH, wpłaty należy wnosić do RUCHU S.A. Oddział Krajowej Dystrybucji Prasy, 00-958 Warszawa, ul. Towarowa 28. Konto: PBK S.A. XIII Oddział Warszawa nr 11101053–16551–2700–1–67. RUCH S.A. zapewnia dostawę pod wskazanym adresem pocztą zwykłą w ramach opłaconej prenumeraty;

na zagranicę

– RUCH S.A. Oddział Krajowej Dystrybucji Prasy, 00–958 Warszawa, ul. Towarowa 28. Konto: PBK S.A. XIII Oddział Warszawa nr 11101053–16551–2700–1–67. Dostawa odbywa się pocztą zwykłą w ramach opłaconej prenumeraty z wyjątkiem zlecenia dostawy pocztą lotniczą, której koszt w pełni pokrywa zleceniodawca.

Prenumerata ze zleceniem dostawy za granicę jest o 100% wyższa od krajowej.

Terminy wpłat na prenumeratę zagraniczną:

do 20 XI na I półrocze roku następnego do 20 V na II półrocze roku bieżącego

Terminy wpłat na prenumeratę krajową:

RUCH S.A.		Poczta Polska	
do 5 XII	na I półrocze roku następnego	do 25 XI	na I półrocze roku następnego
do 5 VI	na II półrocze roku bieżącego	do 25 V	na II półrocze roku bieżącego

Dostawa zamówionej prasy następuje:

– przez jednostki kolportażowe RUCH S.A. – w sposób uzgodniony z zamawiającym,
– prenumerata pocztowa – pod wskazanym adresem, w ramach opłaconej prenumeraty.

RUCH S.A. fulfils foreign customers' orders, starting from any issue in the calendar year:

tel.: (48) (22) 620 10 39; fax: (48) (22) 620 17 62.

Bieżące numery można nabyć a także zaprenumerować roczne wydanie bezpośrednio w Dziale Wydawnictw IPPT PAN, Świętokrzyska 21, 00-049 Warszawa, tel. (22) 826 60 22. Również można je nabyć, a także zamówić (przesyłka za zaliczeniem pocztowym) we Wzorcowni Ośrodka Rozpowszechniania Wydawnictw Naukowych PAN, 00-818 Warszawa, ul. Twarda 51/55, tel. (22) 697 88 35.

Redakcja przyjmuje prenumeratę na wszystkie czasopisma wydawane przez IPPT PAN

Subscription orders for all journals edited by IFTR may be sent directly to the Editorial Office of the Institute of Fundamental Technological Research, Świętokrzyska 21, 00–049 Warszawa, Poland.

All journals edited by IFTR are available also through:

Foreign Trade Enteprise
ARS POLONA,
Krakowskie Przedmieście 7,
00–068 Warszawa, Poland
fax (48) (22) 826 86 73

or

Agencja Reklamowo–Wydawnicza
ARKADIUSZ GRZEGORCZYK
Bitwy Warszawskiej 1920 r., 3
00–973 Warszawa, Poland
tel (48) (22) 822 49 36
fax (48) (22) 822 49 36

Arch. Mech. T. 50, nr 4, str. 673–808, Warszawa 1998.